Continuum and Combined Continuum-Discontinuum Analysis of Wellbore Mechanics and Stimulation Response

Khalid Mohammed M Alruwaili

Submitted for the degree of Doctor of Philosophy

Heriot-Watt University

Institute of Petroleum Engineering

The School of Energy, Geoscience, Infrastructure and Society

August 2016

ABSTRACT

Wellbore drilling and stimulation activities are interlinked processes within the task of borehole construction. Before drilling a well, the initial stress state in the rock can be defined by three principal stresses, with a typical assumption that these consist of the vertical stress (σ_v), the maximum horizontal stress (σ_H) and the minimum horizontal stress (σ_h). After drilling, the stress state changes around the created borehole. The fundamental engineering problem then is to calculate the stresses around the created borehole and/or at the borehole's wall. Numerous analytical and numerical models exist to estimate the stresses around a circular hole, but these models cannot explain the observed phenomena either in the field or the lab. Attention here is focused on models that are commonly used to predict the stress state around a circular opening. These models do not account for the sequence of the physical processes, leading to an inadequate stress state estimation. This research investigates the 2D classical analytical method, along with a comparison of that approach against numerical methods. This investigation reveals that the models are not equivalent. This is not because of mathematical issues, but is due to the fact that the mechanical systems expressed by these models are not equivalent. The drilling model captures the physics of the real process which makes it possible to explain some phenomena observed in field and laboratory tests. The drilling model approach is applied for several sedimentary rock examples. The combined continuum-discontinuum method reveals its capability in calculating rock failure and deformation that is comparable to some published laboratory drilling tests. Also, the simulation results shed light into the complex fracture growth regime around the wellbore. Drilling and Hydraulic fracture simulation is carried out for Berea sandstone using both the continuum and the combined continuum-discontinuum methods. The results are in good agreement which identifies a practical engineering method for larger models. The fracturing initiates in Mode II (shear) near the circumference of the wellbore aligned with the maximum stress. At later stages, Mode I (tensile) fractures also develop and propagate the fracture parallel to the maximum horizontal stress. This fracturing mechanism continues for as long as the pressure is applied.

DEDICATION

This thesis is dedicated to my parents, my wife, my son, my daughter and all of my family members

ACKNOWLEDGMENTS

It has been my privilege to work closely with Professor Gary Couples and Dr. Jingsheng Ma, I have enjoyed the opportunity to learn from their knowledge and experience. Their frequent insights and patience with me are always appreciated. I am very proud of what I have achieved under their guidance and supervision, thank you both.

I am very grateful to Dr. Helen Lewis for her support in helping me run the SAVFEM code. Many thanks to you.

I would like to thank Geomechnica's team for giving me the opportunity to use their software from my research study. Especial thanks to Dr. Andrea Lisjak and Dr. Omid Mahabadi for their prompt responses whenever I encountered problems with FEMDEM code.

Many thanks my examiners Dr. James Somerville and Professor Giovanni Grasselli for their valuable comments.

I would like also to thank Saudi Aramco for their financial support during the course of my studies here at Heriot-Watt University.

Thank you so much to everyone who has helped me along my research journey. So many people have been so kind.

DECLARATION STATEMENT

(Research Thesis Submission Form should be placed here)

LISTS OF TABLES AND FIGURES

Chapter 1 – Introduction

The oil and gas industry spends almost $1.3 billion (according to some estimate) annually on wellbore stability problems (Tare et al., 2002). This budget, which is increasing every year, questions the methods in current use to model wellbore mechanics. The same methods underpin the design of stimulation activities, such as hydraulic fracturing. Thus, the topic of wellbore mechanics warrants a re-investigation.

Wellbore stability problems occur as a results of drilling weak formation which causes sand production and borehole enlargements (Ewy et al., 1994, Partin et al., 2010). Drilling into natural fractures may cause lost circulation and inability to control the wellbore pressure (Power et al., 2003). The chemical and thermal reactions (from drilling fluids) with lithology (especially with shale formations) may develop swelling and expansion of the formation (Tare et al., 2003). A complex geology structure and anisotropic stress contrast may results in wellbore stability problem (Ali et al., 2003). Handling wellbore stability issues needs an in-depth knowledge about the mechanisms which have been the root cause of the instability. The Misconception of the processes in the development of stress states around the wellbore during drilling can lead to incorrect mechanistic interpretations, and thus poor outcomes that result in instability such as breakouts, washouts and collapse of the borehole. Therefore, it is crucial to exactly determine what mechanisms and processes have caused the problems.

Wellbore stimulation is a post-drilling process that is used for enhancing well productivity. The stimulation can range from something as simple as wellbore cleaning of mud filter cake to an extensive hydraulic fracturing stimulation. In this thesis, I will emphasise the hydraulic fracture stimulation process which requires a good estimation of stress state around the wellbore in order to ensure that a suitable course of stimulation treatment can be implemented and carried out successfully. An unsuccessful stimulation treatment can lead to a major capital loss.

Wellbore stability and stimulation have been modelled with considerable variation in sophistication capturing from basic linear elastic behaviours to highly non-linear elastoplastic behaviours of rock masses (McLean et al, 1990). Linear elastic models of wellbore stability have offered important insights into the problems as they can be solved analytically. Non-linear elastoplastic models, on the other hand, can capture

some important aspects of rock post- yield behaviours as rock masses are treated as continuums by finite element analysis. Those models indeed help us gain good understandings into the stress state behaviours and have been widely applied in the industry to real problems in hand as predictive tools. Therefore, it is crucially important to investigate rigorously what would happen if models cannot capture certain behaviours of rocks, model assumptions are not met and what implications can be. Clearly a robust approach is needed to model stress evolution of rocks where a single intact rock mass undergoes elasto-plastic deformation and fragmentation where each component is subject to elasto-plastic deformation internally and interacts with other components following Newton's laws. In this work, such approach is facilitated using a combined Finite-Element Method and Discrete-Element Method (FEMDEM) to enable us to draw consistent and comprehensive picture on what can and cannot be archived with standard models.

The main objective of this thesis is to provide an understanding of the geomechanical processes that underpin the task of making a realistic stress state estimation around the wellbore. I approach this by investigating the classical stress state methods from which many analytical and numerical models are prevailed. This investigation reveals important drawbacks of the current practice of modeling of wellbore stability and subsequently stimulation.

In Chapter 2, a literature review on some of the models used in wellbore stability and stimulation problems are presented. A closer look was taken at the linear elastic models and their relationship with estimating the stress state around the wellbore and fracture initiation. A critical assessment of how these models formulate our understanding of predicting stress state around the wellbore is presented.

In Chapter 3, a comprehensive evaluation of the classical analytical method widely used for estimating the stress state around a circular opening, along with a comparison of that approach against numerical methods are presented. The analysis concludes that the models are not equivalent. This is not because of mathematical issues and numerical artifacts, but is due to the fact that the mechanical systems expressed by these models are not equivalent. This conclusion has clear implications for how one might choose between the methods to predict a stress state around the wellbore.

In Chapter 4, a series of 2D FEM drilling simulations are presented to develop models of realistic stress states of examples sedimentary rock types that are allowed to fracture and fragment. The combined finite-discrete element method (FEMDEM) is used to create the results. FEMDEM method includes a detailed and explicit rock failure process, and also incorporates dynamic rock deformation behaviour as might be related to the consequences of the breakage processes. The drilling stage is considered to be a key boundary condition component to achieve a realistic mechanical state prior to any stimulation work.

In Chapter 5, a 2D Berea sandstone model is used to simulate a drilling process and allow for a realistic stress state formation. The outcomes establish a range of starting points, which exhibit altered stress states and already-failed rocks, for the process of well stimulation. The FEMDEM simulation tool is used to examine how a post-drilling new loading of the wellbore results in the propagation of failures away from the opening into the rock mass.

In Chapter 6 and Chapter 7, a detailed and informative discussions on the key points of this research are highlighted in Chapter 6. A summary of the key findings, conclusions, future research work and recommendations are presented in Chapter 7.

Chapter 2 – Literature Review

2.1 Introduction

Drilling and well stimulation are essential tasks in the oil and gas industry to create the means to access and exploit underground oil and gas resources. The industry has long experience of the techniques involved, as many wells have been drilled and completed across the world. Wellbore stability problems is one of the major issues which costs the industry a substantial expenditure every year (Bradley, 1978). The wellbore stability has become a major concern in horizontal wells and extended-reach laterals, as these type of wells are likely to be more exposed to larger differential stresses which risk the stability of the borehole. Underbalanced drilling challenges the task of ensuring wellbore stability by controlling the mud weight to minimize mud filtrates and unintentional induced fractures; these issues may arise commonly while exploiting unconventional resources.

Drilling engineers have typically adopted simple models to predict the geomechanical processes that impact wellbore stability. All of the methods depend on an estimation of the far-field state of stress that existed prior to drilling a well. The reasons or causes for wells to become unstable (i.e. experience rock failures) during drilling are dependent on the situation. To obtain a better analysis and prediction of wellbore stability, it is necessary to take a closer look at the parameters and conditions encountered during wellbore instability. For example, drilling into a pre-stressed rock formation will cause a disturbance of the stress state around the wellbore to some distance into the rocks. This disturbance depends on the geology (i.e. rock properties), far-field stresses, and mud weight. A major factor, which can (in principle) be determined, is the prediction of the pre-drilling state of stress. The rock properties may or may not be known very well, and the mud weight is in principle known and controlled. Design of wellbore stability involves the adoption of a model that is intended to represent the processes, and thus their effects, in terms of altering the stress state after drilling. The basis for simple formulae to accomplish the calculation is a version of the Kirsch (1898) analytical expression. Nearly all of the numerical methods that are used are validated against this solution. Whether based on the analytical expression or a numerical solution, the analysis is carried out to determine the impacts of the parameters on wellbore stability and hydraulic fracturing design.

The fracturing phenomena was initially recognised from well acidizing operations which were used as mechanisms to create channels into the formation to enhance well productivity. The same phenomenon is observed also in water injection and cement squeezing. An in-depth study was conducted by Farris (1941) to establish a relationship between well performance and stimulation treatment such as acidizing, water injection or cement squeezing. From this study, Farris introduced the idea of intentional hydraulic fracturing to increase oil and gas production from tight rock formations. The first well treatment with this idea was performed in the Hugoton gas field in Grant County, Kansas, in 1947. An acid injection was used in that treatment to stimulate a limestone formation. After treatment, the well productivity did not change. The treatment was performed without any basis from a **MODEL**. A brief details of the field history will be discussed later in this chapter.

In 1948, the Hydraulic fracturing process was introduced through a paper written by Clark (1948). Two successful treatments were conducted in Stephens County, Oklahoma and another one in Archer County, Texas, using a blend of oil and gasoline. Subsequently, applications using hydraulic fracturing operations increased the productivity of wells in tight formations of the Hugoton gas field. The hydraulic fracturing technology not only increased well production rates, but also increased the amount of gas that can be recovered in the field.

The fundamental concept behind fracturing has been developed over time, with advances in modeling design applications continuing up to our current physical understanding of the process. In the following sections, a review on the modeling design of hydraulic fracturing will be presented, and how the treatment design impacted the oil and gas production in the Hugoton gas field and some other fields. I aim to highlight and discuss the most critical components in the wellbore stability and hydraulic fracture modeling design and their impact on the overall treatment.

2.2 Wellbore Stability Background

Before drilling a well, the underground state of stress is in a compression state. The regional stresses can be defined by the vertical or the overburden stress, σ_v and two horizontal stresses, σ_H (the maximum horizontal stress) and σ_h (the minimum horizontal stress). When the well is drilled, the stress state will change as a result of removing the

wellbore region from the underground. The stresses at the wellbore wall are defined as a hoop or tangential stress, σ_Θ which normally acts at the wellbore circumference. The radial stresses, σ_r and the shear stress $\sigma_{\Theta r}$ are defined across the entire domain.

If the stresses disturbance exceed the tensile or shear failure criterion, the wellbore will be instable. To evaluate the potential of wellbore stability, a model must be used to calculate the stress/strain component and then compare them against a given failure criterion either linear (e. g. Drucker-Prager, 1952) or non-linear criterion (e. g. Pariseau, 1968 and Hoek-Brown, 1980).

In general, the wellbore stability models are narrowed down to linear elastic models (Bradly, 1979; Paslay and Cheatham, 1963; Aadnoy, 1987) and elastoplastic models (Westergaard, 1940; Veeken et al, 1989). The differences are in the strength criteria used to predict wellbore instability. The linear elastic models offer more conservative prediction of stress state around wellbore where less conservative stress prediction is provided the elastoplastic approach. In conclusion, the hard rock formation may justify the use of linear elastic models which are based on the maximum and minimum stress (i. e. Mohr-Coulomb). For weak rock formation, the use of non-linear or elastoplastic models may be preferred.

The majority of well designs rely on the history of drilling in a developed field. Logs and imaging tools are used to analyse wellbore breakout and they are useful to predict pore pressure and porosity using density logs. Log-based wellbore stability interpretation is a routine activity in current drilling technology.

Wellbore stability analysis has been previously presented in many publications (Aadnoy and Chenevert, 1987; Bradley, 1979; Cheatham Jr., 1984; Eaton, 1969; Matthews and Kelly, 1967; Wilson and Willis, 1986). The well drilling requires a geomechanical model to estimate the stress path and calculate safe mud weight and fracture pressure while drilling (Bradley, 1979). The model must include rock mechanical, and deformation characteristics when the rocks are subjected to stress conditions that reach failure.

A comprehensive historical review over two decades was made by Papanastasiou and Zervos (2004) on wellbore stability models. They have demonstrated an improvement

in predicting the mud weight moving from linear elastic solution to finite elastoplastic methods. Later in this chapter I will present the most indicative linear elastic wellbore stability models used to compute the stress and/or strain around the wellbore.

2.3 Hydraulic Fracture Background

Breakdown pressure is an essential part of the hydraulic fracturing process. The stress state changes as a result of the drilling is a critical component in calculating the breakdown pressure. Breakdown pressure is an extremely complex problem. It involves different parameters such as injection rate, fracking fluid, rock properties, wellbore size and the state of stress. As a result, many published models used to determine the breakdown pressure. Although numerus models prevail such as the classical breakdown model (Hubbert and Willis, 1972; Bredehoeft et al., 1976; Hickman and Zoback, 1981), the poroelastic model (Haimson, 1968; Schmitt and Zoback, 1989), the fracture mechanics model (Abou-sayed and Brechtel, 1978; and Rummel, 1987), the point stress model (Ito and Hayashi, 1991) and the shear failure model (Callanan, 1981; Morgenstern, 1962; Liunggren wt al., 1988; Panah and Yanagisawa, 1989; Lo and Kaniaru, 1990; Mori et al., 1990), none of these model are generally accepted.

After fracture is initiated at the wellbore wall, a fracture propagation model must be used. In 1947, the first hydraulic fracturing treatment was conducted by Stanolind Oil and Gas at Hugoton gas field. The treatment result was described by Clark (1949). In 1949, Halliburton obtained a patent for a commercial process of hydraulic fracturing treatment. Then, the hydraulic fracturing treatment became the standard well completion in this field. Hugoton gas field is one of the best examples to look at the fracturing results performance and its association with fracture modeling development over time.

The linear elasticity method are usually used to model rock deformation. The power fluid law is used as an expression of the fluid inside the hydraulic fracture. The fracture propagation law uses the linear elasticity fracture mechanics theory. Numerous models using analytical and numerical methods have been developed overtime to design a hydraulic fracture treatment. The classical 2D hydraulic fracture model (Perkins and Kern, 1961; Nordgren, 1972; Khristianovic and Zheltov, 1955; Geertsma and Klerk, 1969; Green and Sneddon, 1950), the Pseudo-3D (P3D) model (Settari and Cleary; 1986) and the fully 3D model. Other numerical methods are used to simulate the interface behaviour between rock grains as a results of rock deformation (Guo et al.,

2008; Zhang et al., 2007; Taleghani and Olson, 2009). The stress state is a dominating factor in the fracture initiation and propagation. A simplified approached of predicting a stress state has been always considered for many fracture models. Later, I will discuss some of the relevant methods to this research and highlight their outcomes.

2.4 Numerical Model Historical Review

The first breakdown pressure was developed by Hubbert and Willis (1957). The model assumes that when the tangential compressive stress exceed the tensile strength, a fracture is initiated in tensile (Mode I). The tensile strength is usually considered as a variable parameters and difficult to obtain. Therefore, it is often ignored from the breakdown model suggested by Hubbert and Willis. Bredehoeft, Wolff, Keys and Shuter (1976) introduced the concept of fracture opening pressure to overcome the tensile strength parameters. The concept was further improved by Hickman and Zoback (1981). They derived the breakdown pressure based on the initial injection pressure cycle and the final pressure cycle. The difference between the two cycles is the tensile strength parameter of the rock.

Haimson (1968) developed a model with the same concept of the first model. The difference is that he added the Boit constant to the model equation and introduced the poroelastic model. His model was argued by Schmitt and Zoback (1989) that the model was inappropriate for low porosity rocks.

Another model was introduced by Abou-sayed and Brechtel (1978) to calculate the breakdown pressure based on fracture toughness, K_{IC}. Iot and Hayashi (1991) introduced a point stress model. It assumes that when the minimum effective stress reached the tensile strength of the rock, the fracture is initiated inside the rock not at the borehole wall. Shear fracture model assumes that when the stress in the wellbore wall reached the shear strength of the rock, breakdown occurs and fracture is initiated.

For hydraulic fracture, the first treatment design used complex charts, monographs and calculations to determine the appropriate fracture fluid volume that need to be injected into the well. The design required to calculate the differential pressure across the perforations based on injection rate per perforation, diameter of the perforation, coefficient of discharge for the perforation and the fluid density. This design method was used until the mid-1960s, when simple program can be used in basic computer. The

PKN model was developed by Perkins and Kern (1961), Nordgen (1972). The KGD model was develop by Khristianovic and Zheltov (1955) and Geertsma and Klerk (1969). These were the two classical models used for hydraulic fracturing treatment design. Green and Sneddon (1950) studied the problem of an elliptical crack under a constant loading. The radial model was developed by Abé, Mura, and Meer Abe in 1976 to account for radial fractures. The hydraulic fracturing process in these models were based on planar analytical solution, considering a tensile (Mode I) fracture propagating in a homogeneous and isotropic medium. Their work was the base of the original development of the hydraulic fracture designs.

The Planar model were extended into pseudo-3D (P3D) models to account for the effect of multiple layers and confining stresses along the height of the fracture (Settari and Cleary; 1986; Morales and Abou-Sayed, 1989). Unlike the PKN and KGD models were the dimensions of the fracture must be assumed. The P3D model calculates variable fracture width and length. Although these models still assume bi-wing hydraulic fracture geometries, the rock properties can be varied along the height and length of the fracture, while the elastic behaviour of the surrounding rock is captured by a continuum numerical solver. Researches have attempted to simplify the problem by modifying some existing 2D/P3D planar fracture models using advance approximation techniques. The result shows that the modified models can simulate hydraulic fracture in a geologically complex reservoir based only on approximations (Green et al., 2007 and Kresse et al., 2013). These models calculate pressure propagation inside the fracture only. The pressure around or between fractures are ignored (Kresse et al., 2013).

The fully 3D model was developed to handle more complex fracture modeling. The model can handle the fracture geometry in arbitrary shape and orientation by removing the assumptions of the P3D fracture model. The development of the fully 3D models is based on the liner elastic mechanics with complex fluid flow pattern inside the fracture (Hossain, 2001). In these models, the fracture can propagate laterally and vertically and also change the direction of its origin depending on the local stresses, rock properties and natural fractures (Economides et al., 1994; Hossain, 2001). At the time, the simulation of fully 3D model could take up to one month to propagate 6 cm of fracture with high power computer (Hossain, 2001). Therefore, these models were used mostly in the academic research.

Other numerical models were developed to create a simulation tool to model the hydraulic fracturing process more realistically in a heterogeneous and anisotropy medium. Among these models are the coupled fluid flow and Discrete Fracture Network (DFN) model which is used to describe the discontinuities in rock mass. Although, these approaches can provide more realistic representation of the rock mass discontinuities, they tend to be limited to model new fracture creations (Dershwitz et al., 2010; Rogers et al., 2011).

To realistically simulate hydraulic fracturing in complex environment, actual calculation of fracture growth in a representative natural fracture network must be developed along with right simulation tool. Such physical behaviour like interaction between fractures, temperature and chemical impact on fractures, existence of stress heterogeneity must be assessed and validated. The interaction between fractures has been studied by many researchers and scientists with different numerical solutions. Last and Harper (1990) are probably the first who studied the impact of fluid flow on natural fractures. McLennan and others (2010) have studied fracture propagation within natural fracture media in three dimensions using Three Dimensional Discrete Code (3DEC). Ben and others (2012) simulated hydraulic fracture with Discontinuity Deformation Analysis (DDA) method. The method uses an implicit formulation for rock deformation. The most relevant work to this research study is made by Fu and others (2011) who have used Loosely Discrete Element Code (LDEC) method to study fracture propagation in geothermal reservoir. All of these models simulated a hydraulic fracturing treatment without considering the drilling stage in the model. They were simply initialized by the far field loads with a pre-existing borehole of fractured network. The LDEC method combines the finite element with discrete element method and solves explicitly the fracture propagation. The method was originally developed by Munjiza (1991). A full description on this method is documented by Munjiza in The Combined Finite Discrete Element Methods (Munjiza, 2004).

Despite the vast requirements needed to develop a more realistic wellbore stability or fracture model, all models discussed above originated based on the fundamental understanding of the stress state principles for homogenous and linear elastic approach. Most or may be all the linear elastic wellbore mechanical models are validated against the so-called Kirsch's solution or a version of this solution for some petroleum engineering problems. In the next section, I will introduce a version of Kirsch's

solution used to describe the stress state around a circular opening. To date, this analytical version is used to directly estimate the stress state around the wellbore or used to validate numerical model with a pre-existing hole for wellbore stability and hydraulic fracturing problems (Serati et al., 2015; Xie et al., 2014; Wang et al., 2009;). The analytical solution devised by Kirsch and many others who followed his path used Airy's stress function to derive and calculate the stresses in an infinite plate with an opening in the middle. Airy's function uses the potential function to calculate stress changes only. It does not account for material/rock displacement and the elastic moduli of the rock. Further investigation of what Kirsch does and calculate will be examined in Chapter 3.

2.5 Review of Stress State around a Wellbore

The far field stresses has been widely recognized as a basic input parameter necessary in the engineering design of underground problems. Quantitative study of the horizontal stresses in rock at a particular location cannot be made since gravitational forces are the only one clearly understood to date. The horizontal stresses can be estimated by several methods (analytical or numerical methods). The knowledge of the in situ stress is a prerequisite to a comprehensive geomechanical modeling. Rock failure will occur when the stresses exceeded the strength of the rock or when the ratio of shear stress to normal stress exceeded the frictional strength of the material. In a numerical model, the far field stresses are performed as an external loading applied to a specific "finite" model (initialization stage) regardless of it size (Figure 2.1).

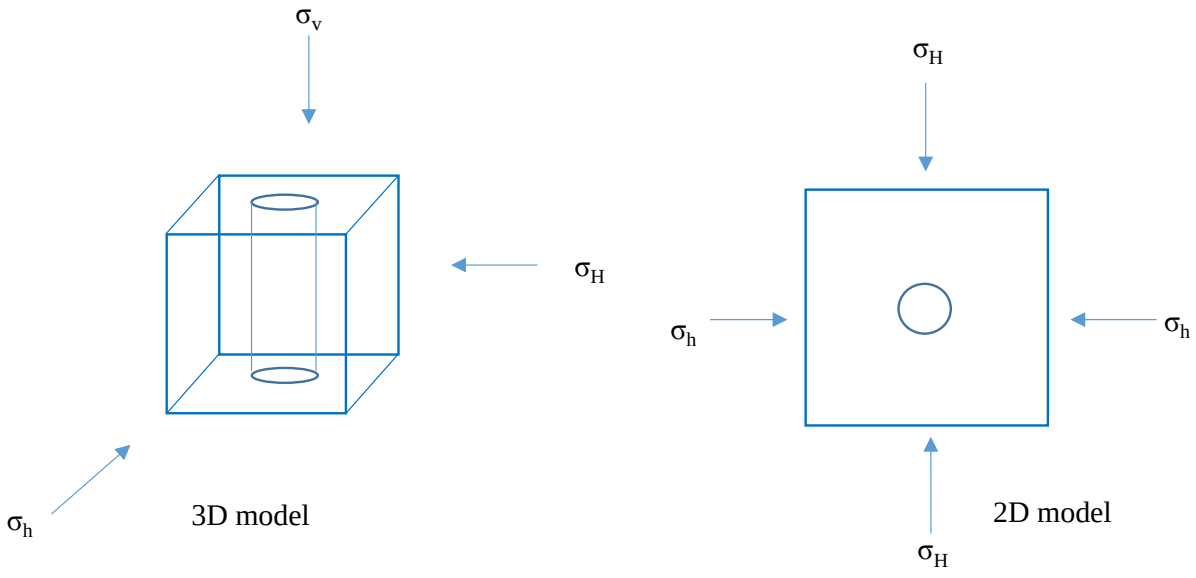

Figure 2.1: 3D and 2D numerical models and the far field stresses

The linear elastic model is widely used in rock mechanics to calculate the magnitude of the stresses after creating the well. The inelastic state or failure is expressed as a high stress magnitude development in the linear elastic model. The analytical expression of Kirsch's solution was exclusively meant for models that are under stress state of elastic condition. Quantitative investigation on the word "Elastic Solution for Elastic Problem" of Kirsch's expression is not available. Since this solution forms the basis and the understanding of wellbore mechanics in many analytical and numerical models used to date, it motivated me to thoroughly examine the solution and provide a comprehensive analysis on this solution in Chapter 3.

After the wellbore is created, Kirsch (or here a 2D expression based on Kirsch solution) calculate the stress state around the wellbore using the following equations:

$$\sigma_{rr} = \frac{\sigma_H + \sigma_h}{2}\left(1 - \frac{R^2}{r^2}\right) + \frac{\sigma_H - \sigma_h}{2}\left(1 + \frac{3R^4}{r^4} - \frac{4R^2}{r^2}\right)\cos 2\theta \tag{2.1}$$

$$\sigma_{\theta\theta} = \frac{\sigma_H + \sigma_h}{2}\left(1 + \frac{R^2}{r^2}\right) - \frac{\sigma_H - \sigma_h}{2}\left(1 + \frac{3R^4}{r^4}\right)\cos 2\theta \tag{2.2}$$

$$\sigma_{r\theta} = \frac{\sigma_H - \sigma_h}{2}\left(1 + \frac{R^2}{r^2} - \frac{3R^4}{r^4}\right)\sin 2\theta \tag{2.3}$$

Where,

σ_{rr}, radial stress

$\sigma_{\Theta\Theta}$, tangential stress

$\sigma_{r\Theta}$, shear stress

σ_h, minimum horizontal principal stress

σ_H, maximum horizontal principal stress

R, "wellbore" radius (i.e. radius of internal "boundary")

r, radial distance

Θ, radial angle, measured anti-clockwise from the direction of σ_h

The linear elastic solution based on a form of Kirsch expression is used to calculate stresses around wellbore transitioning from the pre-drilling elastic state to the post-drilling elastic state. The approach used to validate linear elastic numerical models

against a version of Kirsch equation are only limited to numerical differences that might occur due to the inherited artifacts of the numerical solutions. I am unaware of any quantitative study between the analytical and numerical models to address the validation approach. I will provide this quantitative analysis in Chapter 3.

2.6 Models Derived or Validated Against an Expression of Kirsch Solution

Here I will present some of the models that used a version of Kirsch solution or validated against Kirsch model. The purpose of this presentation is to show the involvement level of this analytical expression into the most critical engineering problems. I will only focus on the stress state concept and failure used in each model.

As mentioned before, Hubbert and Willis (1957) derived the first process-based estimation of the breakdown pressure by reasoning that a fluid (wellbore) pressure equal to the smallest tangential stress would cause a crack to open. It is often referred as a classical or conventional fracture initiation model. The equation is a linear elastic equation which assumes that the wellbore fluid pressure is penetrating or non-penetrating pressure. The penetrating pressure is when the wellbore pressure is equal the formation pressure and the non-penetrating pressure is when the wellbore pressure is not equal the formation pressure. So their expression in calculating fracture initiation is purely based on Kirsch's equation. The breakdown pressure or fracture initiation pressure is a function of the maximum and minimum horizontal stress plus the tensile strength of the rock.

Daneshy (1974) presented a fracture initiation model based on one principal stress. Under his assumption only one fracture can propagate either vertically or horizontally. He formulated his equations based on Kirsch expression and calculated a fracture failure in a tensile mode. He incorporated a poro-elasticity stress term in the equation.

Ong and Roegiers (1996) considered the effect of stress anisotropy without considering the plastic yield, temperature and chemical. The model they presented is based on tensile fracture initiation when wellbore pressure reaches a critical value (a 2D version of Kirsch solution). In their expression, each angle across the wellbore represents a fracture pressure that satisfy the tensile failure at the wellbore wall. The expression is derived 100% from Kirsch's equation

Mitchell and Fulkner (2006) gave a possible explanation for fracturing due to yielding. They explained that the increase of the plastic shear failure zone created shear bands or an unstable state of stress around the cavity. This leads to localised micro-scale fractures and the injected fluids can enter into the created crack to produce local tensile stresses at the fracture tips. The bases of the explanation were based on linear elastic methods.

The conventional continuum mechanics model (based on Kirsch equations) is based on a potential expression (derived from Airy's stress function) of stress concentration around a borehole and does not include the rock elastic properties. Any form of Kirsch expression is based on linear elasticity and assumes a fully non-penetrating conditions. Again, all the models presented above lack the quantitative analysis between Kirsch solution and numerical models that are derived or validated against it. Therefore, a definitive and quantitative conclusion of how Kirsch stress state expression agrees with the numerical models is not available. The drilling is considered an implicit formulation within Kirsch solution. The final equation of Kirsch or any other version derived from it claims that the calculated stress component account for the stress changes due to drilling (or after drilling). Nearly all the models I presented considered that approach without thoroughly investigating how the drilling affect the stress state around the wellbore. Numerical models considered a pre-existing hole and then applied the far field loads at the external boundaries.

Drilling is the stage were engineers experience the first stress disturbance or changes that might cause the instability of the borehole. An analytical solution of the stress state in a plate with a pre-existing hole was published by Kirsch (1898), and this formed the basis for many early studies of rock behaviour around tunnels and shafts which contributed to drilling knowledge. Following along the path pioneered by Kirsch, researchers such as Love (1927), Muskhelishvili (1953) and Savin (1961) published solutions for excavations of various shapes in elastic plates. Their solution are basically a modified mathematical expression of Kirsch equation. The excavated shapes is defined as a mathematical line within an elastic plates. A useful summary of these solutions and their applications in rock mechanics was edited by Brown (1987) in an introduction to a volume entitled Analytical and Computational Methods in Engineering Rock Mechanics. Again, they are all derived from kirsch solution by modifying their mathematical expressions without considering the consequences of the drilling on the

stress state around the wellbore. Kirsch and others solution derived from it define a mathematical constrains not a physical boundary (e.g., numerical models) to the problem. These constrain do not terminate the solution like the numerical models. This is a completely different expressions (analytical vs. numerical) to solve the same problem. I will investigate this by comparing the two approaches in Chapter 3.

There are two different numerical modelling approaches to estimate the state of stress after drilling. The first one starts with a pre-existing hole and then applies the stress load to the model. The second is by applying the loading, and then drilling a hole. Most if not all of the wellbore stability and the hydraulic fracturing modeling deigns often skip the drilling modeling stage or process and ignoring its impact on the stress state changes. Mainly the reason, as mentioned before, is that Kirsch formulated his equation based on a plate with a pre-existing hole and the stresses calculated by the equation representing implicitly the drilling process. Therefore, all numerical models constructed with a pre-existing hole and then subjected to the far field loads to a stress state that assuming that Kirsch equation is the reference stress state that they should use to validate their numerical models. In the next Chapter, I will investigate the stress state under the condition of creating the hole versus a pre-existing hole and make a quantitative analysis to understand the differences between Kirsch expression and numerical model. The linear elastic condition will be applied to the numerical solution.

Based on a certain far field loading condition, the inelastic or fracture region can develops in different size and pattern around the wellbore during or after drilling. The regions that often experience high stress concentrations as a consequence of drilling are near the wellbore. There are different ways to model drilling or rock cutting using numerical techniques. The discrete element method (DEM) and finite element methods (FEM) are the most commonly used numerical methods for rock cutting or drilling analysis.

Rawling, Barton, Bandis, Addis and Gutierrez (1993) conducted a lab experiment on sandstone sample blocks subjected to far field loads. The block samples were drilled (creating a hole) in the middle with different trajectory angles. The results revealed different fracture patterns around the wellbore as a consequence of drilling for different angle. A numerical model based on discontinuum approach were used to demonstrate

the type of failure around the wellbore. The failure mechanisms were dominated by Mode II (shear) type.

In the next section, I will briefly discuss a field performance example versus numerical models. The example show the importance of advancing the knowledge and tool to achieve better results.

2.7 Field Performance versus Models Development History

In April 1986, the Kansas Corporation Commission ruled that infill wells have to be drilled in every 640 acres. With more than 40 years of technology development in hydraulic fracturing, the 1990s were bound to have achieve better performance than the wells drilled in the 1950's. Unfortunately, this was not the case. Figure 2.2 shows the comparison of the Absolute Open Flow Potential (AOFP) ratio for the newly drilled wells in 1990 with 40-year-old wells and categorised by the operators. With the exception of three companies (Arco, Union Pacific and others), the 1990 wells simply duplicated the 40-years-old wells. The AOFP for Arco, Union Pacific and others is better than the rest of the other operators. The most likely reason for better AOFP ratio is that the stimulation procedures used are better than the one used in the original wells. This indicates the change in the treatment designs used for hydraulic fracturing which is a reflection on the modeling techniques.

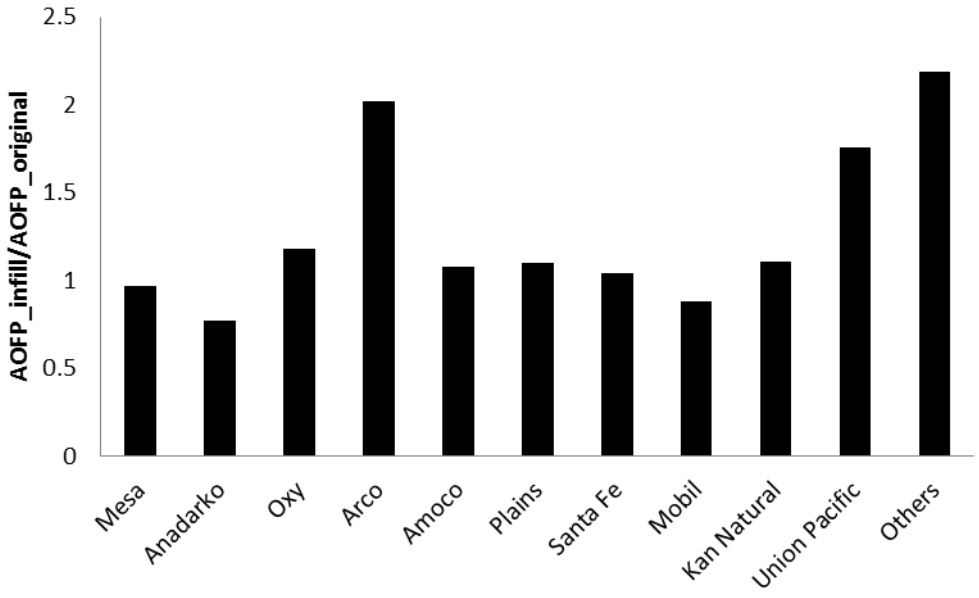

Figure 2.2: Ratio AOFP ration by the operators (After McCoy et al., 1991)

For Union Pacific, we know nothing about what they did to get such higher AOFP ratios than the others. For Arco, the major thing that they did is by basing their fracture

model design on the fully three dimensional (3D) fracture model, the TerrFrac model, as compared to the simpler Pseudo three dimensional (P3D) model, used by most operators. So, sophisticated fracture modeling does have an impact.

In 1996, Mobil published a paper on the performance of the new infill wells drilled from 1994 to 1995 in comparison with the wells drilled in 1991, and this paper shows how the process changes improve fracture treatment designs in the Hugoton gas field. The improved fracture models and the power of computers at that time, have contributed to the success of the hydraulic fracture treatments (Hecker et al., 1996). The results demonstrate a significant improvement in the production through the implementation of new fracture model design with of course gathering field data and evaluating the historical outcomes from the field. The stimulated zone consists of dolomite and limestone pay intervals separated by siltstones. The new process highlighted a drastic change of the treatment design in term of low pad volumes and pumping rate needed instead of large pad volumes and high pumping rate used in the 1991 wells. This was done by eliminating the multi-stage fracturing used in 1991 to using single stage in 1994. The volume of fracture treatment reduced from 450,000 – 500,000 gallons of proppant with 110,000 gallon gelled fluid to almost 50% with an improved gas production. The cost of the treatment was significantly reduced from $239k in 1991 to $140k per well in 1994 (Hecker et al., 1996) see Figure 2.3

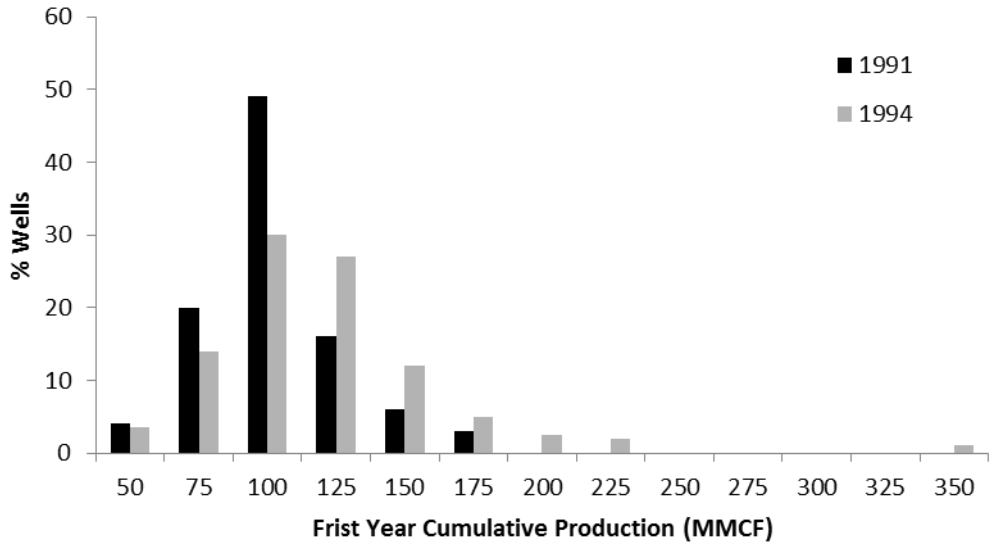

Figure 2.3: Comparison of 1991 vs. 1994 first year cumulative gas production (after Hecker et al., 1996)

A recent fracturing treatment work was performed by PetroChina on Changqing oilfield in 2012, an ultra-tight oil reservoir consisting of sand and shale formations. A fully 3D fracture model was used in comparison with the 2D fracture model that was previously used to design fracture treatment for Changqing ultra tight oil wells. Changqing oilfield consists of three typical reservoir configurations observed at well completions; 1) thick reservoir with aeral continuity, 2) reservoir with laminated siltstone and shale, 3) reservoir at the bottom of the source rock. Based on the fully 3D fracture model simulation, the treatment design called for 3302 barrel of fluid volume and 1547 barrel of sand volumes with pumping rate of 0.628 bbl/min. The regular treatment was 246 m^3 fluid volume and 314.5 m^3 sand volume with pumping rate of 0.262 bbl/min treatments. The oil production of the well with new treatment was significantly higher than the gas production from the regular fracture treatment in reservoir completion number 1 (see Figure 2.4 below).

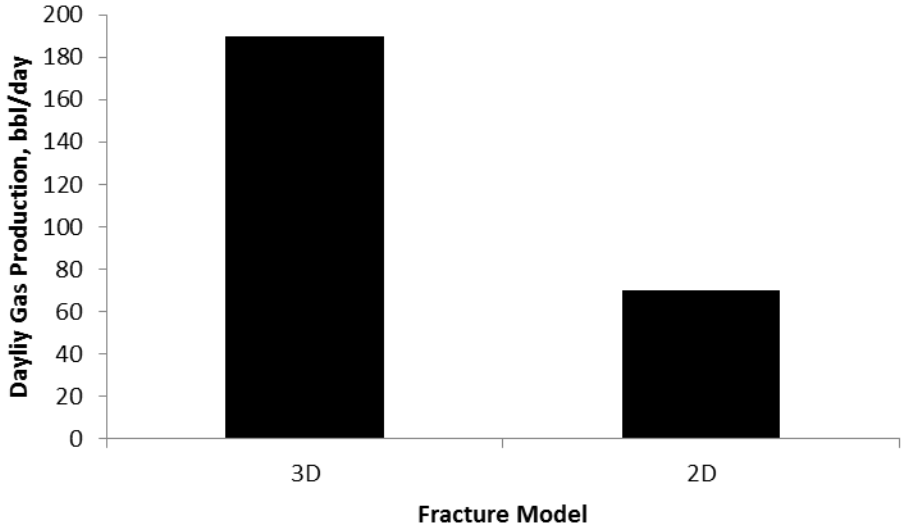

Figure 2.4: Comparison of oil production from new and old fracture treatment

The new treatment processes was also successful in the second type of the laminated siltstones and shales reservoir. The same treatment was unsuccessful in the third type reservoir given that the fully 3D model shows a failed treatment design (Zhuo et al., 2012). Another treatment was performed in the same field using the fully 3D fracture model and predicted an increase of treatment volume from 2445 to 3112 gallons (or an increase by 27%) of the dual-stage treatment in comparison with the single-stage treatment simulated by 2D fracture model. This exercise demonstrates an additional production enhancement by 34% (Liu et al., 2012).

An Unconventional Fracture Model (UFM) was developed in 2012 to design hydraulic fracture treatment in Changqing oilfield. The UFM utilizes fully 3D fracture model with a complete description of the in situ field stress. The company incorporates pre-existing natural fractures and interaction criteria with hydraulic and natural fracture in the treatment design. The initial production test was 649 to 783 barrel/day in the horizontal wells as compare to a 201 barrel/day on average, which is significantly higher when they based their treatment design on the advance fracture models (Liu et al., 2012). This is an important indication on how geomechanics can play very important role in the fracture treatment design.

A review study of methods used to predict wellbore stability in Cyrus Field was published by McLean and Addis (1991). The Cyrus Field in the UK Continental Shelf (UKCS), the wells are normally drilled with an average mud weight of around 1.15 S.G. Over the history of drilling in this field, the wells exhibit no problem with wellbore stability using the recommended mud weight. A study was carried out using numerical and analytical analysis to determine whether the average mud weight of 1.15 S.G is sufficient to prevent spalling of the wellbore wall. Using the linear-elasticity model, the minimum mud weight calculated was 1.24 S.G. while FEM model calculates a minimum mud weight of 1.18 S.G (the actual mud weight used in drilling this section is 1.17 S.G). Based on the predicted and the actual torque while drilling, the linear elastic analysis carried out was extremely conservative and the well could be drilled with lower mud weight without any problem (Child and Cocking, 1989). These observations raises questions on how these model (which are based on Kirsch solution) predict the stress state around the wellbore.

2.8 Summary

In this chapter, I reviewed various methods used to model wellbore stability and hydraulic fracture problems. The wellbore stability problems must adapt a model to calculate the stress/strain component and then compare them against a given failure criterion either linear or non-linear criterion. If the stresses disturbance exceed the tensile or shear failure criterion, the wellbore will be instable and eventually fail partially (breakout) or completely (collapse). Analysis used to assess wellbore stability either used a linear elastic model which is a more conservative model type to estimate stress state and safe mud weight or less conservative model type which includes elastoplastic or shear models.

Breakdown pressure and hydraulic fractures are the two processes involved in stimulating a well. Models to predict fracture initiation and propagation are used on the basis of simple mechanics. These models adapt a version of Kirsch's solution to either directly estimate the stress state around wellbore (based on analytical methods) or validate a numerical model against it. None of these models are generally accepted. The progress and impact of the model development indicated over field operations.

Kirsch or an expression of Kirsch solution forms the basis of the wellbore stability and hydraulic fracture models in term of predicting the stress state around the wellbore. The expression of his solution is based on Airy stress function that describes the stress state as a potential around a circular opening. Nearly all methods, regardless of their numerical formulation, are constructed with a pre-existing hole to model wellbore stability and hydraulic fracture initiation and propagation. Kirsch's equation does not consider rock properties or wellbore geometry deformation and claimed as an "elastic" solution. Kirsch's equation or other derived from it define its boundary as a mathematical constraint which does not terminate the solution if the calculation performed beyond the mathematical boundary (e. g., stress calculation inside the pre-existing hole). I will thoroughly examine a relevant version of Kirsch solution in the next chapter against a numerical models and provide a critical analysis. I am not aware of any extensive quantitative analysis on the validity of the linear elastic analytical solution in comparison with a numerical wellbore models under elastic condition.

I will consider a numerical model with a pre-existing hole subjected to different far field loads and a drilling model which is initialized with the far field stress condition and then drilled. All models in the next chapter will be restricted to an elastic response only. The two models will be compared with a version of Kirsch solution to investigate the stress state around the wellbore in particular.

Chapter 3 – Mechanical Analysis of 2D Wellbore Model

3.1 Introduction

There are several topics which require an understanding of the mechanical state in the vicinity of a wellbore. The drilling operation itself alters that state, by creating the opening, and via thermal changes. One of the purposes of the drilling mud is to counter some of these effects, especially in regards to preventing failure of the wall rocks. Subsequent operations, notably stimulation treatments, are fundamentally related to the mechanical state that exists at the time of the treatment. In order to derive an appropriate estimate of the pre-treatment mechanical state for the analysis of the hydraulic fracturing process, it is necessary to understand how that pre-state is governed by the well construction processes.

In wellbore geomechanical modeling, it is assumed that, before the well opening is created, the local state of stress is only compressional due to simple self-weight conditions and lateral confinement, and as altered by any external loadings. Here, I analyse how the well construction alters the pre-drilling local state of stress, including any feedback from non-elastic responses that result in permanent strains and related stress changes. I do not address any changes relating to thermal effects or the mechanical consequences of chemical reactions. Well drilling causes the release of potential energy that was stored in the rock that is broken up and removed. The removal of the support on the wellbore wall due to the removal of the drilled rock mass causes a change of the stress pattern on and near the wellbore wall, and to some finite distance away from the well. This change can occur within the elastic domain, or may involve additional changes related to plastic deformations, with these responses governed by rock properties and the local conditions. This Chapter describes the analysis of the factors that govern these responses.

The usual strategy for developing an understanding of geomechanical changes induced by drilling involves analytical/numerical methods that calculate the stress state as a consequence of the drilling or subsequent near-wellbore activity (which may involve stimulation of the reservoir; this is examined in Chapter 5). That analysis approach is adopted also in this thesis. In this Chapter, there is a focus on the well construction (drilling) phase, with an aim of assessing the reliability of the several

simulation/calculation approaches for developing an understanding of the local mechanical state immediately after drilling. These approaches range from use of the classical analytical expressions (Kirsch, 1898), to numerical methods that can be operated in a fully-elastic mode or with plastic yielding and thus feedback. In order to derive a full understanding of these methods, a comparison is undertaken between Saleh's (1985) finite analytical solution for a plate with a circular hole (which is shown to be sufficiently equivalent to the Kirsch infinite solution) and equivalent problem solved by the FEM pre-hole model. These two methods give similar results, but the differences leads to an important understanding concerning what the analytical expressions actually means. A third approach, again using an elastic FEM approach, examines how the near-wellbore state is affected by excavating the hole (FEM drilling model). Analysis of the three approaches reveals that each method provides different outcomes.

3.2 Background

All rock in the ground is thought to exist in a state of 3D compressive stress prior to any drilling operations, but that state may not be known very well, which complicates any prediction of the consequences of the well construction process. The usual approach involves making an assumption about the pre-drill state, in which that state is usually assumed to be locally uniform, and possibly uniform over a wide region; that assumption will be addressed later in this thesis.

At first, in this Chapter, a brief introduction, of the main conventional stress assessment, using Saleh's finite solution method ("Saleh" (Saleh, 1985)), and the linear elastic finite element method (FEM pre-hole model), is presented for the calculation of the stress state around an unsupported opening in a model domain with "far-field" loads (expressed as boundary tractions). This is undertaken here by the application of a modified Kirsch's analytical solution by Saleh (1985) for a finite-model 2D domain, and the linear elastic finite element method (FEM linear elastic model), to the case of a pre-existing circular opening located in a finite two dimensional plate. The results of the two methods are compared revealing discrepancies which, up on analysis, leads to an important new insight into the challenge of relating an analytical solution to the real physical world.

The emphasis on the near-wellbore states of stress is pursued on account of the fact that the disturbance of the stress state, during/after the drilling, is the cause of many mechanical responses interconnected with the perturbation and the stability of the

opening. When the mechanical stability limits are exceeded, the rock may respond in several ways, depending on the rock and the extant conditions. One important response is the creation of and then motion along discontinuities (fractures). This Chapter also examines the influence of (potential) newly-created discontinuities on the stability of the opening, and how their activation modifies the stress states in the near-wellbore region. The discontinuities may reduce the strength of the material, increase the fracture permeability and change the (bulk) modulus of elasticity. These effects are studied using the FEMDEM method (the combined finite-discrete element methods).

The main objective of this Chapter is to assess the mechanical state around the wellbore using analytical and numerical solutions. This understanding of the post-drilling mechanical state is an essential starting point for analysing the subsequent processes associated with well stimulation. The analysis of the effects of drilling is based on 2D finite-element and finite-discrete element simulations, and a finite analytical solution. In all cases, the model domain is a finite and square region of 2000mm size, with a 200mm (nominal) diameter "hole" in the middle, representing the wellbore. The conceptual basis for each method is discussed at the point where that method is introduced. In all cases, the Y-direction boundary load is larger than the X-direction load. Since material anisotropy is not considered at this point, the solutions presented can be rotated into any configuration to match the orientation of the principal stresses in a particular setting. In this Chapter, the borehole walls are pressure-free after the hole is created. Based on the concept of effective stress, the results obtained here are equivalent to results for cases with a wellbore and pore-pressure equal to P, if the boundary loads ("framework stresses") are also increased by magnitude P (this is assuming that the material is porous and the pores are fluid-filled). The case where the wellbore pressure is greater than P (which represents a typical overbalance condition) can be obtained, while the response is elastic, by superposing a solution with no boundary loads but a wellbore pressure whose value is higher than P by the amount of overbalance (this loading will be addressed in Chapter 5). Although many combinations of boundary loads were examined in the course of the research, this Chapter describes the outcomes from cases where the major (Y-direction) and minor (X-direction) boundary stresses are -20MPa and -10MPa; -70MPa and -10MPa, or -200MPa and -10MPa. These values are selected because they are associated with outcomes that span conditions from near-isotropic (effective) stress states, to states with high differential stress, and also relate to the range of typical rock yield strengths expressed in terms of effective-stress (these will be argued later).

3.3 Analytical "Linear Elastic" Methods

The analytical approach to the calculation of the stress around an unsupported circular opening is undertaken with the assumption that the material in the model domain is linear, isotropic, homogenous and perfectly elastic (no failure or yielding). The theory of elasticity provides a means of calculating the distribution of stress and strain in a 2D region. The direct solution of elasticity equations, in a domain with a central hole, is far from trivial. An alternative is to calculate the mechanical state by means of simple, analytical (i.e. space coordinates are the parameters) expressions. This method is based on the so-called Airy stress function, which is based on an expression of potential, and which is differentiated to determine the stress components (the details of this method do not need to be repeated here; see Love (1927); or Timoshenko and Goodier (1951); for a lucid explanation). Kirsch (1898) derived the classic analytical solution for the case of an infinite plate with a central "hole", with modifications of this solution being developed by others, extending it to the case for an elliptical opening by Poulos and Davis (1974), Jaeger and Cook (1979) and Hoek and Bray (1977), and a 2D finite plate with rounded corners by Saleh (1985).

In 1898, Kirsch derived his so-called "linear elastic" stress solution for an infinite plate with a circular hole in the middle (that is his description; as shown later in this Chapter, the analytical solution does not match a real elastic solution), under two-dimensional far-field stresses. The solution calculates the full stress components (radial, tangential and shear stresses) at all locations within the infinite domain, as simple expressions involving space coordinates and far-field loads. Material properties are not involved in the solution, but they can be assigned and used in a different formulation that can calculate displacements and hence strains. Kirsch (and later derivative works) did not consider the direct effects of drilling or excavation, and implicitly assumed that these were addressed within the approach. The following images and expressions show the configuration of the Kirsch's infinite solution (see Figure 3.1 (A)) and the finite-domain modification presented by Saleh (Figure 3.1(B)). The Saleh model is used as a reference solution through the remainder of this Chapter.

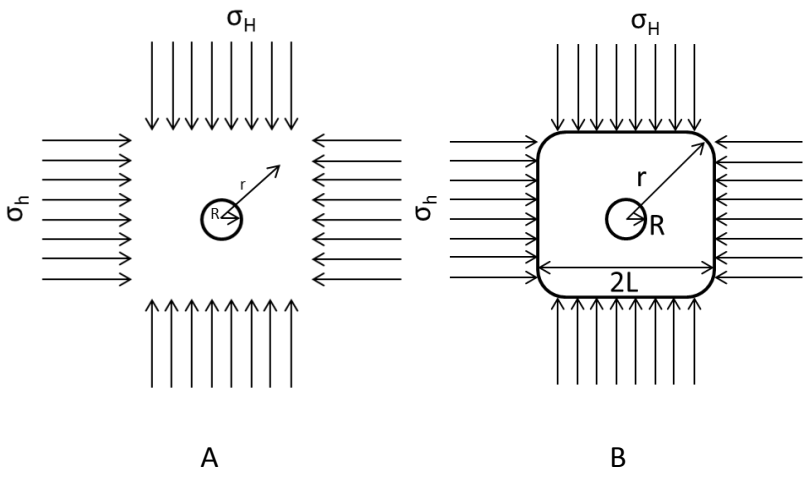

Figure 3.1: Infinite (A) and Finite (B) model domains for the linear elastic analytical solution

$$\sigma_{rr} = \frac{\sigma_H + \sigma_h}{2}\left(1 - \frac{R^2}{r^2}\right) + \frac{\sigma_H - \sigma_h}{2}\left(1 + \frac{3R^4}{r^4} - \frac{4R^2}{r^2}\right)\cos 2\theta \quad (3.1)$$

$$\sigma_{\theta\theta} = \frac{\sigma_H + \sigma_h}{2}\left(1 + \frac{R^2}{r^2}\right) - \frac{\sigma_H - \sigma_h}{2}\left(1 + \frac{3R^4}{r^4}\right)\cos 2\theta \quad (3.2)$$

$$\sigma_{r\theta} = \frac{\sigma_H - \sigma_h}{2}\left(1 + \frac{R^2}{r^2} - \frac{3R^4}{r^4}\right)\sin 2\theta \quad (3.3)$$

Where,

σ_h, minimum horizontal principal stress; here this is σ_x

σ_H, maximum horizontal principal stress; here this is σ_y

R, "wellbore" radius (i.e. radius of internal "boundary")

r, radial distance

θ, radial angle, measured anti-clockwise from the direction of σ_h; here this is σ_x

In 1985, Saleh derived a finite analytical solution based on Kirsch's solution as shown in Figure 3.1 (B). Saleh's solution is given below:

$$\sigma_{rr} = \frac{M^2(\sigma_h + \sigma_H)}{2(M^2 - R^2)}\left(1 - \frac{R^2}{r^2}\right) + \frac{M^2(\sigma_h + \sigma_H)}{2(M^2 - R^2)^3}\left[(M^4 + R^2.M^2 + 4R^2) + \frac{3M^2(M^2 - R^2)R^4}{r^4} - \frac{4(M^4 + R^2.M^2 + R^2)R^2}{r^2}\right]\cos 2\theta \quad (3.4)$$

$$\sigma_{\theta\theta} = \frac{M^2(\sigma_h + \sigma_H)}{2(M^2 - R^2)}\left(1 + \frac{R^2}{r^2}\right) - \frac{M^2(\sigma_h - \sigma_H)}{2(M^2 - R^2)^3}\left[(M^4 + R^2.M^2 + 4R^2) - 12.R^2.r^2 + \frac{3M^2(M^2 + R^2)R^4}{r^4}\right]\cos 2\theta \quad (3.5)$$

$$\sigma_{r\theta} = \frac{M^2(\sigma_h - \sigma_H)}{2(M^2 - R^2)}\left[-(M^4 + R^2.M^2 + 4R^2) - 6.R^2.r^2 + \frac{3M^2(M^2 + R^2)R^4}{r^4} - \frac{2(M^4 + R^2.M^2 + R^4)R^2}{r^2}\right]\sin 2\theta \quad (3.6)$$

Where,

$M = 0.577L\sqrt{3.08 - \cos 4\theta}$, distance from the centre to the model corners

L, the model edge length

Other terms are as defined above. Note that the terms, added by Saleh to create a finite domain, alter the calculated stresses at the r = R boundary of the "hole", but only by a small amount as demonstrates next.

The conceptual design for the underground engineering problem was traditionally considered with an infinite boundary, but Saleh (1985) provided a modification to identify finite boundaries. Thus, one could choose to use either approach if only the analytical reference case is desired, but that choice does not exist in the case of numerical models, which must be formulated on a finite domain regardless of the size of the engineering problem. Engineers and researchers have typically considered a relatively large model size as a method to mimic the state of stress of an infinite-domain problem. For our purposes, and due to the complexity of the numerical code we used for this research, a reasonable model size must be selected to overcome the issue of excessive simulation time. To assess the effect of model size, I calculated the stresses at critical points, using the finite-domain Saleh solution, and compared those with the

infinite solution of Kirsch. The stresses are calculated for various model lengths (L) as a function of angle (Θ). The stress differences tend to diminish between the two analytical solutions as the length of the model approaches the value of 1000 mm (Fig 3.2). When plotted over the model domain, the differences between the two analytical solutions are readily seen as being concentrated near the "hole" and along the boundaries (Fig. 3.3). At 1000 mm length (L), the stress differences between 0° and 90° are 0.2%, 2.4% and 1.3% in the radial, tangential and shear stresses, respectively (Fig. 3.4). Based on this comparison, I claim that the use of the Saleh solution is justified for the model domain (L = 2000, r = 100) that I am considering.

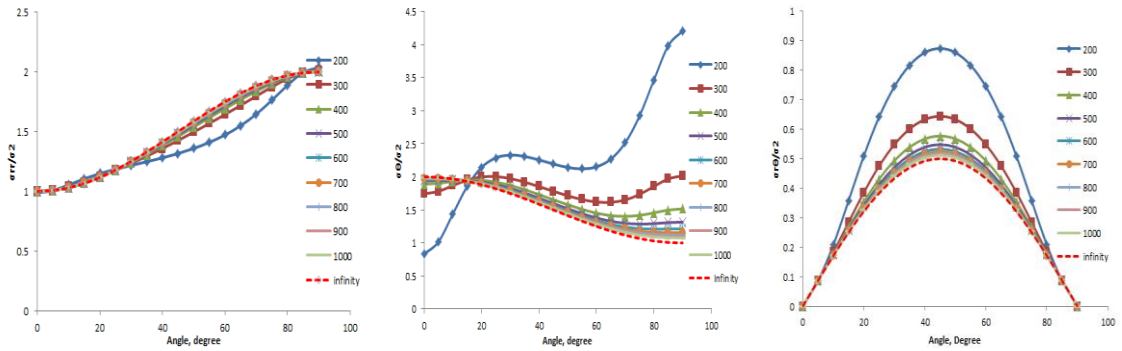

Figure 3.2: Comparison of the finite (Saleh) and infinite (Kirsch) solutions as a function of model size (L). These results all have R = 100mm.

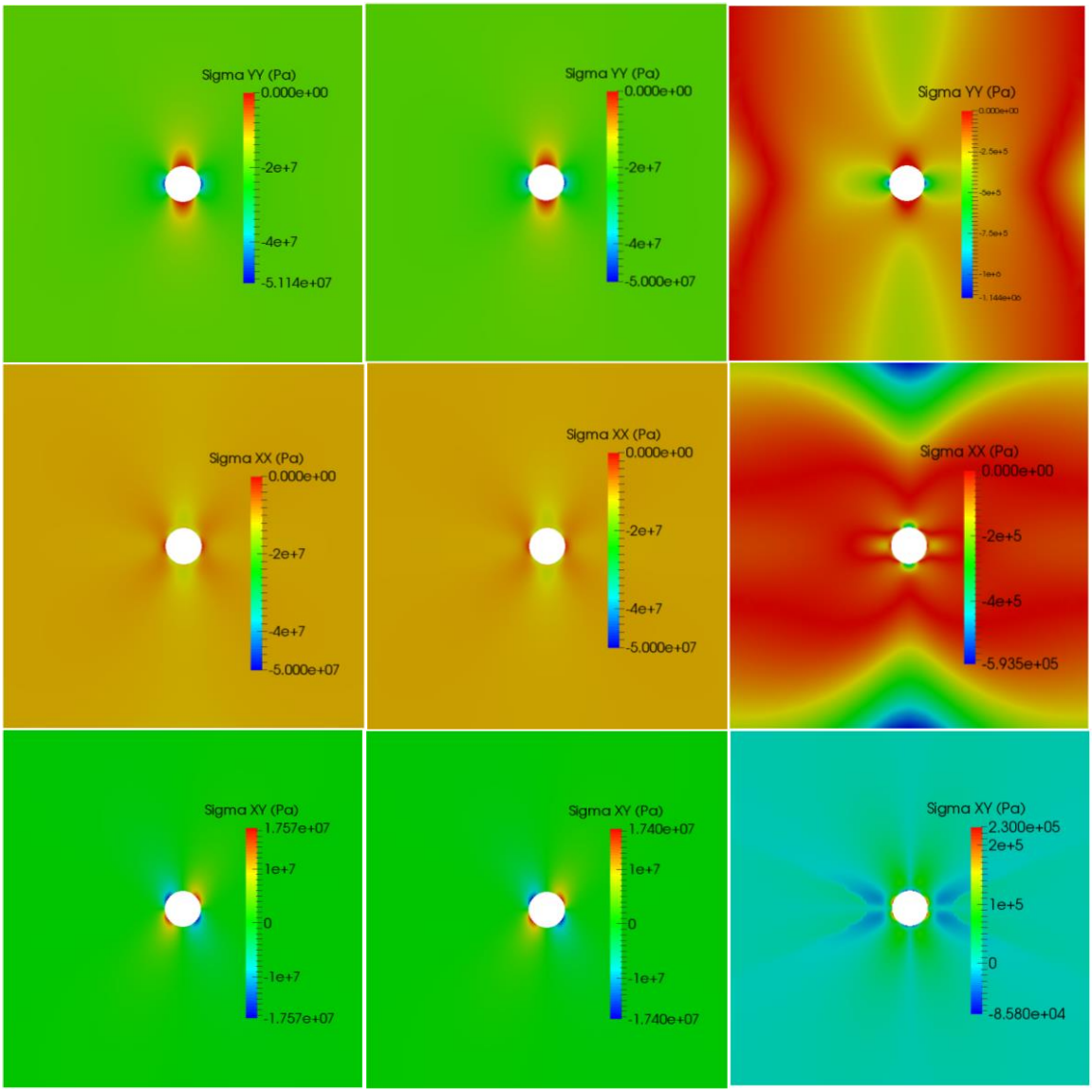

Figure 3.3: 2D Saleh's finite (left), Kirsch's infinite (right) and the stress difference between Saleh and Kirsch's infinite solution for (σ_H= -20MPa, σ_h= -10 MPa)

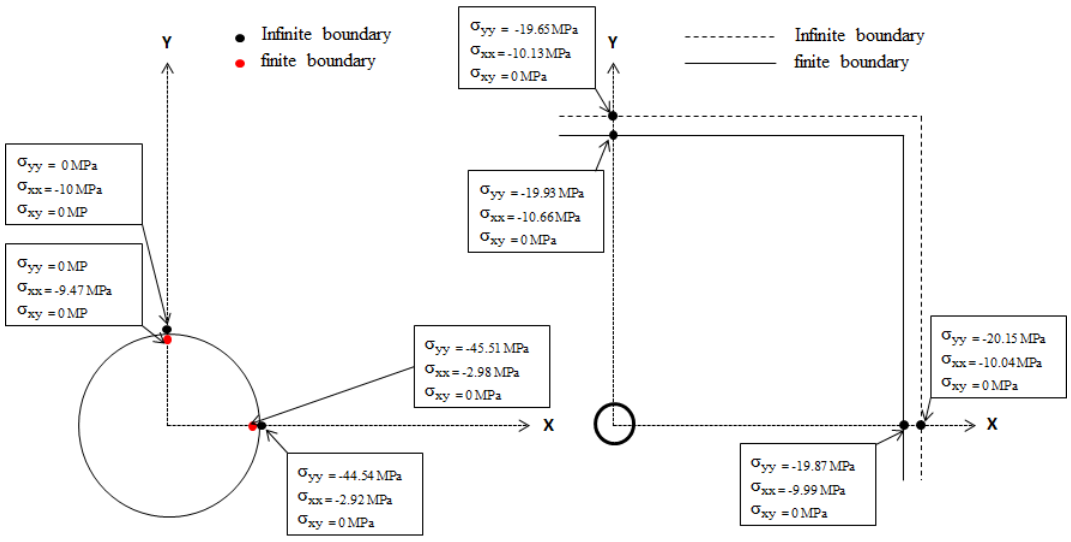

Figure 3.4: Stress values at wellbore and far-field boundaries for σ_H = -20MPa and σ_h = -10MPa.

Although, the Kirsch analytical solution is usually state as defining the stress state in a model with a hole in its centre, this is not quite true. The Kirsch solution (and others derived from it afterwards) is based on a stress function that exists across the entire 2D space. The stress function is defined in such a way that the stress components (i.e. σ_r – the radial, and σ_t the tangential, principal stresses – or their Cartesian equivalents expressed as σ_x and σ_y) have assigned values along a circular line (an internal "boundary" condition) at a fixed radius (for σ_r), and along the relevant edges (classical boundary conditions) of the square model region. The solution of the stress function still exists inside the "wellbore", and also in the far region beyond the square edges – so none of these constraints are actually at a boundary, since no boundaries actually exist. Inside the "wellbore" region of the domain, the radial stresses are tensile (even when the far-field stresses are compressional), because that is the characteristic of the Kirsch solution. The existence of these tensile stresses is irrelevant if one takes the point of view that they are "not there", because they apply to spatial locations within the void space of the wellbore opening. However, that simple dismissal may be the reason that no one seems to have appreciated there are differences between the Kirsch (or here, Saleh) solutions of the inferences that can be made if are considers the mechanical problem a fresh. Their differences relate to the fact that real wellbore boundary is not at a constant radius, due to motions that occur after removal of the rock by drilling. The un-considered discrepancy between approximate reality and the situation of the analytical solution is not insignificant (as shown below), so there is a good reason to examine the issue carefully.

At the origin of the model domain (in the centre, where r = 0), the analytical solution is undefined, since the expression for radial stress has the term "r" in the denominator, and this is of course zero in value at this location. As will be demonstrated shortly, the analytical expressions maintain the zero value of the radial stress along the line of constant radius, r = R (the nominal wellbore radius), regardless of any value of σ_x and σ_y. This is an important point, because the analytical solution is usually stated to be applicable for a 2D region with a contained hole, and that is not quite correct. If a circular hole exists in a plate, and the plate is loaded by σ_x and σ_y, the hole changes shape to an ellipse. The Kirsch/Saleh analytical solution does not alter the position in space where the radial stress is assigned to be zero. When points move across that line, as they must do in reality, these real motions alter the positions where the condition σ_r = 0 would be appropriate. Thus, the adoption of the analytical solution introduces a non-physical characteristic (i.e. the lack of material motion) whose impact needs to be

ascertained, relative to judging the value of the analytical solution for use in calculating near-wellbore mechanical states.

In the approach based on the use of the analytical expression, the effect of the (non-existent) hole is implied to be the difference between a reference state that has the far-field stress (σ_y and σ_x) everywhere, and the stress state calculated by the expressions. These "changes" are largest in the region just beyond the distance "r = R", so just within the wall rock region. As will be demonstrated within this Chapter, these locations are where there are the largest discrepancies between the analytical calculations and those which are more realistic. Of course, these near-wellbore locations are where we have most interest relative to wellbore stability or to how a stimulation will operate, hence there is a compelling need to understand how any model drives its answers at these problems. I will emphasise these differences between analytical and numerical solutions in the comparisons that follow.

3.4 Numerical Methods Using FEMDEM Application

The finite element method (FEM) is a numerical simulation process through which the deformation of a continuum, with a large number of degrees of freedom, can be approximated by solving the equations (such as those which describe the elastic material response) by dividing the continuum into local elements, each with a specified but finite number of unknowns, or degrees of freedom, which normally are the displacements and forces at specified points in each of the elements (Zinckiewicz, 1971). The calculation method is one in which the local expressions of force/displacement equilibrium are assembled into a global set of equations that is solved by minimising the total system energy.

3.4.1 Non-drilling elastic model (FEM pre-hole Model)

The FEM pre-hole model analysis described here is based on a 2D finite, square region that contains a pre-existing, perfectly-circular opening. A symmetrical mesh composed of triangular elements is created, with small elements around the opening to enable fine resolution of the stress state, and to obtain more accurate results with fewer numerical errors. The edges of the triangles around the opening are, of course, straight lines (chords), but the nodes that defines the triangles have coordinates that lie on the circle. A relatively coarse symmetrical mesh is used away from the opening so as to limit the simulation time and manage the memory cost.

The model consists of 11807 triangular elements that are defined by 5969 vertex nodes; the radius of the pre-existing opening is 100mm and the model dimensions are 2000mm

high by 2000mm wide (see Figure 3.4). The average element length along the circumference of the opening is approximately 0.125mm. The mechanical properties used are shown in Table 3.1. These parameters are the ones used in Y-Geo, which is a code based on the FDEM simulation system developed by Munjiza (1992), and later modified by Mahabadi, Lisjak, Munjiza and Grasselli (2012). Y-Geo is an open-source software system that has become a recognised simulation tool to solve complex engineering problems that involve the creation of discontinuities (fractures). The key element to this tool is the solution that combines the calculations of finite displacement, finite rotation and finite strain deformation with the discrete element calculation. Being an explicit formulation, Y-Geo solves Newtonian equations of motions via iterations that allow loads to be equilibrates. In this Chapter, the FDEM approach was used to specifically analyse the mechanical behaviour of an opening, and the material around it, during and after "drilling" (by which I mean the creation of the opening). More details on the methodology of FDEM can be found in The Combined Finite-Discrete Element Method authored by Munjiza (2004). The model input parameters are shown in Table 3-1.

Here, the FEM pre-hole model is created by using FDEM in a mode where there is no opportunity for failure (or inelastic behaviour). The use of FDEM for the FEM calculation facilitates a subsequent comparison between elastic-only cases and those where failure is allowed (demonstrated later in this Chapter).

Table 3-1: Model input parameters

Parameter	**Value**
Young's Modulus (GPa)	53
Poisson's Ratio	0.23
Friction Coefficient	1.27
Density (kg/mm^3)	2650
Viscous Damping (kg/mm.s)	5.9E+6
Cohesion (kg/mm.s^2)	2.6E6
Tensile Strength (kg/mm.s^2)	5E+6
Mode I Frac. Energy (kg/s^2)	394000
Mode I Frac. Energy (kg/s^2)	478000
Contact penalty (kg/s^2)	5.3E+10
Tangential and Frac. penalty (kg/mm.s^2)	5.3E+10

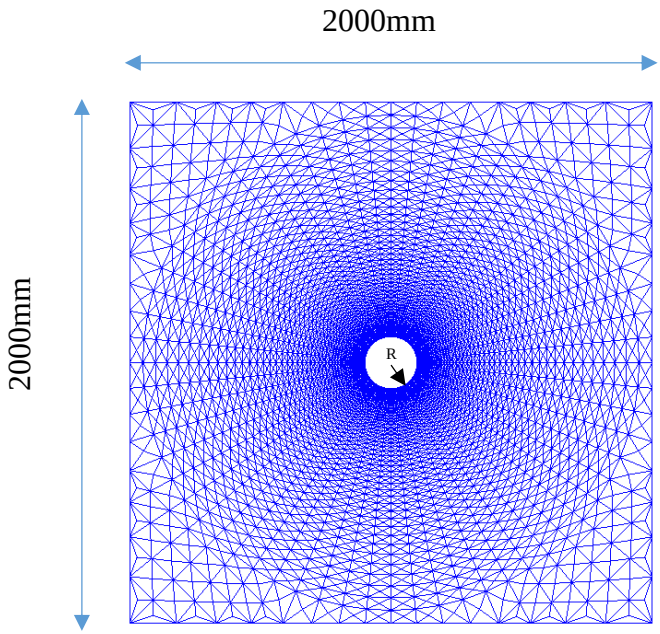

Figure 3.5: FEM pre-hole Model

3.4.2 Drilling elastic model (FEM drilling Model)

In this approach, the model mesh is the same as for the case with a pre-existing hole, except that the to-be-excavated hole region is also meshed. That "inside-the-opening" region of the model is then progressively "removed" from the simulation, the excavation is accomplished in the simulation through the reduction of Young's modulus for the elements inside the hole. The element stiffness is reduced gradually from 5.3e10Pa to 5.3E9Pa and then to 5.3E8Pa (so, a reduction of 100x in stiffness). The elements are then removed completely from the centre of the model. The model runs until an equilibrium of stress state is reached after each reduction removal step.

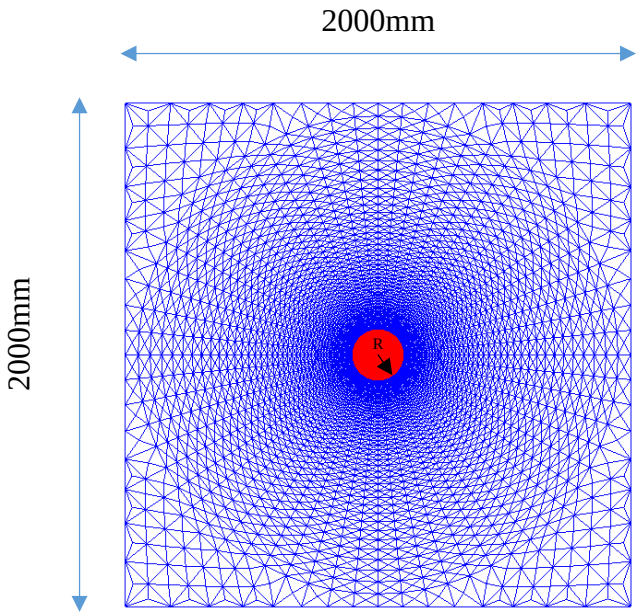

Figure 3.6: FEM Drilling Model

3.5 Mechanical State Comparisons of the Analytical and Numerical Models

The three models introduced above (Saleh analytical solution, FEM pre-hole model and FEM drilling model) could all be claimed as a suitable method for deriving the state of stress around a borehole. However, although the three approaches calculate similar distributions of stress state, there nevertheless are differences that are not trivial. Here, I compare the three methods via three far-field loading cases, with the intention of identifying how the differences in calculated numbers are dependent on the case situation. I then use those comparisons and my analysis of them to identify the method that is preferred. Three loading cases (Table 3-2) are used to explore whether different loading conditions lead to larger or smaller differences between the analysis methods. In these cases, I keep the minor principal stress (σ_h) constant at -10MPa and increase the major principal stress (σ_H) from -20MPa to -70MPa to -200MPa.

Table 3-2: cases for wellbore mechanical analysis

	Case One (Low)	**Case Two (Medium)**	**Case Three (High)**
$\sigma_H = \sigma_y$ (MPa)	-20	-70	-200
$\sigma_h = \sigma_x$ (MPa)	-10	-10	-10

3.5.1 Case One ("Low stress": σ_H = -20MPa, σ_h = -10MPa)

Recall that the simulation/calculation methods used here are "dry". Assuming that classic effective stress is valid, the analysis presented here is applicable to cases where the pore pressure P_{pore} equals the borehole pressure P_{well}, with the σ_y and σ_x component magnitudes being the same as effective stresses, σ_y' and σ_x'.

This "Low" case has the smallest far-field stress difference, which translates (with the dependencies associated with the linear elastic model) into smaller stress differences in the perturbed areas around the wellbore. All else being equal, smaller stress differences would tend to allow many rocks to remain mostly within elastic strain conditions, and so this loading case might be argued as the one most appropriately represented by the purely-elastic restriction adopted in this Chapter. The combination of this set of boundary conditions, and the mechanical properties (see Table 3-1), provide the closest comparison with Saleh's finite-domain stress solution (which does not depend on material properties such as stiffness). The fact that an elastic numerical solution needs to be "tuned" in order to approximate the analytical solution will be examined later in this Chapter.

3.5.1.1 An investigation of the differences between all methods (Case One)

The circular opening that defines the pre-hole model configuration does not remain circular. Displacement of the edges of that opening occurs in the FEM pre-hole model. Along the two coordinate directions, the radius of the hole is reduced to 99.9079mm and 99.9804mm, in the y-direction and x-direction, respectively. The previously perfectly-circular opening has been changed into an ellipse. This change into an elliptical shape is not a major surprise, but it has often been expressed perhaps without adequate analysis (Hudson and Harrison, 1997) that a pre-existing hole would change into an ellipse that has its minor axis (which is parallel to the most-compressive far-field stress component) shorter than the original radius, while the major axis becomes longer than that initial radius. That is not what is observed in the FEM pre-hole model result: both axes are shorter than the original borehole radius. There is, therefore, an issue in making comparisons between the analytical solution, and the one obtained by the FEM pre-hole elastic solution. The same displacement observation is found in FEM drilling model but the magnitude of in motion y and x directions are smaller than the one obtained from FEM pre-hole model. From the stress state point of view (Figure 3.7 and 3.8), the values of stress components at the "wellbore wall" obtained, from FEM drilling model, differ by approximately a factor of two in comparison with the values calculated by Saleh's model and by a lesser factor in comparison with the values

obtained from FEM pre-hole model on both axes. The stress state obtained from the FEM drilling model is significantly smaller.

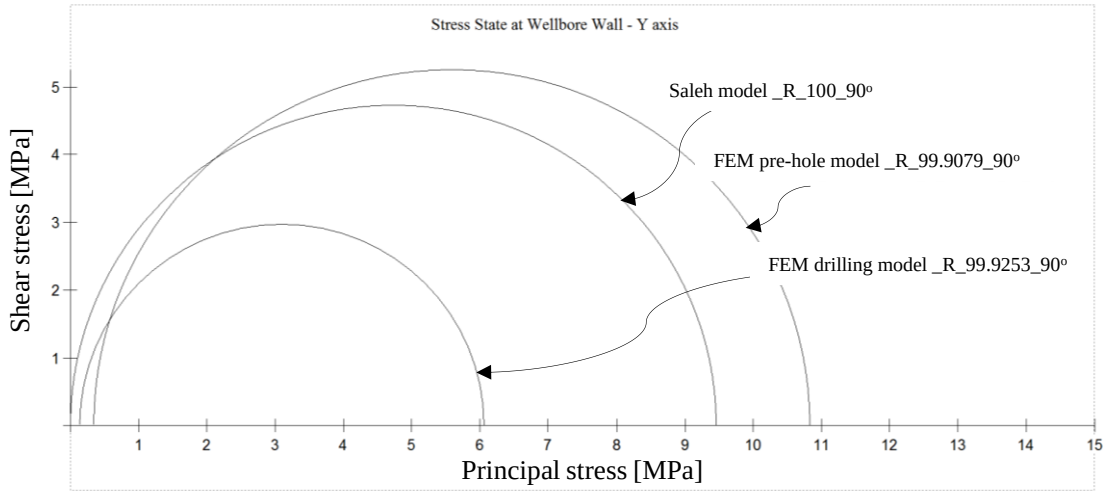

Figure 3.7: Stress state at wellbore wall – Y axis for (σ_1 = -20 MPa and σ_2 = -10 MPa)

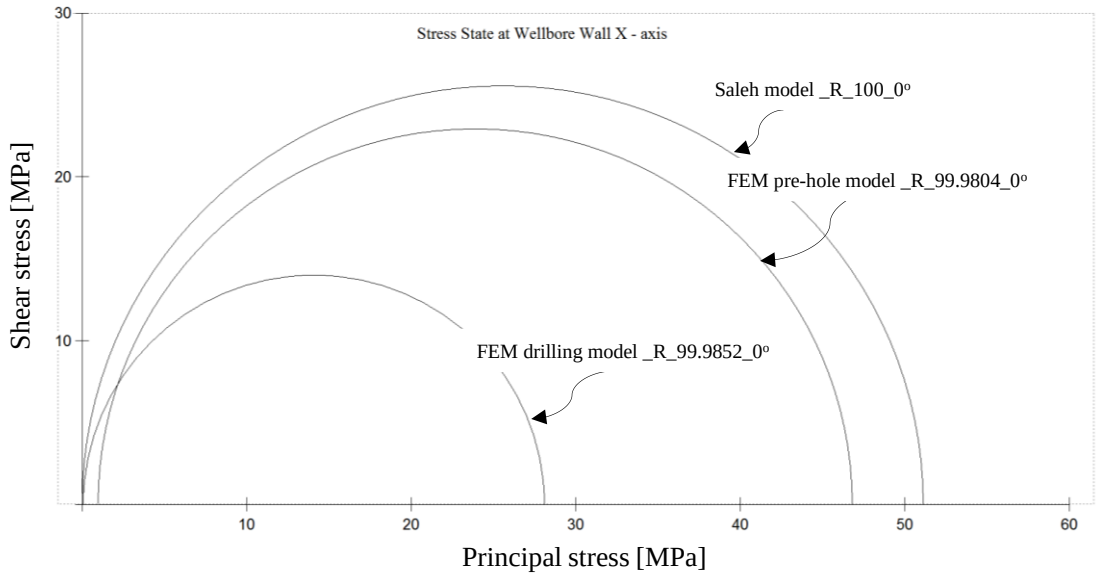

Figure 3.8: Stress state at wellbore wall – X axis for (σ_1 = -20MPa and σ_2 = -10MPa)

Figure 3.9 shows the calculated major and minor stress values for Saleh's solution, the FEM pre-hole model and the FEM drilling model at 99.9079mm (FEM pre-hole final radius) of the opening at the intersection y-axis. FEM drilling model has no stress value at this point because the opening radius did not move this far after drilling (see the next paragraph for a comparsion at a radius 102 to all model). The major stresses are -10.84MPa and -9.47MPa in the FEM pre-hole and Saleh's models, respectively. The minor stresses are -0.351MPa and +0.008MPa in the FEM pre-hole and Saleh's models, respectively. In terms of comaprision, the calculated stress value drived from Saleh's model might be expected to match, with may be small diffrences, FEM pre-hole model

for this ideal case. Saleh is calculating a positive (tensile) minor stress, while FEM pre-hole model is calculating a negative (compersion) stress. With Saleh's solution, at points "inside" the nominal hole, the radial stress would be tensile indicating "pulling" towards the opeining. That is not the case for FEM pre-hole model. The preception behind Saleh's solution being a universal elastic solution is fundmentally inaccurate. I will investigate the dependancy of the FEM solutions in term of material properties, later in this chapter, and these outcomes further reinforce the conclution that the analytical experssion is not a universal solution to elastic problems.

At x-axis (r = 102mm), Saleh's solution is calculating a σ_1 of -49.36MP while the FEM pre-hole and FEM drilling models are calculating -46MPa and -12MPa respectively. At y-axis (r = 102mm), Saleh's σ_1 is -10.07MPa while FEM pre-hole and FEM drilling are -11.34MPa and -5.54MPa resepectivly.

In Figure 3.10, the same comparsion is made at 99.9253mm radius (FEM drilling model radius after equilbration) at 90 degrees on the y-axis. The major stresses are -10.99MPa, -9.47MPa and -6.07MPa in the FEM pre-hole, Saleh and the FEM drilling models, respectively. The minor stress is -11.08MPa, +0.007MPa, and -0.137 MPa in the same model location, respectively. Saleh's model again calculate a tensile stress at this raduis as expected, while the FEM pre-hole and FEM drilling models indicate a compressional stress at this raduis.

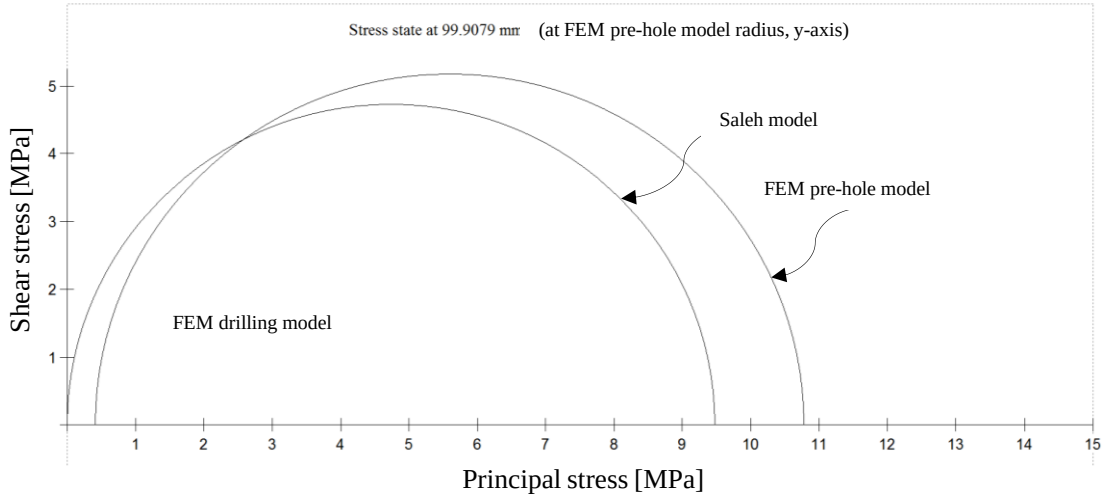

Figure 3.9: Stress state at 99.9079 mm (FEM pre-hole model radius) - Y axis for (σ_1 = -20 MPa and σ_2 = -10 MPa)

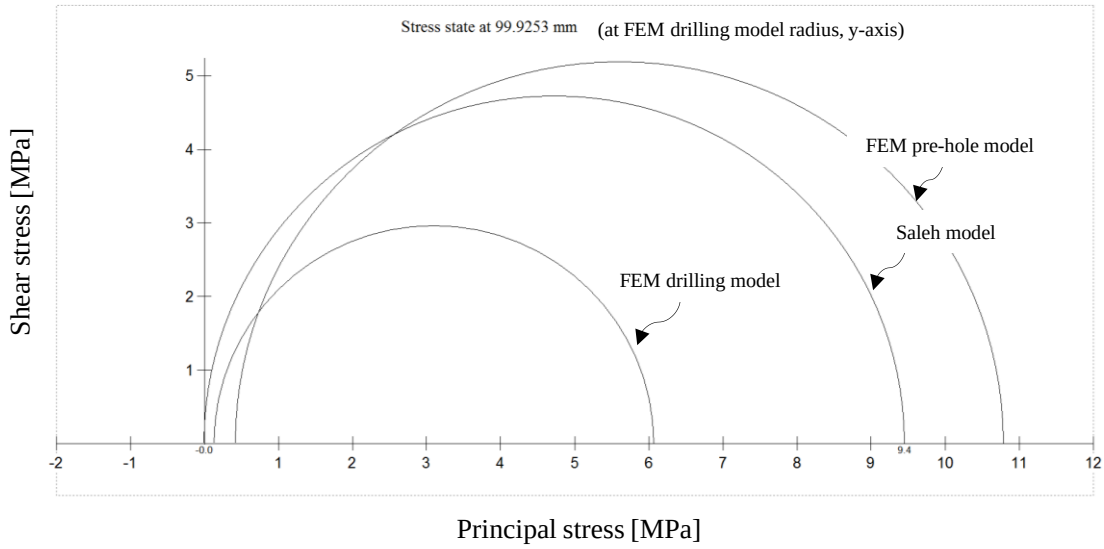

Figure 3.10: Stress state at 99.9253mm (FEM drilling model radius) - Y axis for (σ_1 = -20 MPa and σ_2 = -10 MPa)

Figure 3.11 illustrates the calculated major and minor principal stresses at the x-axis position of the "hole", calculated by Saleh's model, FEM pre-hole model and FEM drilling model, at 99.9804mm (FEM pre-hole model final radius). The major stresses are -47.8MPa and -51.51MPa in FEM pre-hole model and Saleh's model, respectively. The minor stress are -0.668MPa and +0.01MPa in FEM pre-hole and Saleh's models, respectively. In the FEM drilling model, these locations are inside the hole. As usual, Saleh is calculating tensile radial stress because this radius is inside the hole. The FEM pre-hole model, which might be expected to be in close agreement with Saleh's model, is calculating a compressional radial stress at this radius, and so the results do not agree.

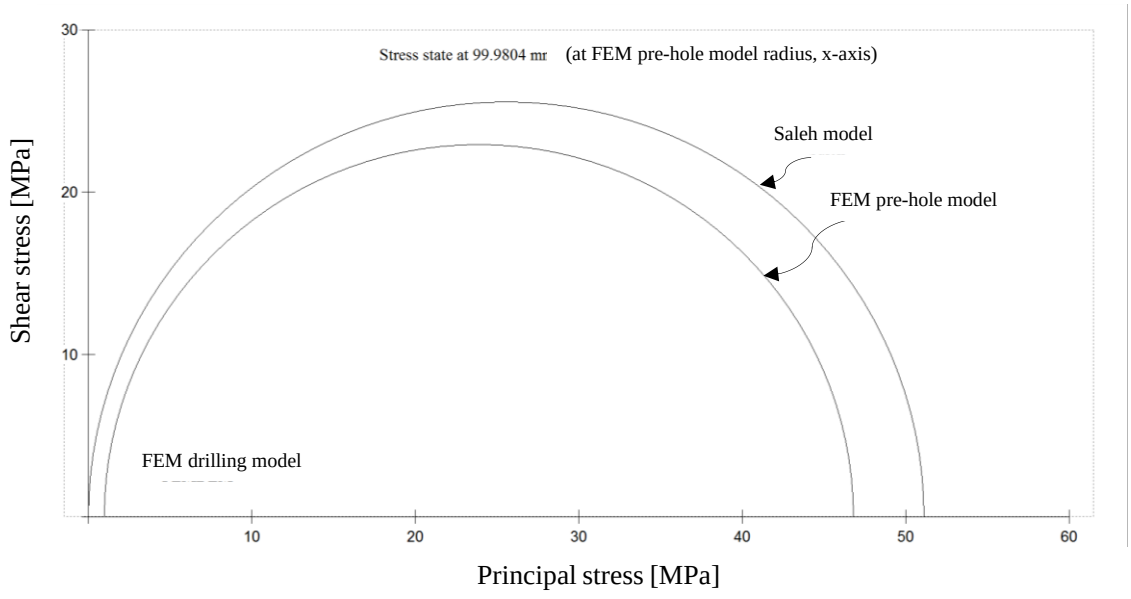

Figure 3.11: Stress state at 99.9804mm (FEM linear elastic model radius) - X axis for (σ_1 = -20 MPa and σ_2 = -10 MPa)

The comparison is also made at 99.9852mm radius (FEM drilling model final radius). The major stresses are -47.8MPa, -51.16MPa and -28.175MPa in the FEM pre-hole model, Saleh's model and FEM drilling model, respectively. The minor stress are -0.668MPa, +0.0075MPa, and -0.07MPa in the respective location. At this radius, the FEM drilling model shows a significant smaller value, by a factor of two, than the one derived from FEM pre-hole model (Fig. 3.12).

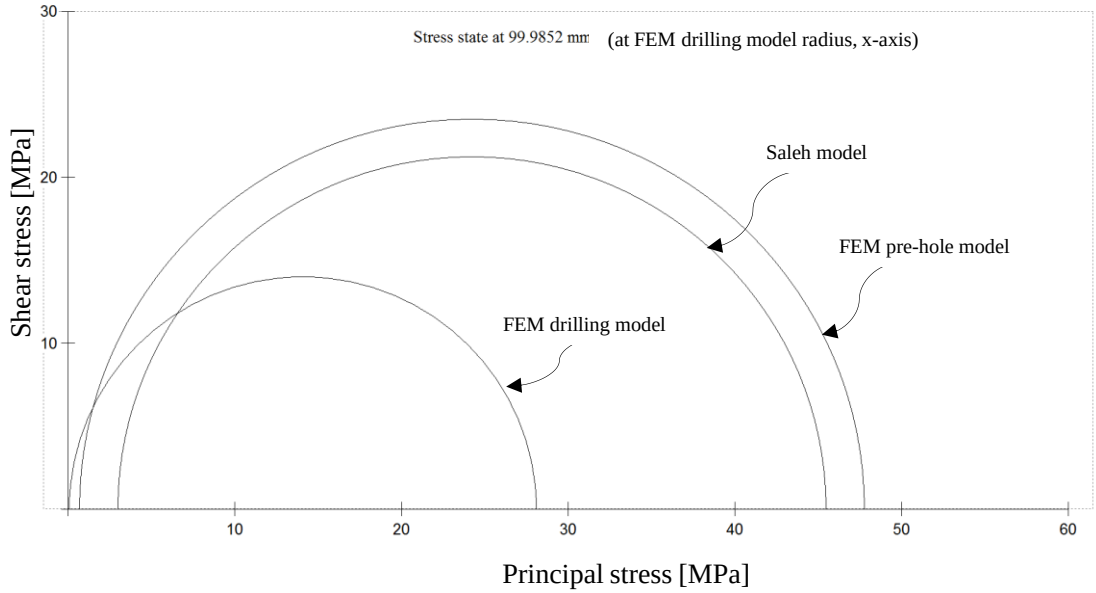

Figure 3.12: Stress state at 99.9852mm (FEM drilling model radius) - X axis for (σ_1 = -20 MPa and σ_2 = -10 MPa)

3.5.1.2 Saleh's solution versus FEM pre-hole model (Case One)

I first compare the Saleh's solution with the FEMDEM (but fully-elastic) model with the pre-existing hole (for simplicity, here I call this the FEM pre-hole model) (Figure 3.13). The stress components calculated by this FEM pre-hole model vary, as a function of distance from the wellbore, in approximately the same way as those calculated with Saleh's solution. I quantify the differences by calculating a percentage difference: this is derived by subtracting the relevant stress value of Saleh from the related value calculated by the FEM pre-hole model, and then dividing by the stress value of Saleh's solution. This, negative differences indicate that the FEM pre-hole model calculates a smaller value of stress at that location. The calculated differences are then plotted along the dimensionless distance from the wellbore (see Figure 3.13). The numerical values for the stress components (σ_{yy}, σ_{xx} and σ_{xy}, at 100mm radius, that is, on the wellbore

wall, on the 90°, 0° and 45° radial lines) are shown in Figure 3.14. It is clear that the two methods give similar results, but they do not agree exactly.

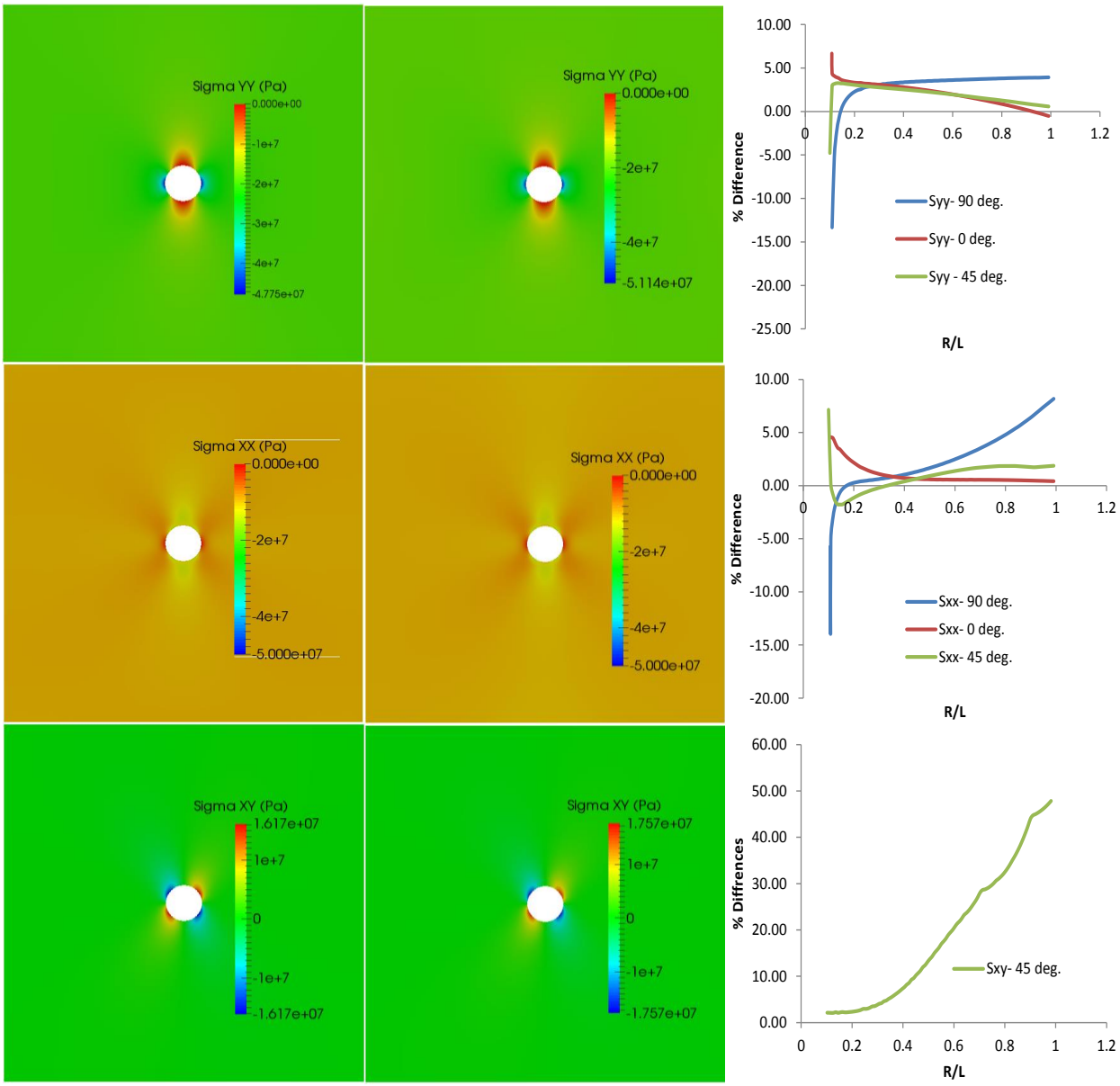

Figure 3.13: FEM pre-hole model (Left), Saleh (Middle) % difference (Right) – Case One. Note: the values of shear stress (σ_{xy}) along y-axis (90°) and x-axis (0°) (line of symmetry) are zero in both methods. Therefore, they are not shown here

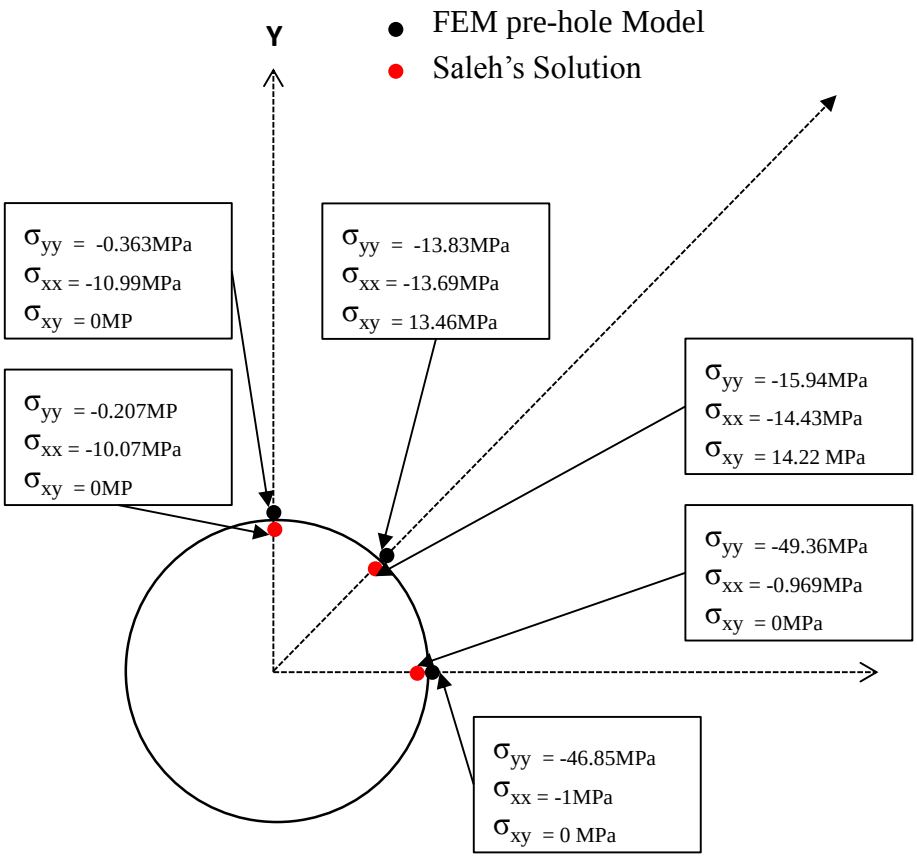

Figure 3.14: Stress values obtained at 102mm radius of the wellbore (refer to the infinite solution in Figure 3.4 for comparison)

The differences between these two models need to be explained. The answer reveals a little-recognised aspect of the analytical solution, and has significant implications for the use of that solution to estimate stress states around a borehole.

In the FEM pre-hole model (and in the other numerical simulations that are introduced elsewhere in this thesis), displacements occur on all of the model boundaries. These boundaries, both those at the domain edges, and the boundary that defines the pre-existing hole, have assigned boundary conditions expressed as stress components (tractions). The nodes (vertices), which define the model mesh along these boundaries, all experience displacements during the calculation. Those displacements are not known in advance (that would be a different type of boundary condition), and are simply consequences of calculating a solution to the problem posed: namely, what deformation distribution is the result of that loading, given the starting configuration and material properties?

In the FEM pre-hole model, the originally-circular central boundary becomes altered to an approximate elliptical shape, and the external boundaries also move. On the face of

the internal boundary, the condition $\sigma_r = 0$ "follows" the movement that is calculated for the nodes located there. In contrast, for the analytical solution, the state $\sigma_r = 0$ is specified to occur at a constant radial distance r = R. That specification is often called a boundary condition in the analytical solution, but there is no boundary, only a line along which a specific state is defined (which is also true of the external "boundaries" in the Saleh solution). Such analytical expressions can be manipulated (not shown here) to allow the calculation of displacements (this requires the addition of material properties; see Sanford (1959)), but this consideration seems to be rarely investigated for the Kirsch/Saleh solutions.

Because of the displacements in the FEM pre-hole model, there are no locations that are truly consistent between the two methods, and at which the stress states could be definitively compared. Here, I illustrate the characteristics of the differences at two radial distances that are large enough to be within the solid part of the FEM pre-hole model in each of three radial directions. At 107mm radius, Saleh's solution is under estimating σ_{yy} in the pre-hole elastic solution at 90^o (y-axis) by almost 18%, while at 0^o and 45^o, Saleh's equations over and under estimate σ_{yy} by 5%, respectively. At the slightly greater radial distance of 108mm, Saleh is under estimating σ_{xx} by almost 6% at 90^o, while at 0^o and 45^o, Saleh is over estimating σ_{xx} by almost 4% and 6½%, respectively.

Figure 3.15 and Figure 3.16 show the major and minor principal stress values for Saleh's solution and the FEM pre-hole model. Three different points were selected at radii of 100mm, 250mm and 500mm for comparing the principal stress values along the Y and X axes. The magnitudes of the principal stresses in the FEM pre-hole model are slightly larger, by 15% compared to the corresponding values of Saleh's model, for r = 100mm along the Y axis. The magnitudes of the principal stresses at r = 250mm and r = 500mm are similar in both models, reinforcing the observation that the differences are mainly in the near-wellbore parts of the models. Along the X axis, the FEM pre-hole model has slightly smaller principal stress magnitudes compared to the corresponding values in Saleh's solution at r = 100, 250 and 500mm (Figure 3.16). The stress difference is larger at r = 100mm and smaller away from the opening at r = 250 mm and 500 mm along both axes, as is the case with along the Y axis.

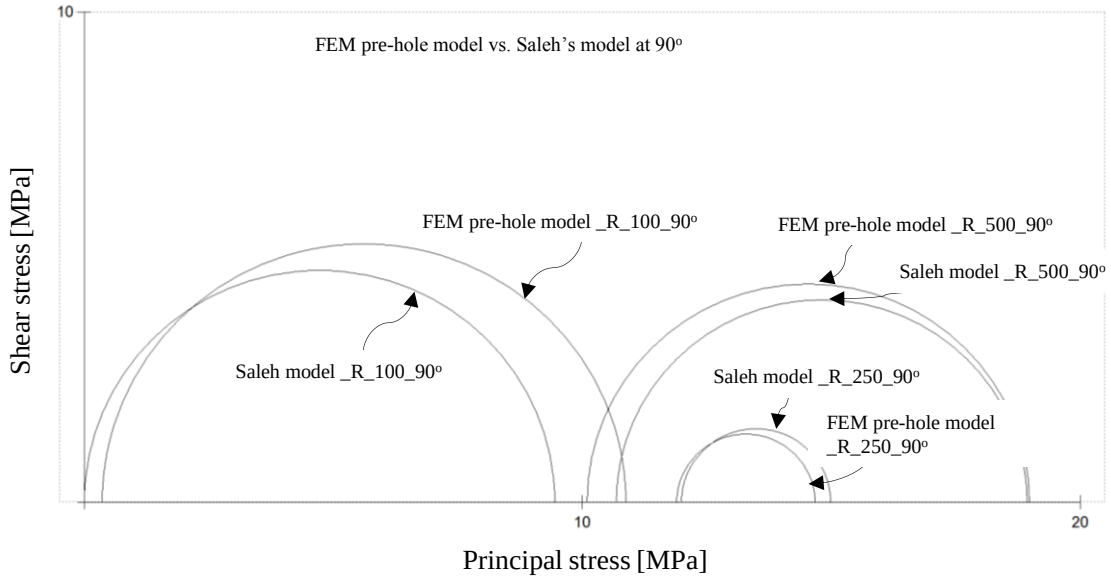

Figure 3.15: Stress state at r = 100, 250 and 500 mm (Y – axis) for σ_H = -20MPa and σ_h = -10MPa

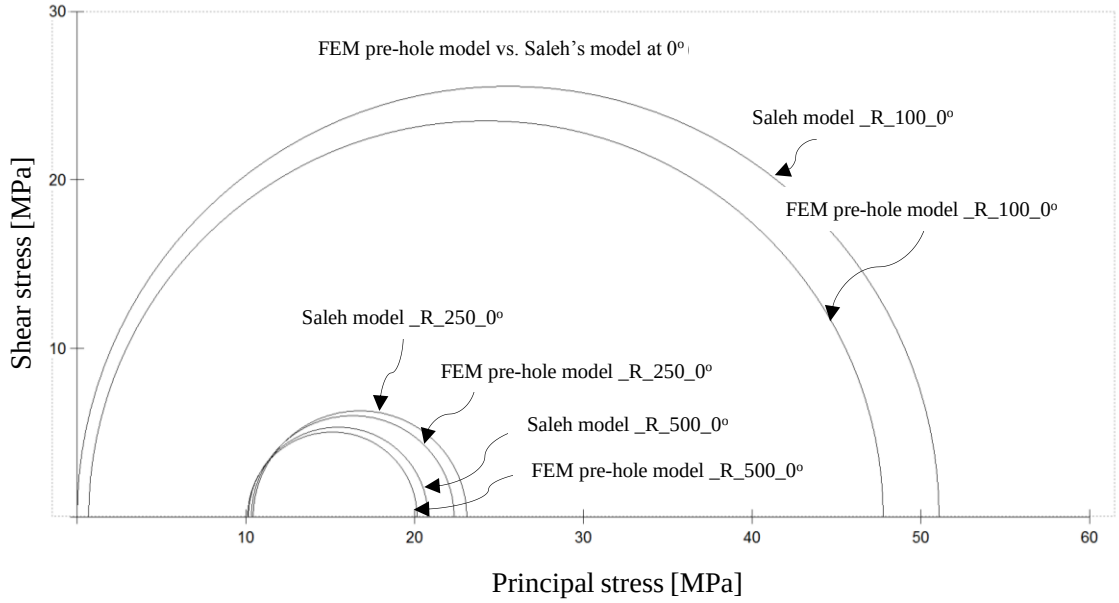

Figure 3.16: Stress state at r = 100, 250 and 500mm (X – axis) for σ_H = -20MPa and σ_h = -10MPa

3.5.1.3 Saleh's solution versus FEM drilling model (Case One)

The FEM drilling model has a pre-existing uniform "far field" stress state that is perturbed by excavating the material inside a circular boundary, to approximate the drilling process. I use the FEMDEM code again, restricting it to an elastic-only response, hence I call this model the FEM drilling model. This simulation provides another comparison with Saleh's solution. As noted above, the drilling process is implemented by reducing the stiffness of the elements within the borehole outline, by a

factor of 10x, then 100x, before assigning a zero stiffness. The progressive reduction of stiffness causes the remainder of the model domain to respond, causing a stress state (Figure 3.17) that has a usual appearance similar to those of the Saleh and FEM pre-hole models, but the stress magnitudes are very different. It is the end stage after excavation is completed which is used in the comparisons that follow.

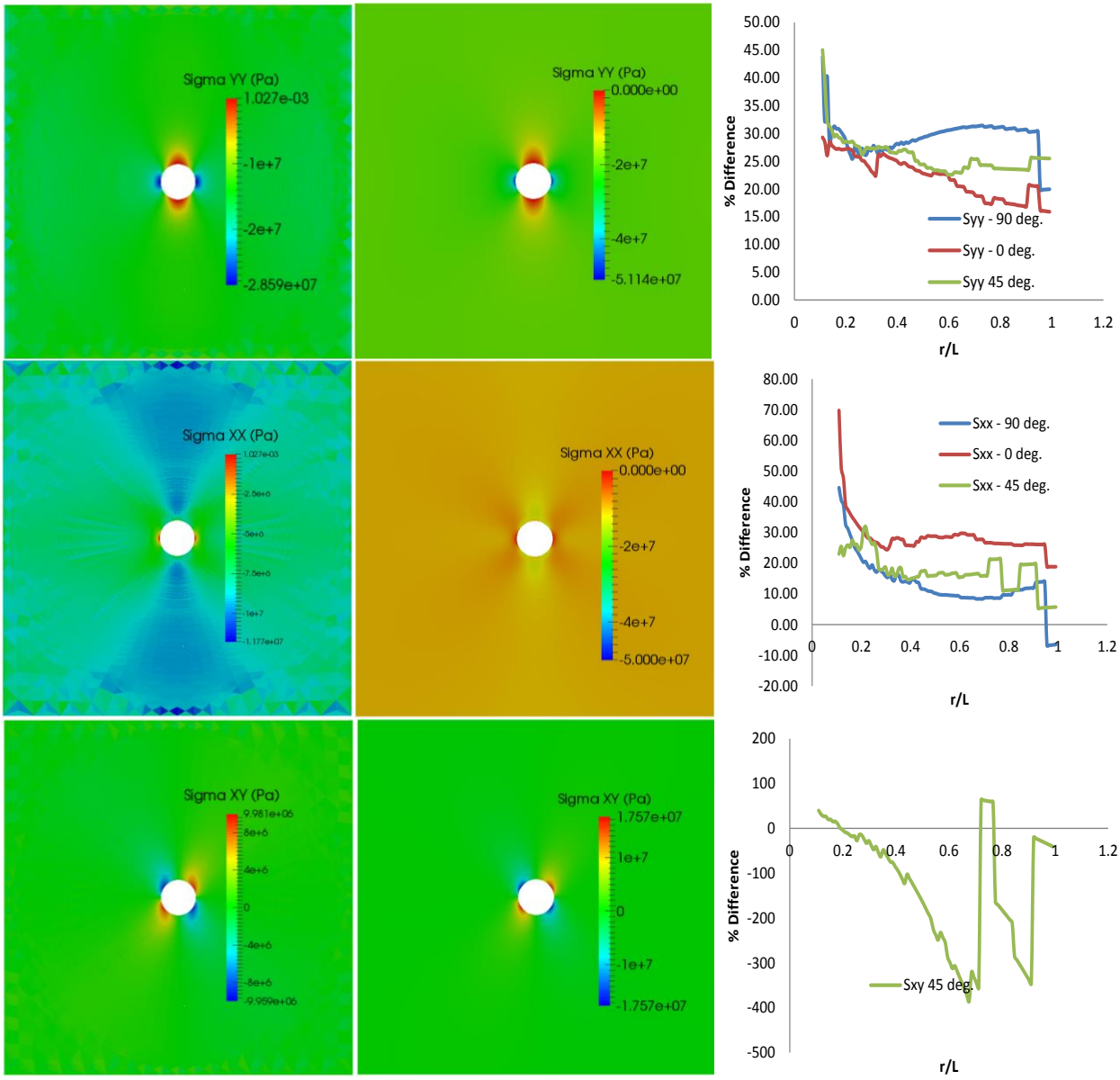

Figure 3.17: FEM drilling model (Left), Saleh (Middle) % difference (Right) – Case One. Note: the % difference plot looks choppy because each element in the FEM drilling model is moving during equilibrium and at every stiffness reduction of the elements in the region to-be-created hole (wellbore's elements)

The changes in stress state, caused by the drilling – which is here represented by the excavation of the region inside of an initially-perfectly-circular opening – are compared with the Saleh's solution. A quantitative stress difference is calculated between the two

models. The stress difference between FEM drilling model and Saleh's model is approximately -50% in σ_{yy} and σ_{xx} between hole and model's edges (Fig. 3.17).

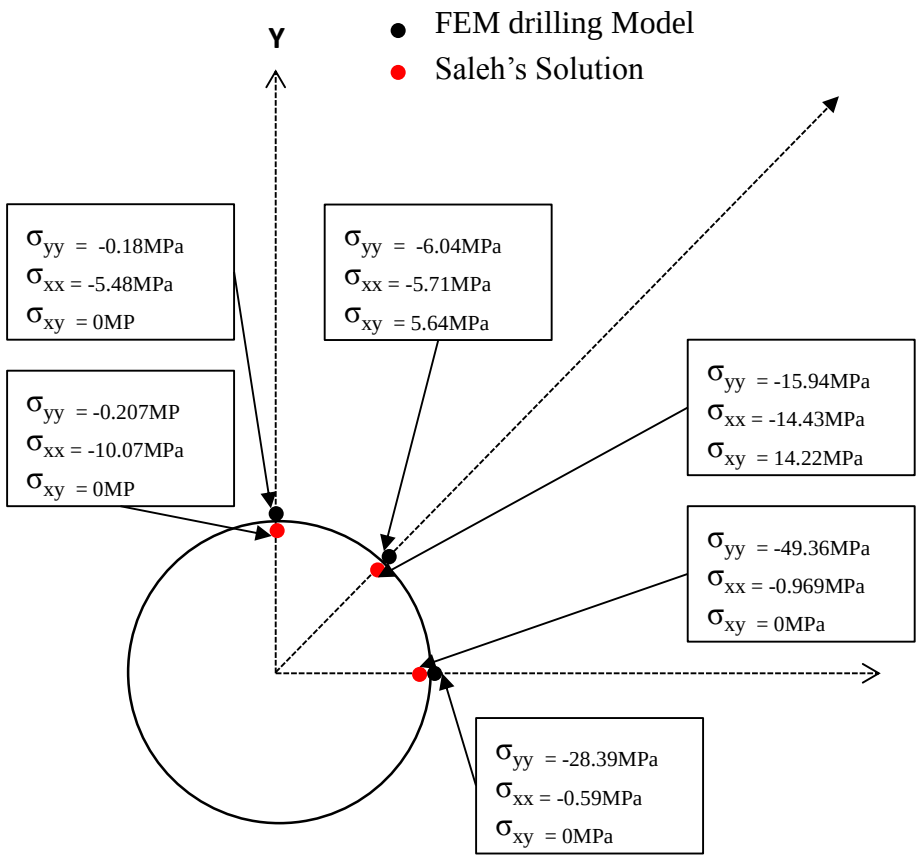

Figure 3.18: Stress values obtained at 102mm radius of the wellbore

It is perhaps easiest to understand the differences between these models if the stress states are depicted graphically, using Mohr-Coulomb plots at several locations.

Figures 3.19 and Figure 3.20 illustrate the differences in the major and minor principal stresses between pairs of the three models. Considerable differences are observed at R = 100mm, 250mm and 500mm along both Y and X axes. At the wellbore radius, the major principal stress in the FEM drilling model differs by approximately a factor of two, in comparison with Saleh's solution. This difference is so large that it cannot be simply ignored as being a minor effect from different methods. When comparing Saleh's solution and FEM drilling model, the stress states are radically different along the y-axis, between the hole and the model edge. The differences are less along x-axis at large distances. The differences between the models are large enough to raise a concern over using the typical elastic-until-failure approaches to assess wellbore stability, since the contrasts in near-hole conditions revealed by the set of methods could lead to an incorrect assessment if the inappropriate model is chosen for that purpose.

FEM drilling model which arguably is a better model because it captures the essence of the well construction process, results in near-wellbore stress states that are significantly different compared to those normally used in wellbore geomechanical problems. If it accepted that the drilling model is better reference framework, the results summarised here indicate that the usual "reference" case for the stress state around a borehole needs to be replaced with a more-realistic estimation that includes the impacts of creating the opening.

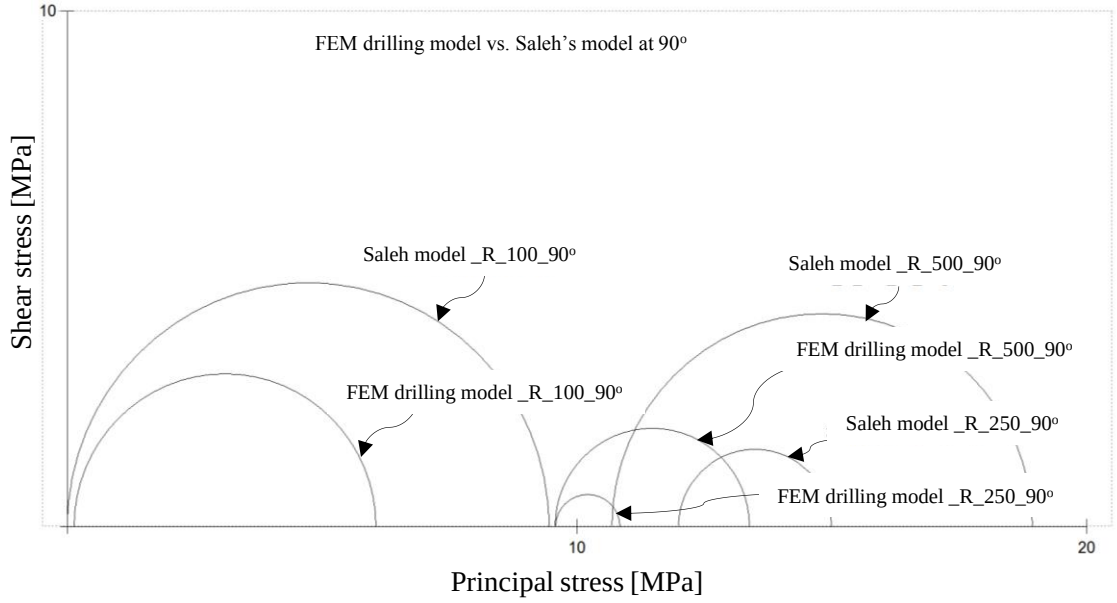

Figure 3.19: Stress state at r = 100, 250 and 500 mm (Y – axis) for σ_H = -20MPa and σ_h = -10MPa

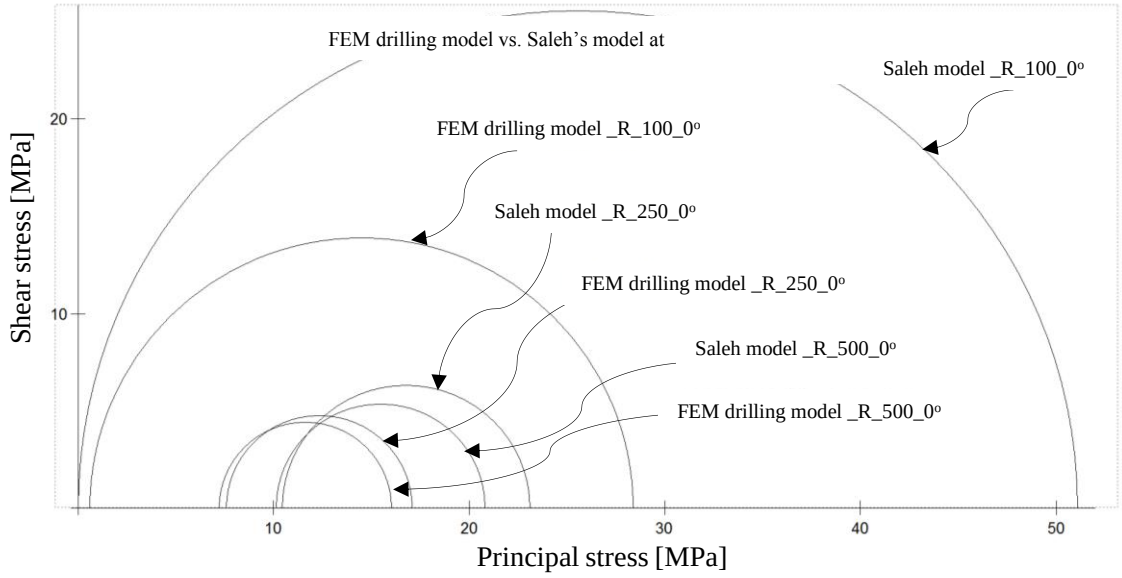

Figure 3.20: Stress state at r = 100, 250 and 500mm (X – axis) for σ_H = -20MPa and σ_h = -10MPa

Saleh's solution for the low-stress difference loading (Case One) differ markedly compared with the FEM drilling model. In the following sections, I show that the medium stress scenario (Case Two) and high stress scenario (Case Three) also exhibit significant differences for the stress state prediction. In Case Two and Case Three, the loading might be expected to reach yield and failure for many rocks, but the models are restricted to an elastic-only response.

3.5.2 Case Two ("medium stress": σ_H = -70MPa, σ_h = -10MPa)

In this case, the three models all show a visually similar appearance (Fig. 3.21). A closer investigation reveals that the major and minor values for the stress components differ. If all were plotted with the same scale-bar limits, the difference would not be possible to determine with accuracy, from the colour displays only. There are comparable apparent visual similarities for the σ_{xx} and σ_{xy} components (not shown).

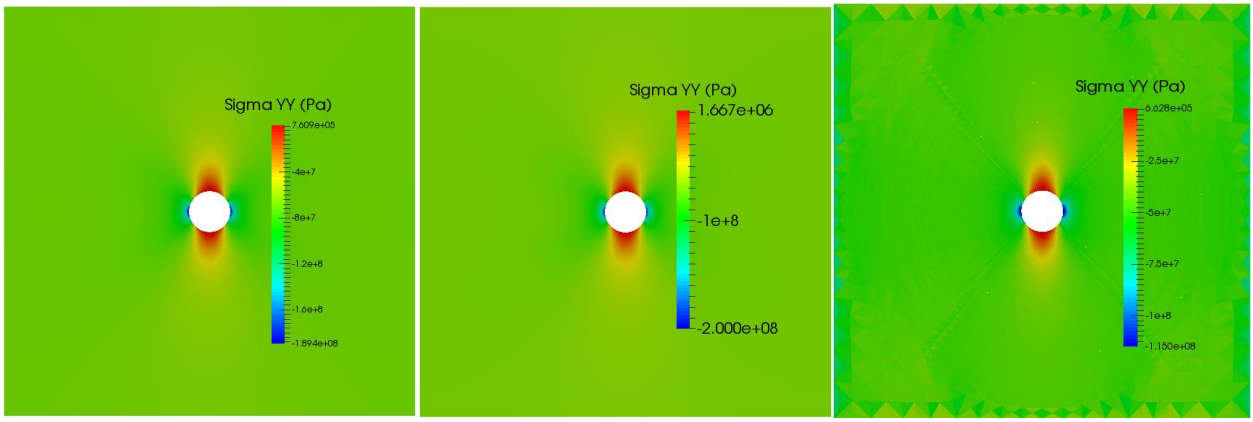

Figure 3.21: Distribution of the σ_{yy} stress-component in the three models. From left to right, these are: Saleh, pre-hole, and drilling results. Note: the right most image (the FEM drilling model) looks odd at the boundary – this is caused by the fact that the model edges has moved far enough so that the plotting algorithm being used "sees" non-existent parameter values along the nominal coordinates

Perhaps a more compelling display of the differences is to show them in the σ-τ space of the familiar Mohr-Coulomb diagram (Figure 3.22). In the following, I calculated the major stress differences between all models. The differential stresses between Saleh's solution and FEM pre-hole model are inconsistent by up to 65% at r = 102 mm, 3% at r = 250 and 500mm along the y-axis. Along x-axis, the differences are smaller by 6% at r = 102mm and 3% at r = 250 and 500mm. When I compare the major stresses between Saleh's solution and FEM drilling model, the differences are markedly larger. Along y-axis, the stress differences are 85% at r = 102mm and 35% at r = 250 and 500mm.

Along x-axis, the stress differences are 42% at r = 102mm, 35% at r = 200mm and 33% at r = 500mm.

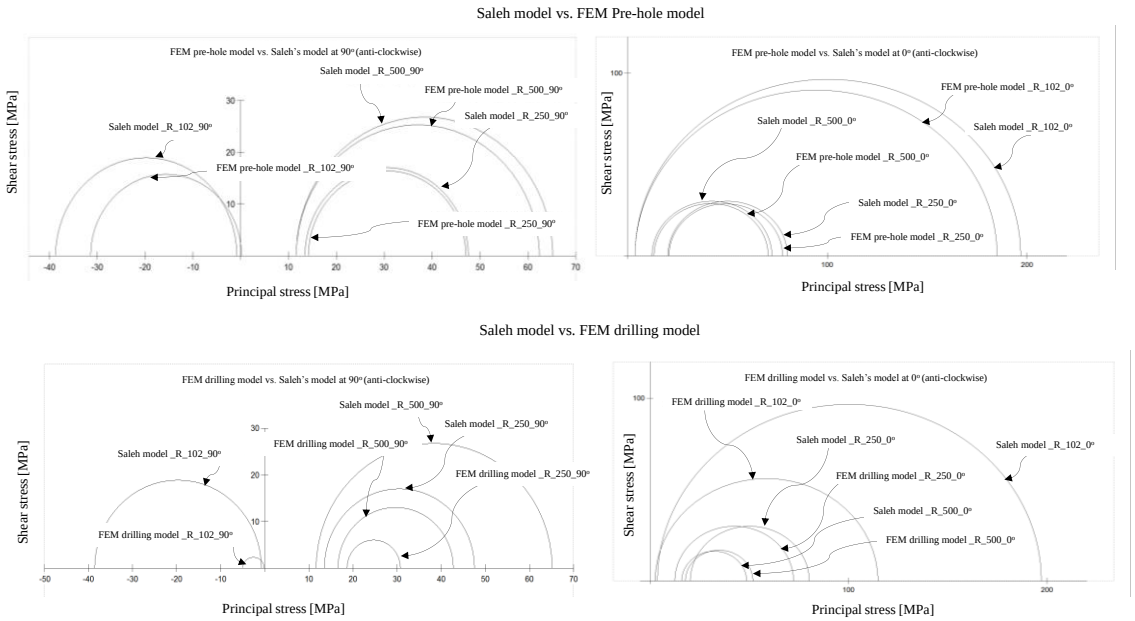

Figure 3.22: Mohr-circle depictions of stress states at the wellbore margin.

It is clear that the three calculation methods produce significantly different results. The pre-drill and Saleh answers are "similar", but do differ by 65+% at r = 102mm along y-axis. However, the FEM drilling model and Saleh's solution results differ by 85% at r = 102mm (y-axis). The choice between the pre-drill or analytical method would introduce some predictive difference (e.g., estimation of safe mud weight). The difference between the drilling and Saleh methods and FEM pre-hole are larger than would be acceptable in many or all applications. The results reinforces the hypothesis that the major differences occur near wellbore wall. Therefore, the choice of the modelling method could have a significant impact on subsequent predictions, and may have important economic consequences.

3.5.3 Case Three ("High stress": σ_H = -200MPa, σ_h= -10MPa)

In this case, the model is subjected to a high magnitude of major far field stress of σ_H = -200MPa in the Y direction, and minor far field stress of σ_h= -10MPa in X direction. The loading is designed to be extreme so that it leads to an instability of the wellbore after drilling. Saleh's solution will be compared with FEM pre-hole model and the FEM drilling model.

To draw a reasonable comparison between Saleh, the FEM pre-hole and the FEM drilling models, a radius point is selected at 103 mm on Y and X axis. Saleh's solution

is over estimating the major stress by 95% along y axis and 40% along x axis in comparison with the FEM drilling model. When comparing the results between Saleh and the FEM pre-hole model, they differ by 80% along y axis and 2% along x-axis a factor of 55x (Figure 3.23).

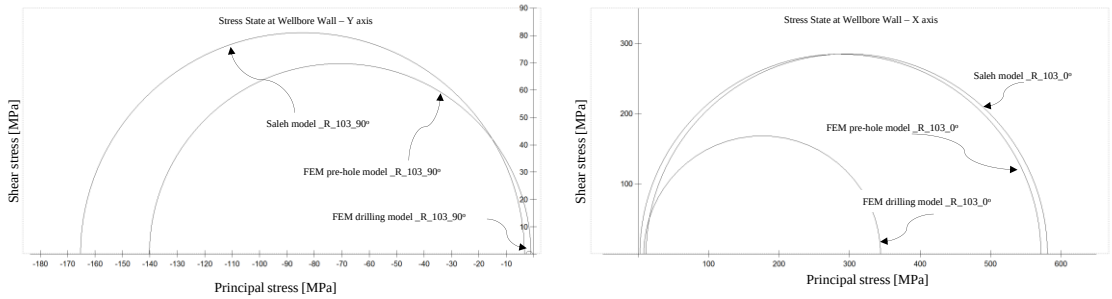

Figure 3.23: Mohr-circle depictions of stress states at the wellbore

The reality of the stress state near wellbore is significantly different when we allow failure to occur in the drilling model (See chapter 4), here I show σ_{yy}, σ_{xx} and σ_{xy} in a pure elastic material (model with infinite strength) (Fig 3.24). The magnitude of the stress around and away from the opening is significantly less from the corresponding values derived from the others. A comprehensive analysis on the failure mode will be discussed in the next chapter.

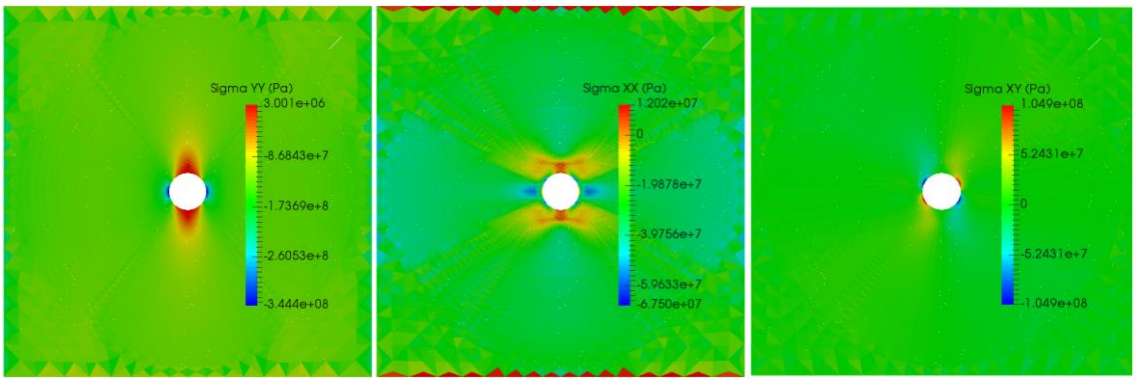

Figure 3.24: Distribution of the σ_{yy}, σ_{xx} and σ_{xy} stress-component (from left to right)

3.6 Material Sensitivity

Above, I have shown that the Saleh's solution to the FEM pre-hole model produces different results (by 10%). Since the analytical expressions are often states as calculating an elastic solution, this difference is puzzling. Could it be that there is some set of elastic parameters for which the two methods agree? Here, I run a series of pre-hole model which have different values of Young's modulus and Poisson's ratio that are selected to perform material sensitivity on wellbore wall's stress state for Saleh's solution, FEM pre-hole model and FEM drilling model. All FEM models are simulated

under σ_H = -20MPa and σ_h = -10MPa far field load and they are all restricted to elastic-response only. The table below summarises the values of Young's modulus and Poisson's ratio used in this series of models.

Table 3-3: Young's modulus and Poisson's ratio properties

Poisson's ratio	0.45	0.35	0.25	0.15
E_1 (GPa)	100	100	100	100
E_2 (GPa)	10	10	10	10
E_3 (GPa)	1	1	1	1

Figure 3.25 show the stress state after the wellbore wall at y axis and x axis. As I increase the material stiffness, E, with constant value of Poisson's ratio of 0.45, the differences between Saleh's model and FEM pre-hole model are within 10% to 5% at y axis and x axis. Between Saleh and FEM drilling model, the difference exceeds 50% for E = 1GPa and decreases when the stiffness is higher on y-axis and x-axis. Obviously, Saleh's solution do not fit any of this set of models.

At Poisson's ratio equal to 0.35, the difference become smaller between all models except for the FEM drilling model, when E = 1GPa; the difference exceeds 50% at y axis and differ by 2x when E = 100GPa at x-axis.

At ν = 0.25 and ν = 0.15, the major stress fall above and below Saleh's model at y and x directions respectively with radical differences. The outcome of these results reinforces the idea that different elastic properties can lead to a different stress state at wellbore's wall. However, Saleh's method does not fit any elastic model, which makes the analytical solution unrealistic, and this it cannot be said to be an elastic solution.

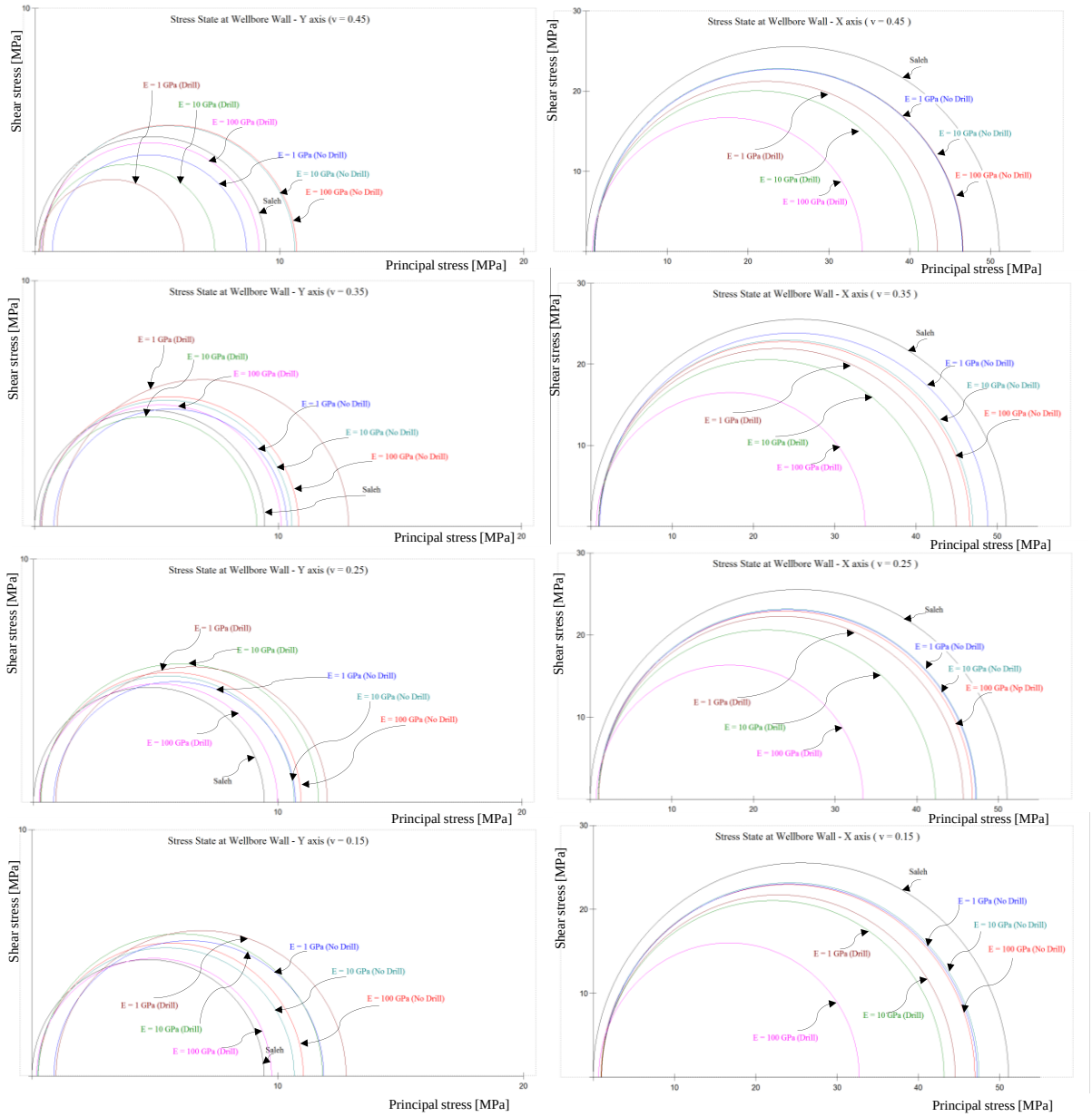

Figure 3.25: Mohr-coulomb plots at wellbore wall, here Drill refers to "FEM drilling model" and No Drill refers to "FEM pre-hole model"

3.7 Summary

Three different far field loadings are used to perform a comprehensive comparison between analytical and numerical models of stress states around a circular opening. All models show stress states that differ from each other. In the numerical models, material points move as elastic deformations take place, which are represented as nodal displacements. Such displacements happen with the FEM simulations described here; such displacement in the numerical models are likely to be similar to the motions that takes place in physical reality. The square boundaries move, and become non-straight,

and the nodes that started as being located on a perfect circle move also. They move inwards, but in such a way that they form a slight, approximately-elliptical shape. In the drilling model, the nodes that lie along the to-be-created hole were also located along a perfect circle before loading, and they also move inwards when the far field load is applied, and again as the "hole" material is removed, so they move more than do the same nodes of the mesh of the pre-hole model. The two FEM models represent different physical processes: in the pre-hole model, the concept is loading of a plate with a central hole; in the drilling model, the concept is to create a hole in a plate that previously has a uniform state. The drilling model seems much closer to what I imagine to occur when I create an opening in the already-loaded subsurface.

The stress free circle could be expected to exist only in an unloaded state after the creation of a perfectly circular hole – a circle not compatible with the far-field loads in any scenario. The analytical solution devised by Kirsch was clever and suitable approximation that was appropriate for its time, but not physically sensible. It served a purpose when numerical simulations did not exist, but that is not the current situation.

Similarly, the tractions on the exterior of the analytical model are constant along coordinate lines. This latter point is not the case for Kirsch's original "infinite" model, of course. However, that is not important, as Saleh's solution is almost indistinguishable from the Kirsch solution when the model size exceeds 1500mm as our example does. The Saleh solution is not strongly influenced by its introduction of a finite "boundary", and this is not the basis for the discrepancies around the central "hole".

When I re-calculate the analytical solution at the coordinates around the hole in the FEM model, the radial stress component is tensile, while the tangential stress component is slightly altered to a value closer to that of the numerical solution. However, the changes in magnitudes are far smaller than are the discrepancies, so the answer cannot be that we are comparing states from different locations. There is simply a fundamental difference between the analytical solution(s) and those derived from numerical simulation of a mechanical process.

The FEM pre-hole model is slightly dis-similar to the analytical solution, but the drilling model calculates stress states that are very different, in locations close to the wellbore. Choosing one model over the other leads to a significant difference in the state that is calculated – with differences on the order of 2x and higher as far field loadings have large magnitude with large stress difference. Since these calculated post-well states are used as the starting point for other assessments, the choice should be

made on the basis of which modelling approach best captures the physics of the real process. The approach that meets this criterion is the FEM drilling model.

The full scope of that work is to be reported in the next chapter, with this single illustration intended to demonstrate that the numerical approach to calculating wellbore geomechanical states creates a model that can be used to investigate other questions in physically-realistic ways.

The analytical solution also shows no agreement whatsoever with FEM simulations when elastic properties are changed. This makes it difficult to believe that the analytical solution calculates an elastic stress state at all. Its mathematical expressions designed to image the pattern of stress state across the entire model are somehow similar to FEM simulations, but they are not quite right in term of the physical reality.

Chapter 4 - 2D Fracture Mechanical Model

4.1 Introduction

In Chapter 3, I showed that the drilling model results in a near-wellbore stress state that is very different to the states that are derived from either the analytical method or from a pre-hole elastic solution. The drilling model is arguably, a more realistic model, as it better captures the process of creating the well opening. However, the drilling model presented in Chapter 3 does not account for any effect related to rock failure and potential feedback. Therefore, in this chapter, a series of FEM drilling simulations are presented to develop models of realistic stress states in 2D models of examples sedimentary rock types that are allowed to fracture. I used the combined finite-discrete element method (FDEM) to create the results. FDEM method includes a detailed and explicit rock failure process, and also incorporates dynamic mechanical behaviour as might be related to the consequences of the breakage processes. The method combines continuum and discrete mechanical algorithm to simulate a realistic geomechanical engineering problems. The drilling stage is considered to be a key boundary condition component to achieve a realistic mechanical state prior to any stimulation work. Here, I extend the results from Chapter 3 to consider the role of rock failure relative to the near-wellbore mechanical (stress) state. The tangential, radial and shear stresses are calculated and analysed. These FDEM calculations in turn provide a quantitative analysis to the fracture propagation and highlight the type of rock failure in each model.

4.2 Background

The rock mass into which a well is drilled already is in a pre-existing state (the so-called, in situ or far field stresses). Real world experience demonstrates that wells can develop localized damaged zones (breakouts) at the vicinity of the wellbore along the direction of the far field minor principal stresses. The breakout initiates at the borehole wall, where the models depict the highest compressive tangential stress to occur during or immediately after drilling. Both lab experiments of the process, and image logs of actual wells, support the idea that breakout is caused by shear fracture whose origin seems to be compatible with large differential stresses that develop in the wall rocks adjacent to the direction of the minor principal stress. It has been also reported that a definitive correlation between breakout dimensions and the inferred magnitude of the major principal stress exists in the field, and in experimental studies (Bell and Gough, 1979; Shamir and Zobak, 1992; Haimson and Herrick, 1986; Lee and Haimson, 1993).

A comprehensive analysis of the breakout in several theoretical, numerical and experimental studies are provided by Dyskin and Germanovich (2000). In general, fracture patterns during or after drilling can be more complex and often difficult to model in shale than sandstone reservoirs. Under a uniaxial compressive stress, it has been observed that the clean sandstone with only 12% clay content exhibits a linear elastic deformation with no ductile behaviour prior to failure. In other word, the some sandstone does not exhibit a significant plastic-strain deformation prior to rupture. This makes the mechanical failure of sandstones less complex. In shales, the mechanical behaviour under a uniaxial compression exhibits a ductile behaviour prior to failure. This allows the shale specimen to reach high degree of strain deformation prior to rupture. In return, the shale can illustrate a complex fracture pattern after failure (Jizba, 1991). The material texture of shale is softer and highly deformable under almost any sets of stress changes that might be caused by drilling or fracturing. In this chapter I will extend the drilling model simulations such that realistic material behaviour (failure) are allowed. I select four sandstone rock types to simulate rock failure as a result of drilling. I use the combined finite-discrete element code, FDEM, which is capable of predicting explicitly the mechanical state behaviour and fracture geometry due to drilling to examine how the non-elastic responses of these materials can alter the mechanical state related to drilling.

4.3 Material property

Rock properties determine how rocks may fail such as in drilling; they are required in any case to set up the FDEM models and knowledge of the parameters is used to interpret calculation results. Zipf (2006) tabulated a suite of material properties for different geological materials. In this chapter, I used Zipf's published properties for sandstones (here I call it Sandstone A) and subsequently simulated and analysed drilling models that were subjected to two different far field loads; σ_H = -20MPa, σ_h = -10MPa, which is the same loading examined in Chapter 3, and a loading with greater stress magnitude where σ_H = -70MPa, σ_h = -30MPa. I assumed two different sandstone properties with less strength to simulate the impact of softer sandstone formations on the wellbore stability.

I will use the property of the sandstone in FEM drilling models to demonstrate and analyse the resulting mechanical state and fracture pattern that develops. I will display the tangential, radial and shear stresses profiles and illustrate the mode of rock failure in

each of the models. Table 4-1 shows FDEM mechanical input parameters obtained from Zipf (2006).

Table 4-1: Models FDEM input parameters

Rock Samples	**Sandstone X**	**Sandstone Y**	**Sandstone Z**
Young Modulus (GPa)	15	8	3
Poisson ratio	0.3	0.2	0.26
Cohesion (MPa)	14	8	1.2
Friction Angle	34	28	22
Tensile Strength (MPa)	5.2	2.7	0.3
Viscus Damping (kg/(m.s))	6.3E+6	4.6E+6	2.8E+6
Mode I Fracture Energy (kg/s^2)	560,000	319,000	47,500
Mode II Fracture Energy (kg/s^2)	1,120,000	638,000	95,000
Density ((kg/mm^3))	2650	2500	2600
Contact Penalty (kg/s^2)	1.5E+11	0.8E+11	0.3E+11
Tangential Penalty ($kg/s^2/mm$)	1.5E+10	0.8E+10	0.3E+10
Fracture Penalty ($kg/s^2/mm$)	7.5E+10	4E+10	1.5E+10

4.4 FEM drilling models

Drilling simulations were conducted using FDEM code on a 2000mm by 2000mm square 2D model (the same model used in Chapter 3). The model consists of 15904 elements and 7985 nodes. A 200mm diameter curricular region was designed to be excavated in the middle of the model. The far field stresses were applied at the square boundaries of the model, with major far field stress σ_H in the y-direction.

The simulation procedure involves loading, drilling and resting (allowing the stresses to reach an equilibrium state). The initial stress state is established during the loading stage until all nodes become static, which is an indication that the stress state is correctly determined. The loading time for each rock type was different. The softer rocks took more time to reach equilibrium than the stiffer rock. The displacements of the nodes are much larger in the soft rock than in the stiff one. After reaching the equilibrium stress state condition, a zero displacement boundary condition is assigned to the nodes at the external boundary of the model to prepare the model for the next phase – the drilling stage. The drilling procedure is undertaken by reducing the stiffness of the elements in

the drilling region – the region to be excavated. Two loading stages were considered to reduce the rock stiffness by one order of magnitude for each stage and then the elements of the drilling region are removed from the model. The total simulation of drilling time in all models was 0.2 seconds. The final stage was the resting stage. During this stage the model was set to respond after the elements are removed from the centre of the model, to reach equilibrium. Each model was checked to see if the elements had stabilized. At this point, the simulation procedure ends and detailed analysis is conducted.

4.5 Stress state analysis and breakout characteristics

A stress analysis and description of breakout characteristics are provided for each sample. The stress variations in x, y and xy directions are illustrated in 2D, and fracture geometries are presented in time sequence to show the development of the breakout region and the failed rock in the wider region across the model.

4.5.1 Sandstone X model

The first type of sedimentary rock I examined is the sandstone X sample, which is a common type of rock in oil and gas reservoirs. The FEM drilling models highlight the dominant failure mode around the wellbore. Figure 4.1 shows the sandstone model under two different magnitudes of far field loads. Model A and B illustrate the σ_{yy}, σ_{xx} and σ_{xy} in two dimensions. The stress disturbance affects a much smaller part of the domain in model A than in model B. The tangential stress shows positive stress above and below the wellbore in both models as an indication of tensile stress. The tangential stress, indicates positive stress (tensile) in left and right region of the wellbore in model A and negative stress (shear) in model B. Model A exhibits similar mechanical behaviour and wellbore geometry deformation to the example discussed in Chapter 3. Model B is demonstrating a typical wellbore breakout as a result of higher far field load. The wellbore in model B is losing its integrity during drilling. Figure 4.2 illustrates the mode of failure in both models. Model A shows no failure during the drilling. The wellbore remains very stable at all drilling stages. In model B, the stability of the wellbore is less and a mix of tensile and shear failures starts at a very early stage of the drilling along the minor stress direction. The failure continues to grow after removing the elements completely from the centre. The indication of fracture geometry and pattern can be clearly identified.

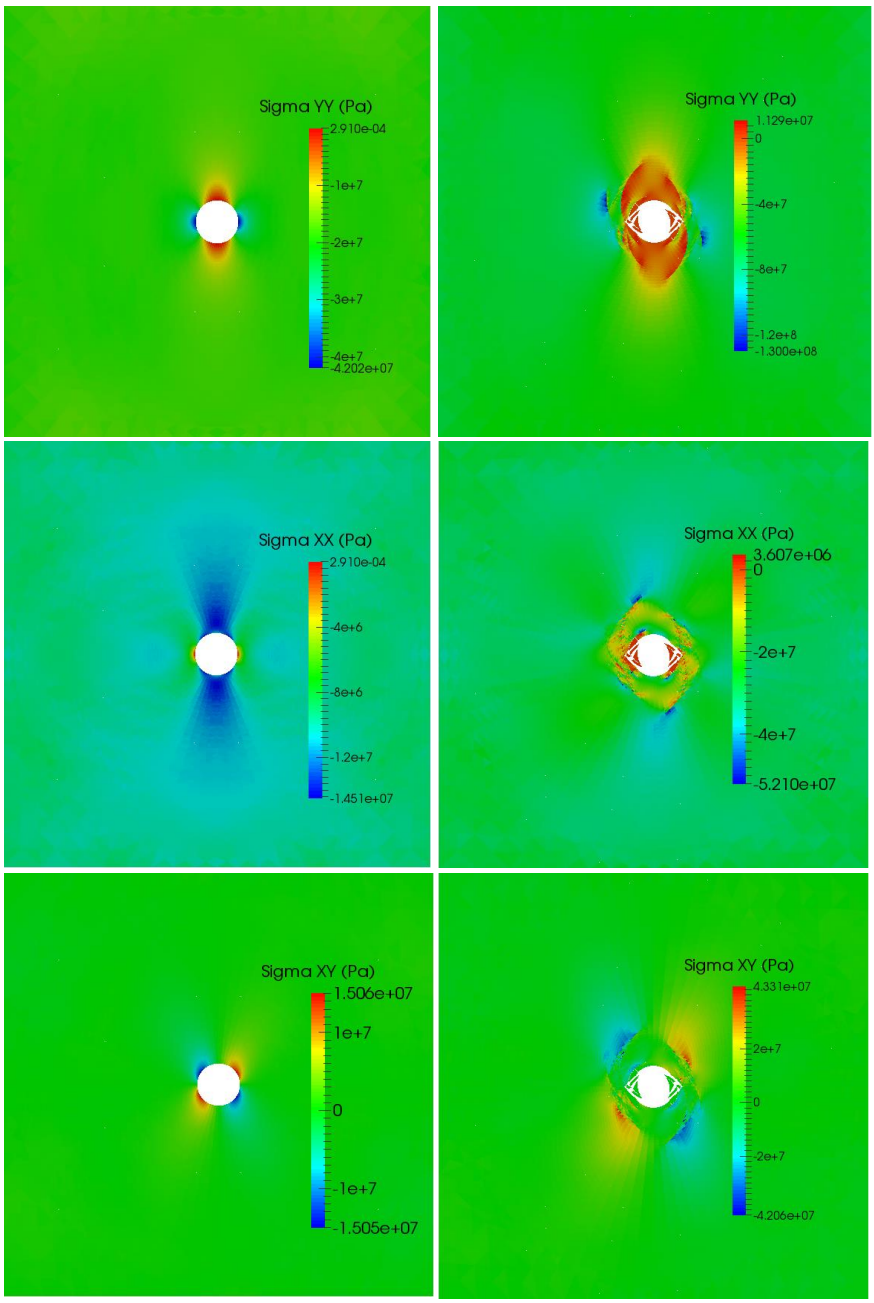

(A) σ_H = -20MPa, σ_h = -10MPa (B) σ_H = -70MPa, σ_h = -30MPa

Figure 4.1: Sandstone X model

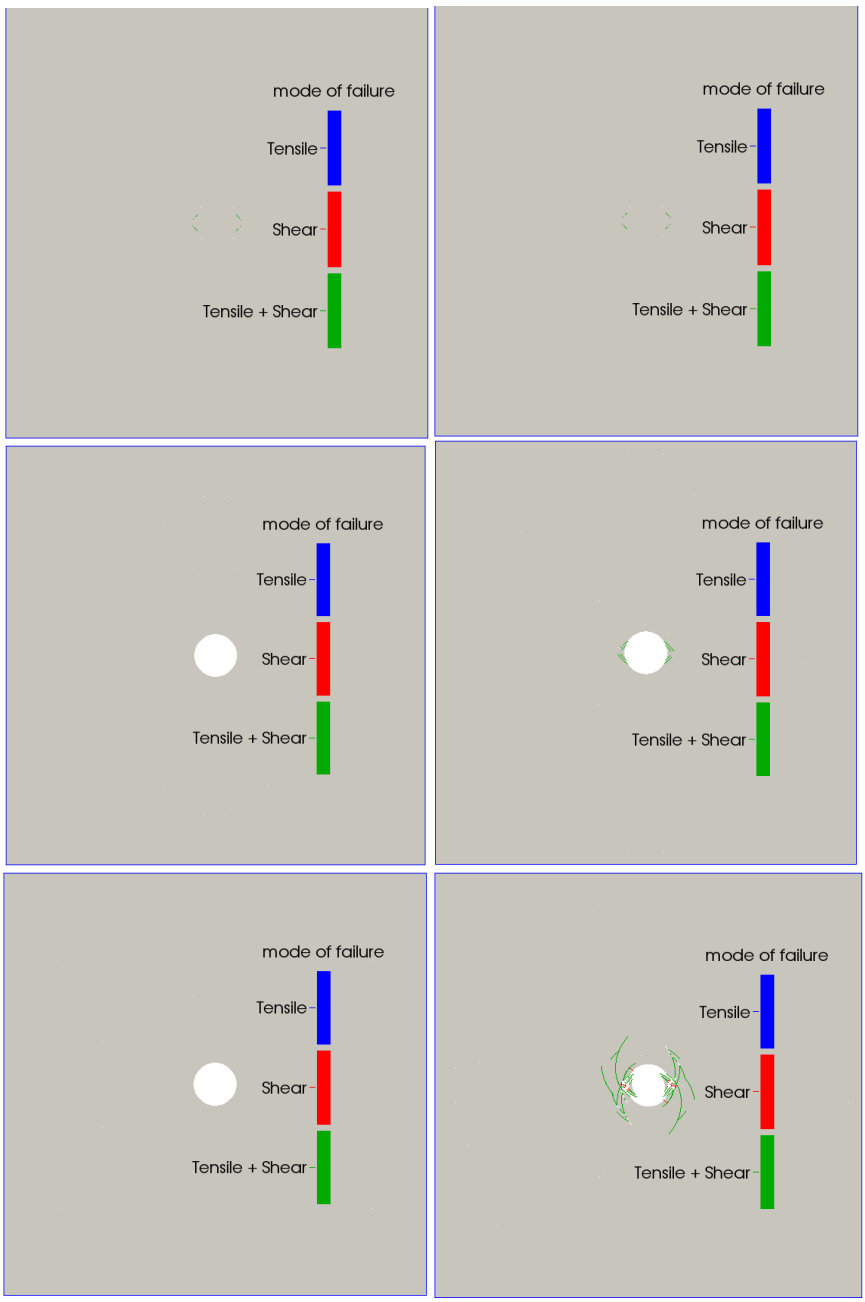

(A) σ_H = -20MPa, σ_h = -10MPa (B) σ_H = -70MPa, σ_h = -30MPa

Figure 4.2: Sandstone X model (mode of failure)

4.5.2 Sandstone Y model

The second rock type is the sandstone Y sample. The model has the tendency to fail under the stresses associated with almost any disturbance. Softer sandstone rock type sometimes dominates the type of rock in oil or gas reservoirs and the drilling into this type of rock could be problematic if it fails. Figure 4.3 shows the stress state of the model A and B after drilling. Completely different stress patterns are observed for the two different sets of major and minor principal far field stress. The stress disturbance caused by the drilling is much larger than was seen in sandstone A model. The stress

disturbance in model A is significantly less than in model B as was observed in the sandstone example. Figure 4.4 shows the mode of failure in the siltstone models. The siltstone can deform quite substantially under the larger stress difference during drilling (see Figure 4.4 (B)). The wellbore stability becomes an issue under the far field loading with high differential stress. The mixed mode of failure can again be seen in both models. Model A has four extended tensile-shear fracture propagations at the tip of the breakout region along x-direction (called intersecting conjugate of shear planes). The tensile-shear fractures in the breakout region occur after removing the rock from the wellbore and continue to propagate after the stress equilibrates. In Figure 4.4 (B), the tensile-shear fracture occurs in the breakout region during the drilling. A multiple tensile-shear fractures were occurred around the wellbore. The wellbore is significantly de-stabilized during the drilling, as rock starts to lose its strength and integrity. The magnitude of the far field stress loads can play very important role in signifying the risk of wellbore stability in softer rock such as siltstone. An extra care is required to overcome the issue of wellbore stability in siltstone rocks.

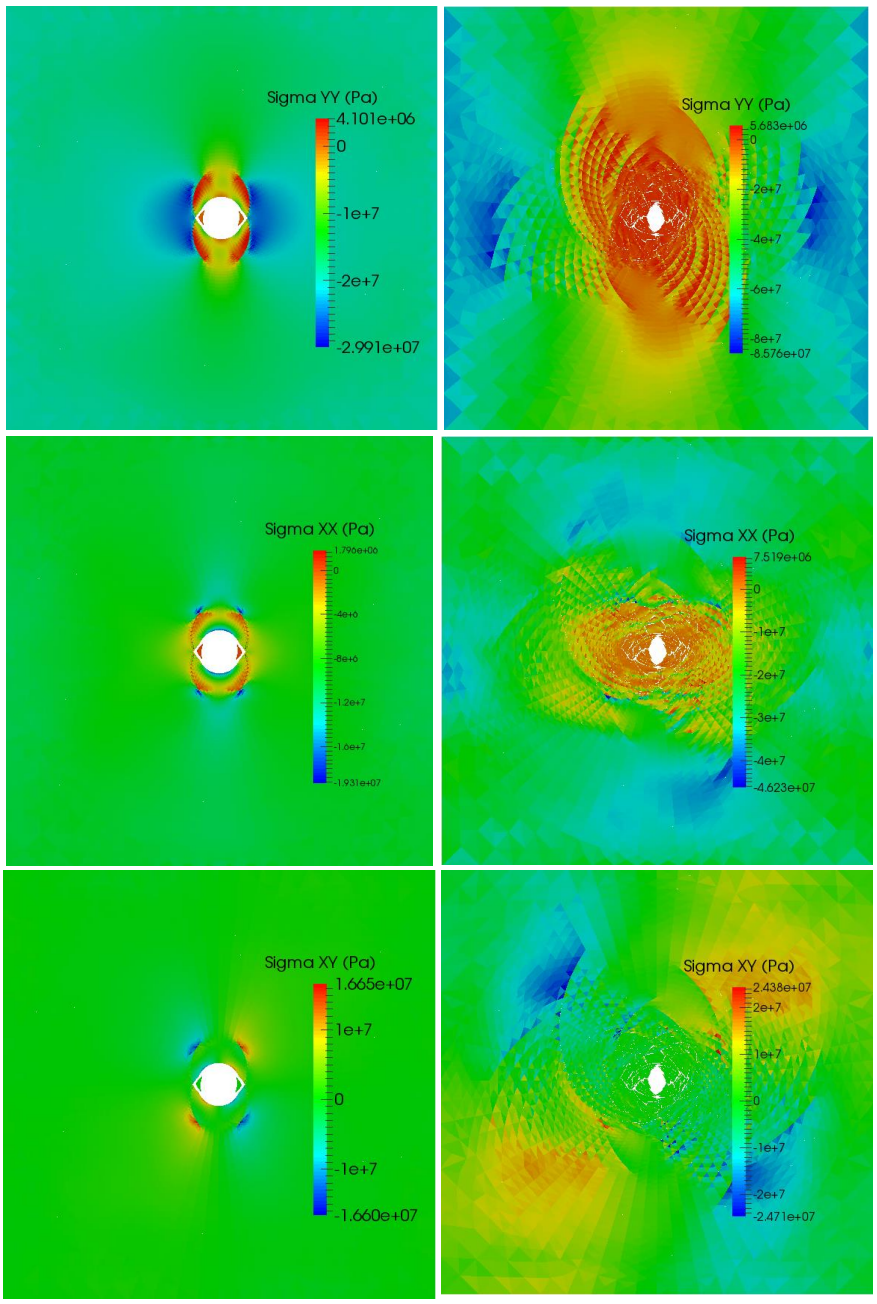

(A) σ_H = -20MPa, σ_h = -10MPa (B) σ_H = -70MPa, σ_h = -30MPa

Figure 4.3: Sandstone Y model

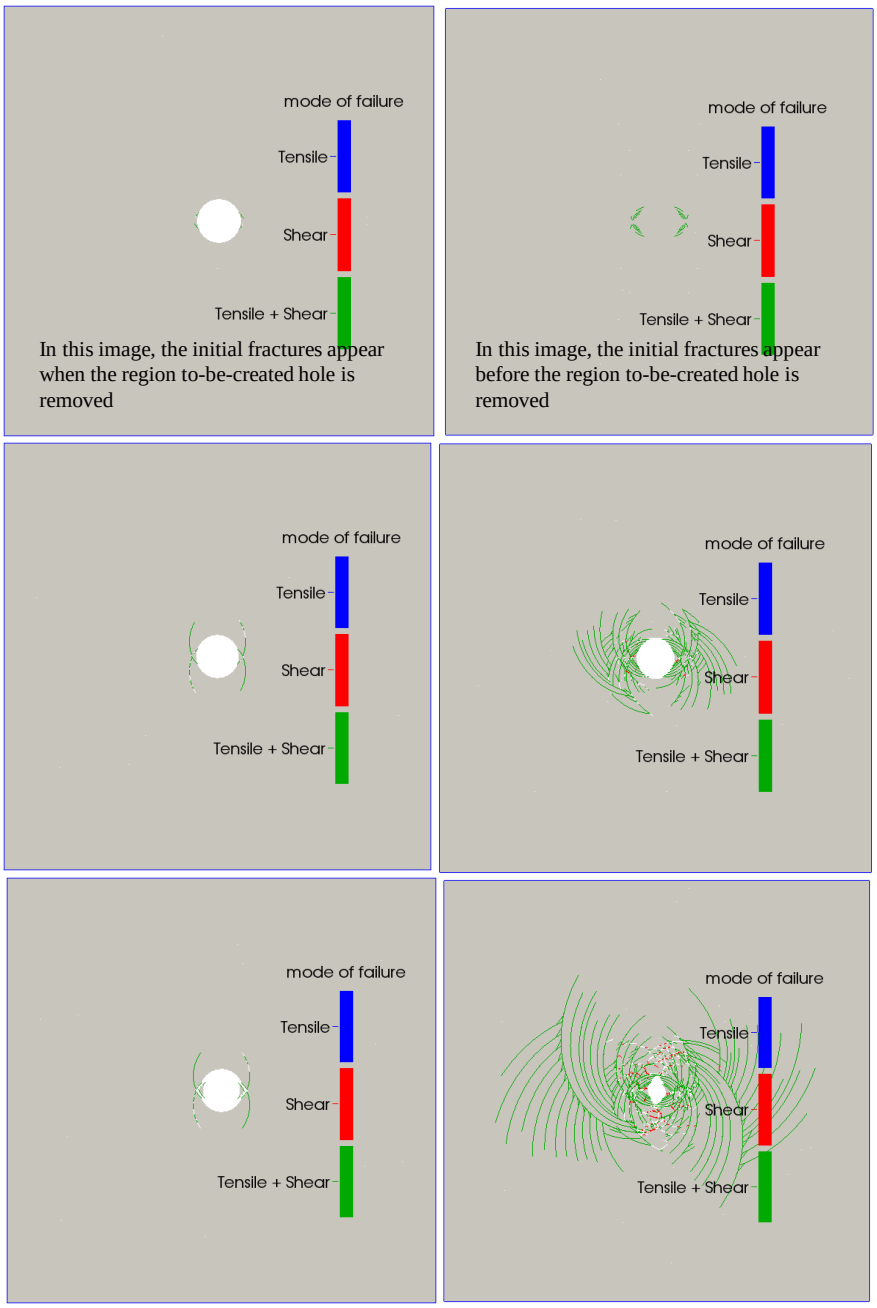

(A) σ_H = -20MPa, σ_h = -10MPa (B) σ_H = -70MPa, σ_h = -30MPa

Figure 4.4: Sandstone Y model (mode of failure)

4.5.3 Sandstone Z model

The third rock to be examined is the sandstone Z sample. I intend to demonstrate the mechanical behaviour only to understand the complexity of the rock and also shed some light on wellbore stability under the effect of drilling and far field loads. Figure 4.5 shows the stress pattern under two different magnitudes of far field stresses. The level of disturbance is much greater than in the other two types of rock examined. Figure 4.6 (A) and Figure 4.6 (B) illustrates tensile-shear fractures. In Figure 4.6 (B), the model

shows rock tensile-shear failure away from wellbore before drilling began which is directly related to the effect of far field load while exceeds the Mohr-Coulomb failure for this material. It suggested that under certain far field stresses and rock type, the targeted area for drilling could be surrounded by failed rock which can increase the risk of losing the wellbore. The risk of having failed rock will likely reduce the material strength and increase the chances of rock displacement into the wellbore. For this particular model, the whole area in Figure 4.6 was dominated by opening and sliding fracture modes as stresses reached an equilibrium.

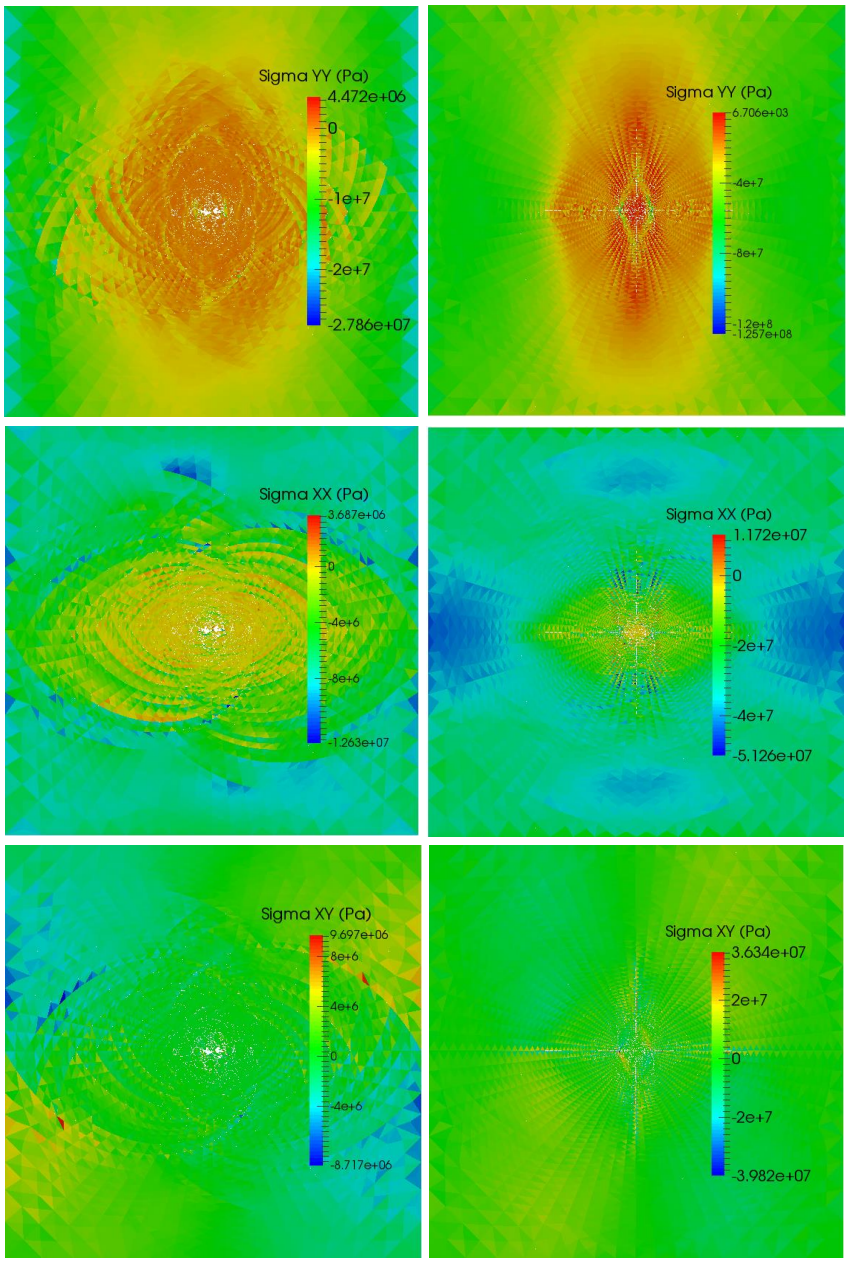

(A) σ_H = -20MPa, σ_h = -10MPa (B) σ_H = -70MPa, σ_h = -30MPa

Figure 4.5: Sandstone Z model

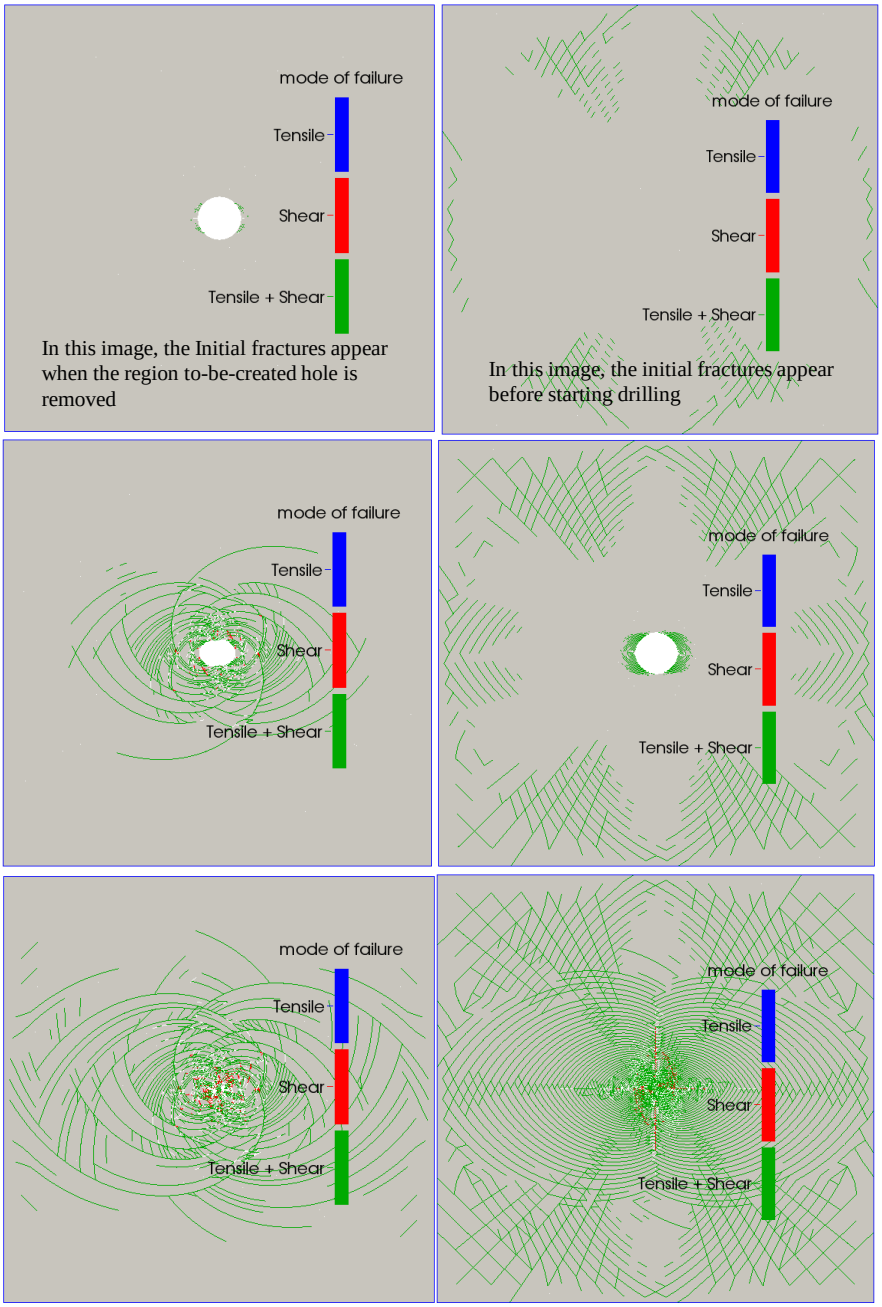

(A) σ_H = -20MPa, σ_h = -10MPa (B) σ_H = -70MPa, σ_h = -30MPa

Figure 4.6: Sandstone Z model (mode of failure)

The following diagram summarize the fracture pattern propagation in each of the above model (Figure 4.7).

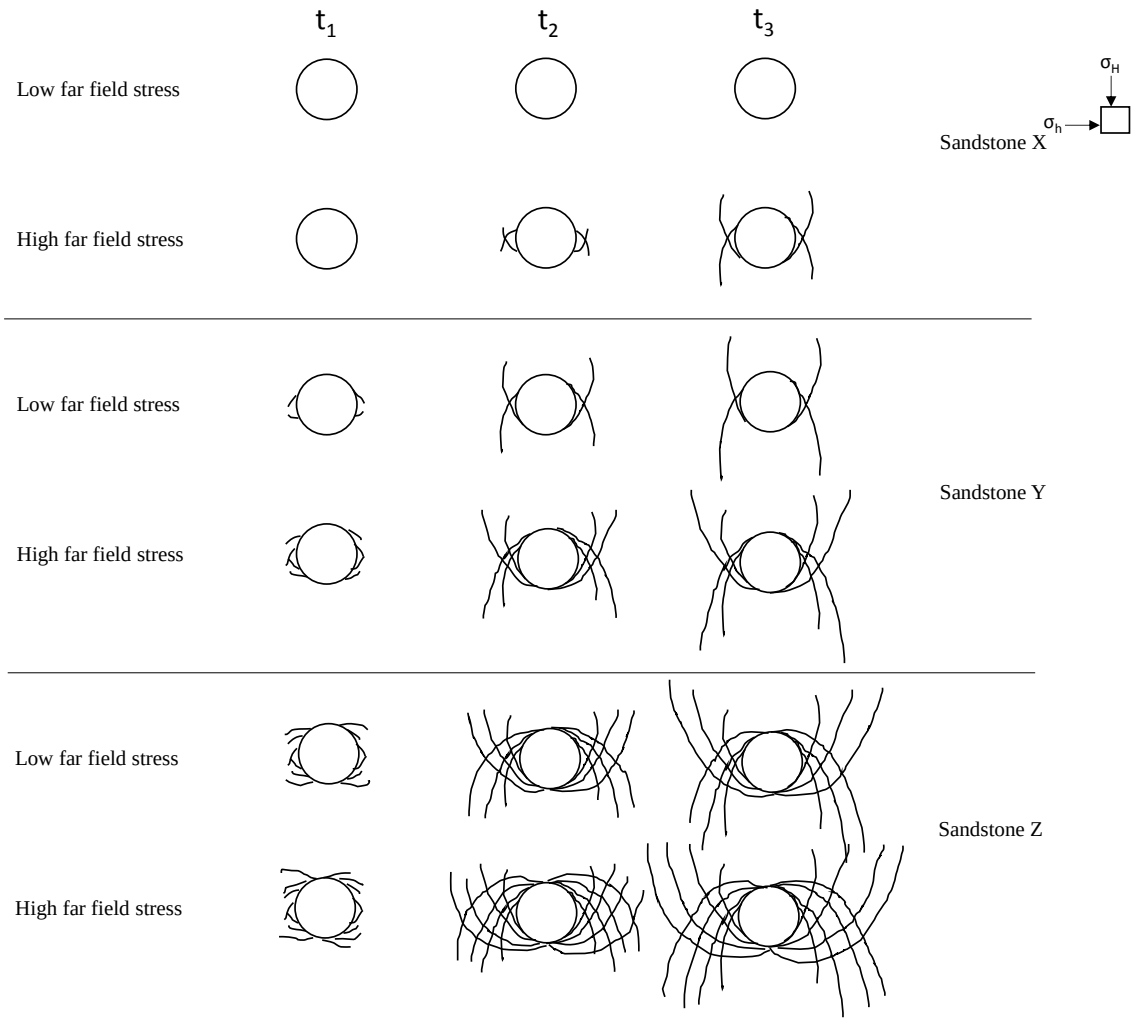

Figure 4.7: diagram of fracture propagation (breakout(s)) versus simulation time (t_1: early time; t_2: middle time and t_3: late time) for sandstone X, Y and Z models

4.5.4 Berea sandstone model

Berea sandstone has been extensively studied in the literature for its mechanical behaviour and petrophysical properties. It has been known for its homogenous characteristics at the scale of lab blocks used for experiments. I examine the drilling responses with Berea sandstone to provide a FEMDEM reference case that I will use in Chapter 5, where I consider the same drilling problem with a completely-continuum method that uses a well calibrated material model for Berea sandstone. The continuum approached represents rock failure or inelastic responses as local strain in a pure plastic framework.

4.5.4.1 Stress state of Berea sandstone using FEMDEM approach

Two far field stress conditions are studied on Berea sandstone. The stress state developments in Berea sandstone are shown in Figures 4.8 to Figure 4.14, which illustrate the progressive changes relating to the creation (excavation) of the hole. Here I

show the tangential stress, σ_{yy}. No rock failure occurred under the low far field stress (Figure 4.8). The tangential stresses around the wellbore are such that the wellbore remains stable in both models. A mixed of mode failure occurs away from the model centre after 0.105 second of simulation drilling time at the higher far field load (Figure 4.9). The failure was mainly due to the effect of the far field stress condition. At the low far field stress condition, the model shows no failure near or away from the hole. At higher far field loading conditions, failure occurs on a few distinct shear planes (here, the term "planes" refers to zones of localized shear deformation with small but finite thickness and length) (See Figure 4.8 and Figure 4.9 for σ_H = -70MPa, σ_h = -30MPa). The following input properties are used for the model similar to those for Berea sandstone: E = 20GPa, ν = 0.38, μ = 0.3, ρ = 2650kg/m^3, viscus damping = 1.83E+6kg/(m.s), cohesive = 1.4E+7kg/(m.s^2), tensile strength = 6E+6 kg/(m.s^2), G_I = 4,600N/m, G_{II} = 28,000N/m, contact penalty = 2E+11kg/s^2, tangential penalty = 2E+10kg/s^2/m, fracture penalty = 1E+11kg/(m.s^2), viscus damping = 7.28E+6kg/(m.s)

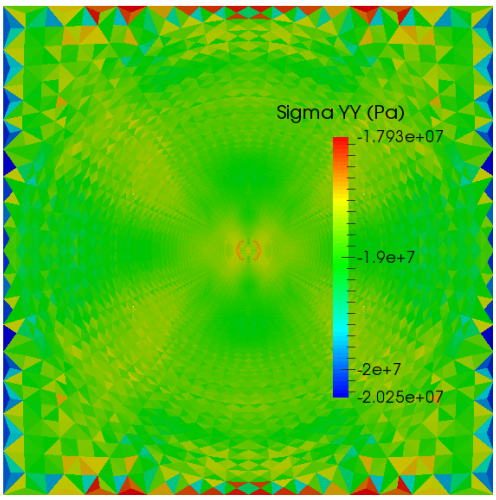

σ_H = -20MPa, σ_h = -10MPa

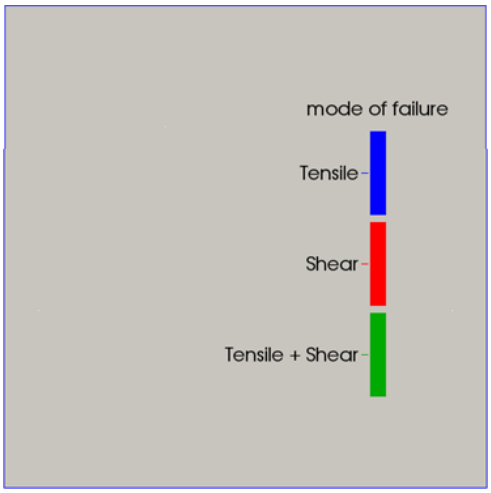

σ_H = -20MPa, σ_h = -10MPa

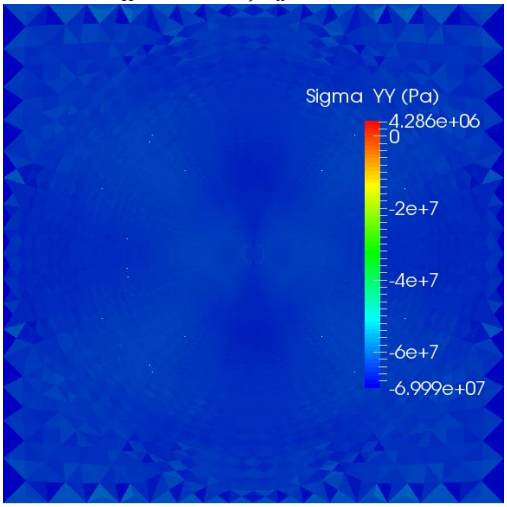

σ_H = -70MPa, σ_h = -30MPa

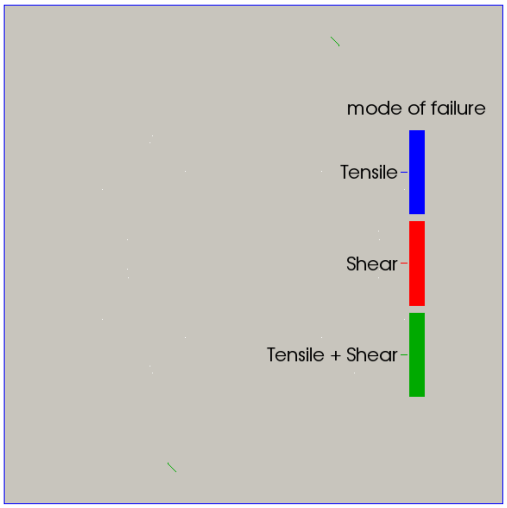

σ_H = -70MPa, σ_h = -30MPa

Figure 4.8: Berea sandstone after 0.085 second (stress state and mode of failure under initial stress state)

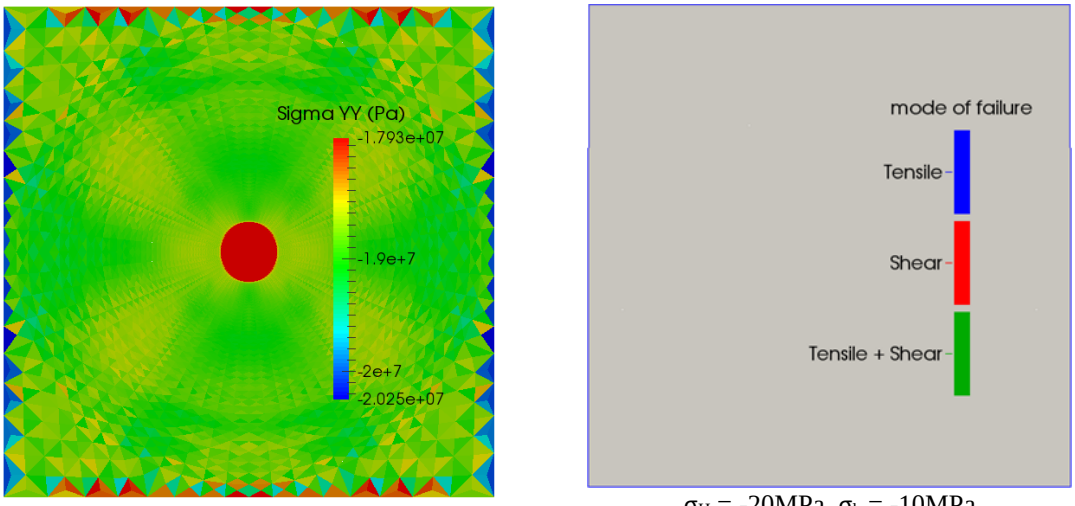

σ_H = -20MPa, σ_h = -10MPa

σ_H = -20MPa, σ_h = -10MPa

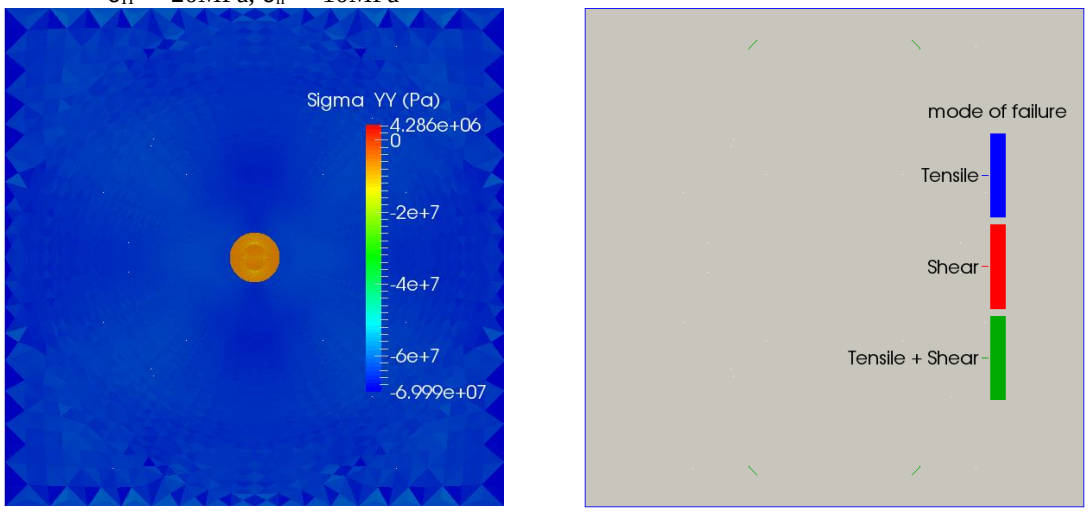

σ_H = -70MPa, σ_h = -30MPa

σ_H = -70MPa, σ_h = -30MPa

Figure 4.9: Berea sandstone after 0.105 second (stress state and mode of failure at initial drilling stage)

Figure 4.10 and Figure 4.11 shows the early and middle drilling stages (Note: the rock stiffness in the region to-be-created hole is reduce by an order of magnitude in the early stage and by two order of magnitude in the middle stage) in Berea sandstone models respectively. No breakout occurs at the early stage of drilling in both far field stress conditions. The failure that occurred away from the wellbore continues to grow in the high far field load. At the middle drilling stage, an initial localized damaged zone formed around the borehole (initial breakout) along the minor principal stress for the higher far field stress load (see Figure 4.11). No initial breakout formed at this stage in the low far field load condition. Extensive field observations and laboratory experiments suggest that breakout orientation is typically aligned with the direction of the minor principal in situ stress (Bell and Gough, 1979; Shamir and Zobak, 1992;

Haimson and Herrick, 1986; Lee and Haimson, 1993). My simulation results concur with what has been found to date in the literature.

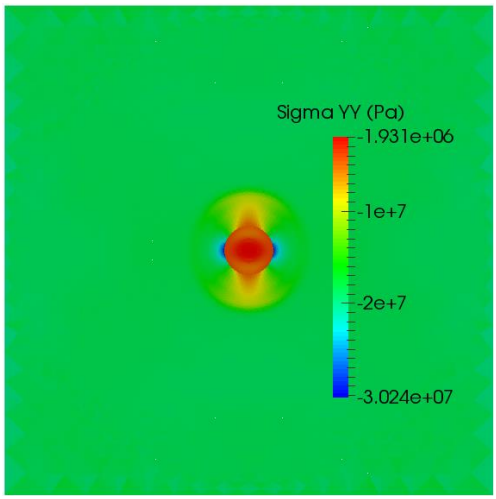

σ_H = -20MPa, σ_h = -10MPa

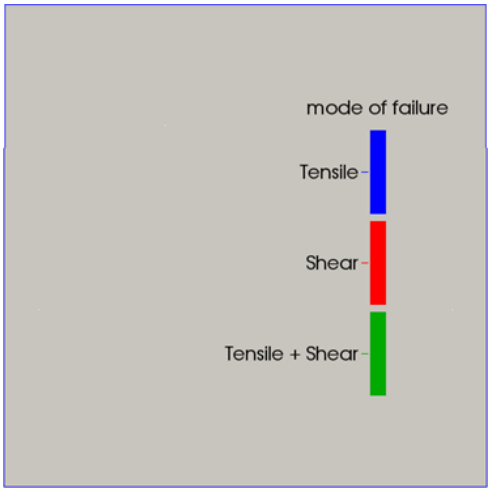

σ_H = -20MPa, σ_h = -10MPa

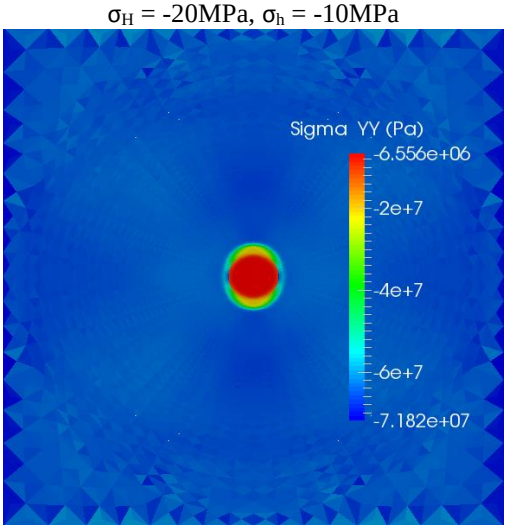

σ_H = -70MPa, σ_h = -30MPa

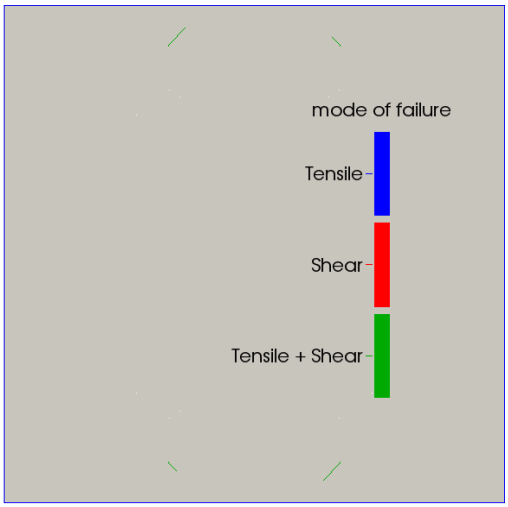

σ_H = -70MPa, σ_h = -30MPa

Figure 4.10: Berea sandstone after 0.15 second (stress state and mode of failure at early drilling stage)

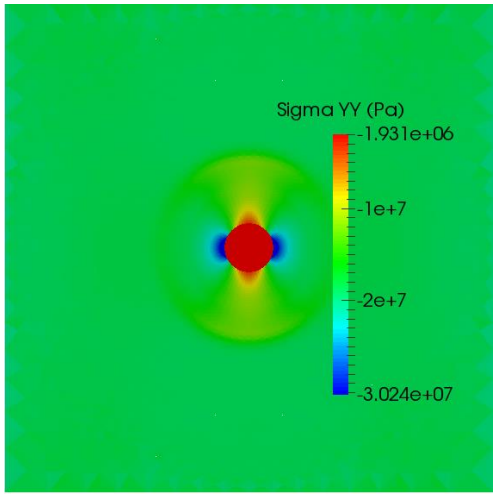

σ_H = -20MPa, σ_h = -10MPa

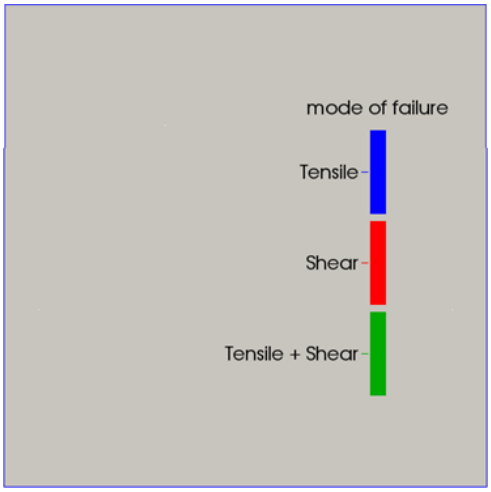

σ_H = -20MPa, σ_h = -10MPa

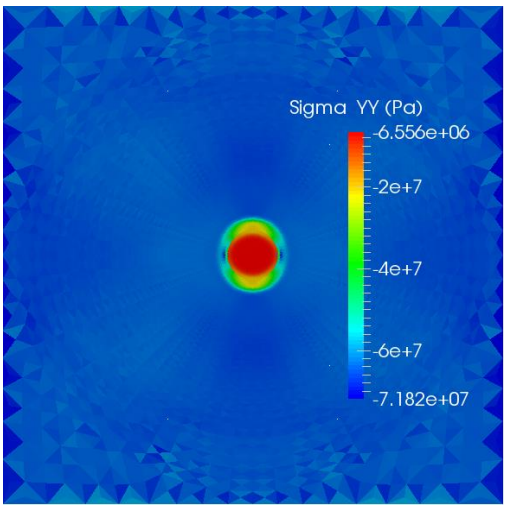

σ_H = -70MPa, σ_h = -30MPa

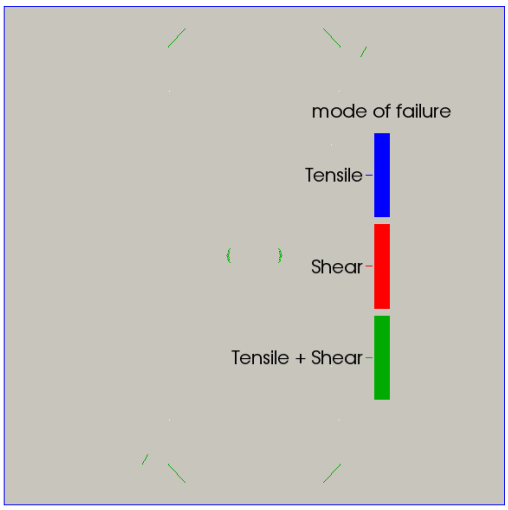

σ_H = -70MPa, σ_h = -30MPa

Figure 4.11: Berea sandstone after 0.2 second (stress state and mode of failure at middle drilling stage)

A multiple breakouts can be developed during or after drilling depending on the magnitude of the major and minor far field loads and rock mechanical properties (see Figure 4.15). During the late drilling stage, two breakouts are countered in the higher far field load and the failure growth in the entire model continue. The low far field stress load model shows no indication of breakout during the late drilling stage. The breakout occurs when the stresses exceed the compressive strength of the borehole wall (Zoback et al., 1985; Bell, 1990). The multiple breakouts or the borehole enlargement is caused by the intersecting conjugate shear planes, which causes part of the borehole wall to fall off (see Figure 4.12 and Figure 4.13). The breakout continue to grow and become larger along x axis due to hole geometry changes (hole become larger from its initial size) and the localised compressional stress zone grows further into the model in the x direction. The mechanism of failure combines both the sliding (shear) and opening (tensile) mechanisms. The breakout continues to grow and reach the boundary of the model as the stress changes taking place and wellbore stability diminishes as shown in Figure 4.14 as a result of rock failure.

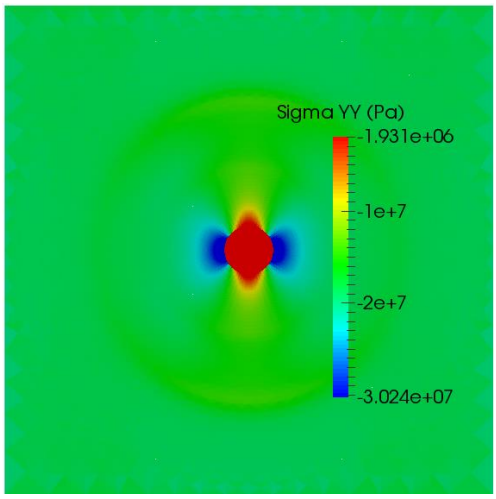

σ_H = -20MPa, σ_2 = -10MPa

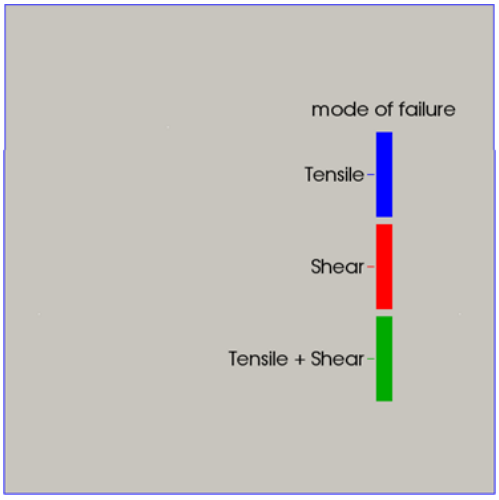

σ_H = -20MPa, σ_h = -10MPa

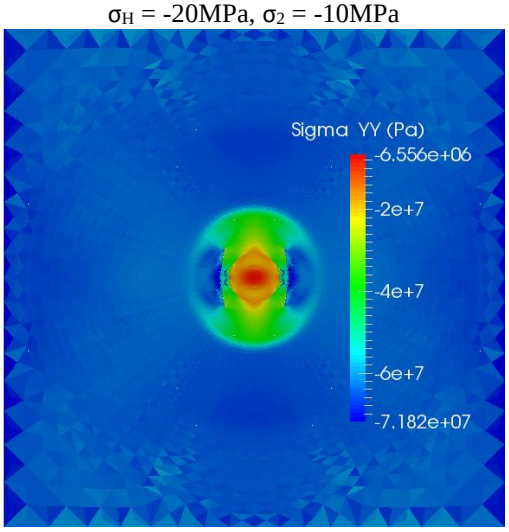

σ_H = -70MPa, σ_h = -30MPa

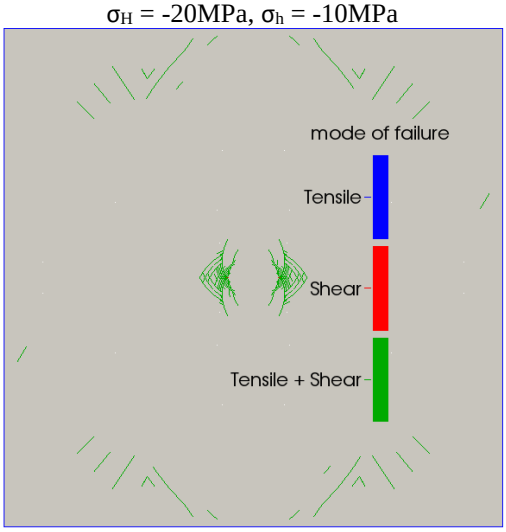

σ_H = -70MPa, σ_h = -30MPa

Figure 4.12: Berea sandstone after 0.2 second (stress state and mode of failure at the late drilling stage)

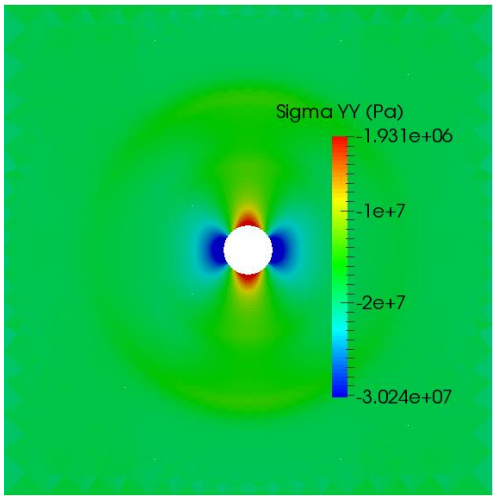

σ_H = -20MPa, σ_h = -10MPa

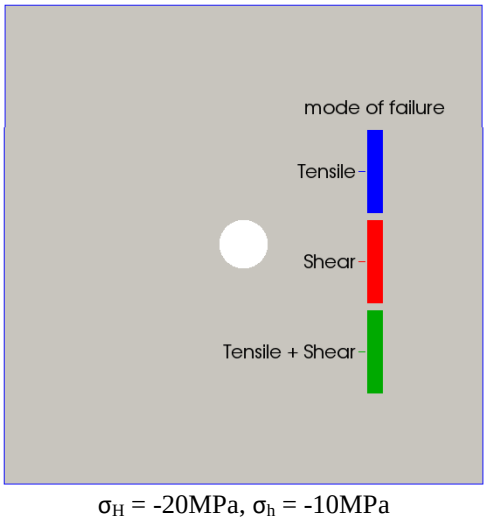

σ_H = -20MPa, σ_h = -10MPa

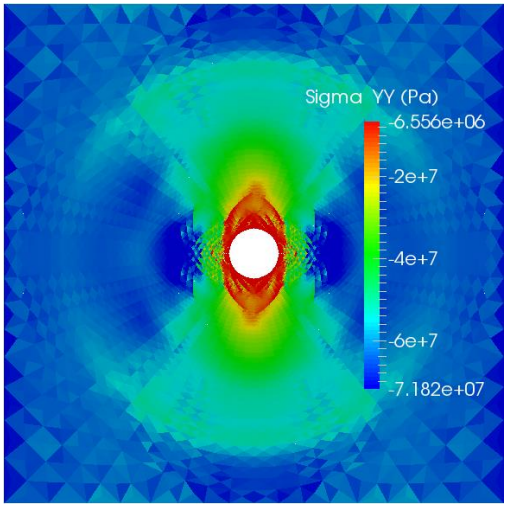

σ_H = -70MPa, σ_h = -30MPa

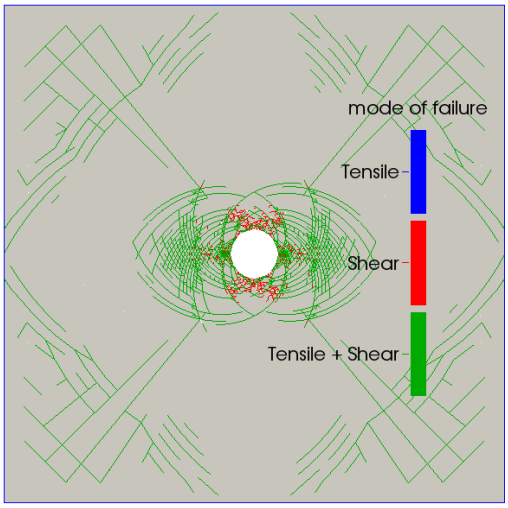

σ_H = -70MPa, σ_h = -30MPa

Figure 4.13: Berea sandstone after 0.2 second (stress state and mode of failure after removing the rock from the wellbore)

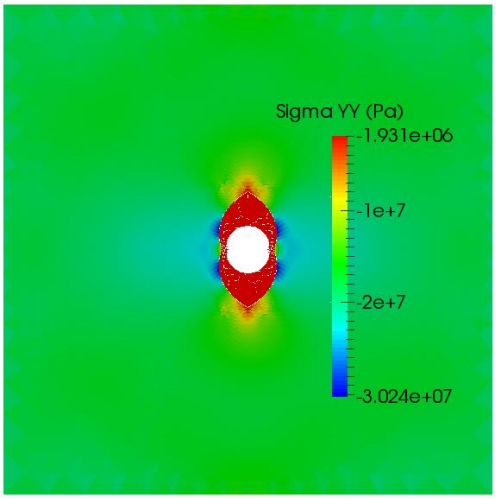

σ_H = -20MPa, σ_h = -10MPa

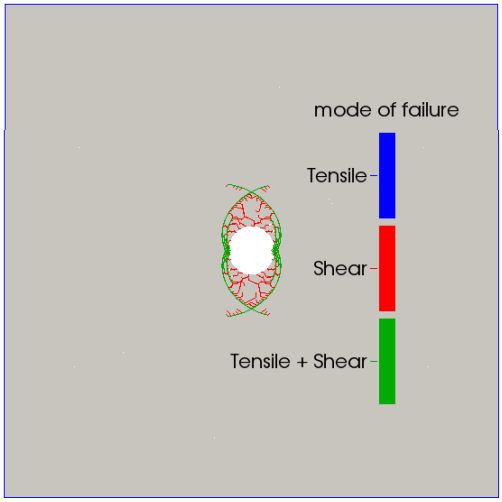

σ_H = -20MPa, σ_h = -10MPa

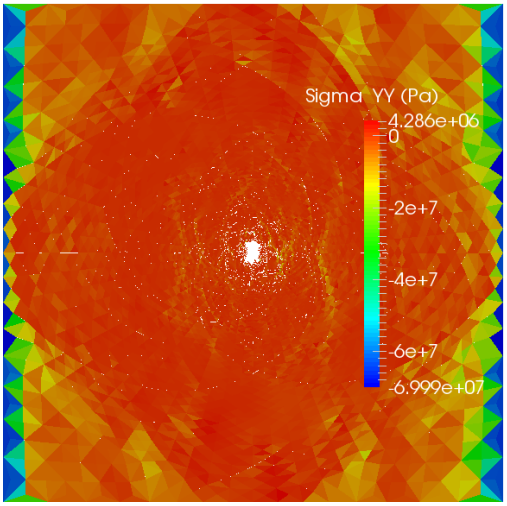

σ_H = -70MPa, σ_h = -30MPa

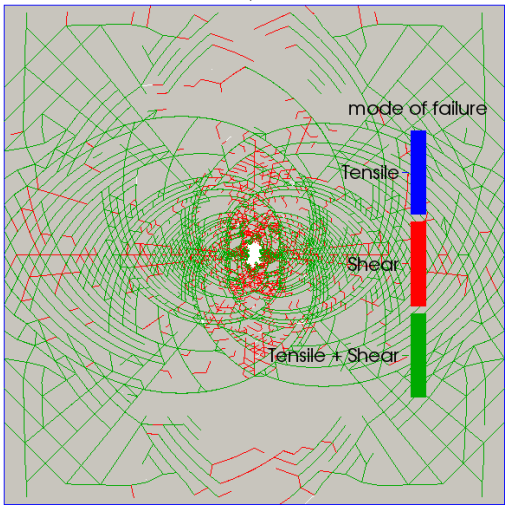

σ_H = -70MPa, σ_h = -30MPa

Figure 4.14: Berea sandstone stress state and mode of failure at equilibrium

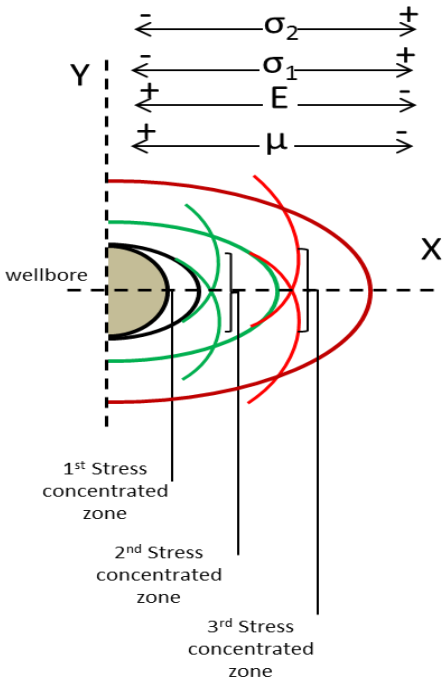

Figure 4.15: diagram of multiple breakouts of Berea sandstone. 1st stress concentration zone developed at the early drilling stage as a result of the buildup stress concentration. The breakout continues to develop as the loading is taking place and model iterate to reach equilibrium. Each breakout develop a conjugate shear fractures causing the rock to fail and spall off. The mechanical properties can affect the magnitude of rock failure

4.5.4.2 Berea sandstone stress analysis

Figure 4.16 and Figure 4.17 show the tangential stress, it is σ_{yy} at the intersection with x-axis, versus simulation time, for both low and high far field stress contrasts. In the first patch of four elements (near the wellbore – along x-axis), drilling is significantly affecting the adjacent element to the wellbore and causing the first element to fail after reaching the maximum compressional stress (see Figure 4.16 (A)). The next three elements retain a certain magnitude of tangential stresses after reaching the maximum compressional stress. The second patch of four elements (after the first patch) shows almost similar behaviour among each other but none of the elements failed (see Figure 4.16 (B)). The third and fourth patches have no indication of localised compression stress and maintained roughly the initial state of stress. Therefore, no failure was occurred into these two patches (see Figure 4.16 (C) & (D)).

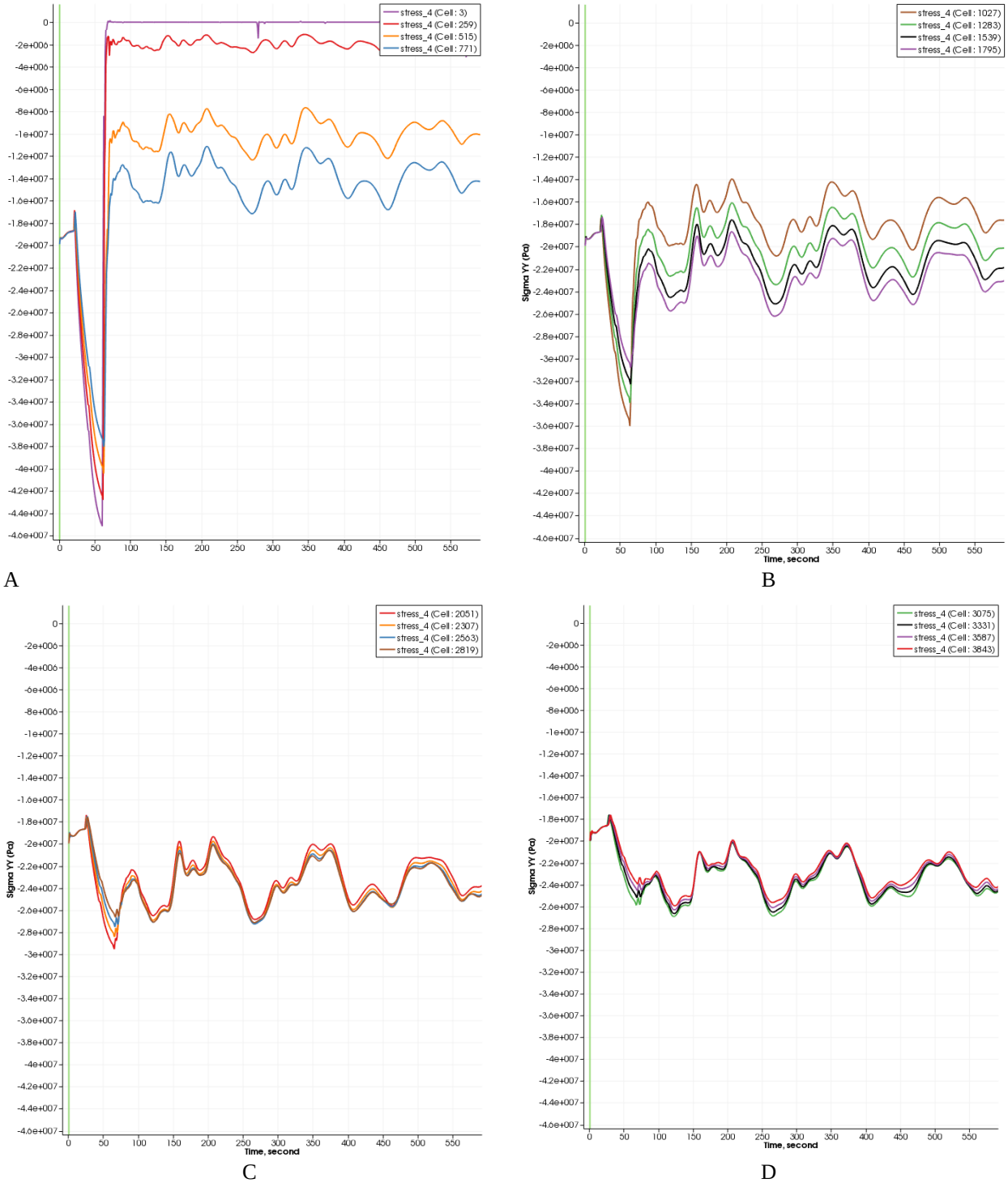

A B

C D

Figure 4.16: plots of stress versus time in Berea sandstone (σ_H = -20MPa, σ_h = -10MPa). Note: A is the first four elements adjacent to wellbore along x-axis, B is the next four elements to A, C is the next four elements to B and D is the next four elements to C.

Figure 4.17 shows the magnitude of tangential stress, σ_{yy} along x-axis, versus simulation time for the higher far field stress contrast of Berea sandstone model. Figure 4.17 (A) shows the first patch of four elements next to the wellbore on x-axis. After drilling is completed, the four elements reached to the maximum compressional stress magnitude and then gained another localised compressional stress during the stress

changes. The first element next to the wellbore took the highest compressional stress before it fails. The amount of compressional stress needed to fail the next three elements is less. Along x direction, the second patch of four elements indicated another localised stress which is an indication of second breakout (see Figure 4.17 B). The remaining two patches (three and four) of eight elements have similar behaviour and they do also indicate additional breakouts along x - axis (Figure 4.17 (C) & (D)).

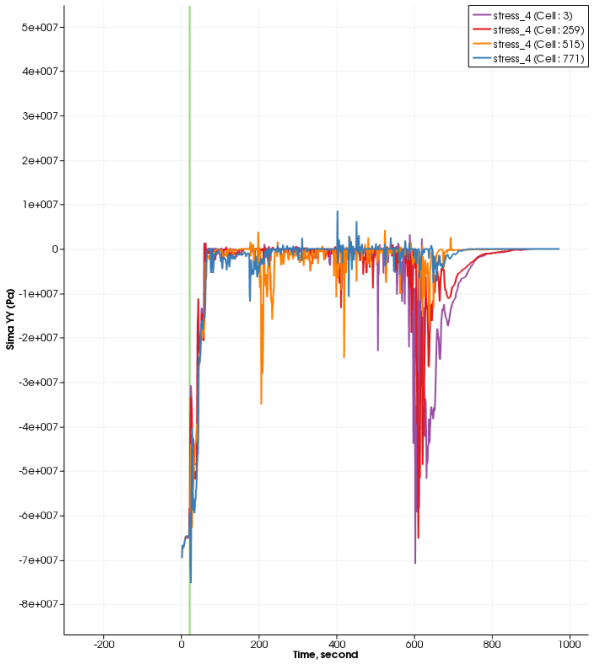

A

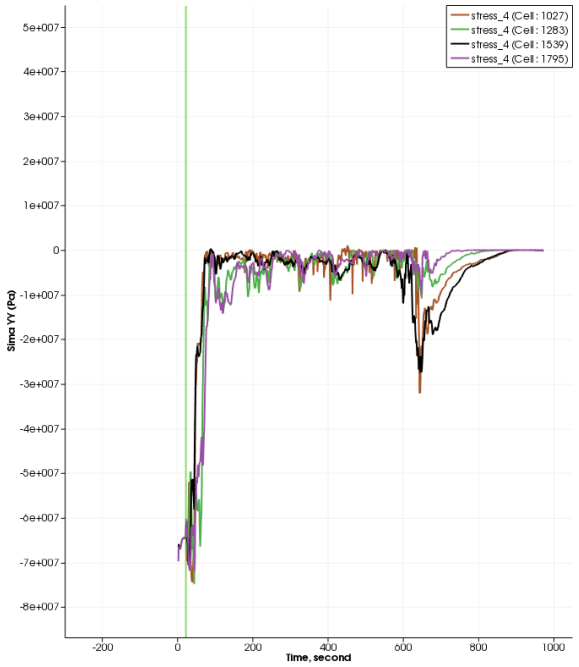

B

C D

Figure 4.17: Tangential stress versus time in Berea sandstone (σ_H = -70MPa, σ_h = -30MPa). Note: A is the first four elements adjacent to wellbore along x-axis, B is the next four elements to A, C is the next four elements to B and D is the next four elements to C.

In the following section, I will introduce some of the lab experiments done on Berea sandstone and some other sandstone samples. These experiments show the effect of drilling under the far field loads. My simulation showed similar fracture pattern observed in a some lab experiments. I intend to show the failure pattern only in the following lab experiments and show that FEMDEM code can be a reliable tool to validate against lab work.

4.6 Some Lab experiments examples

Here I show some lab experiments on Berea and some other sandstone samples. A fracture like breakout has been observed and reported in loosely bounded particles of Berea sandstone block (Haimson, 2003). A V-shape or dog-eared breakouts have been also reported by Haimson for low porosity Berea sandstone (see Figure 4.18). Haimson (2003) reported in his experiment an increase region of breakout in Berea sandstone due to the increase of the major principal stress.

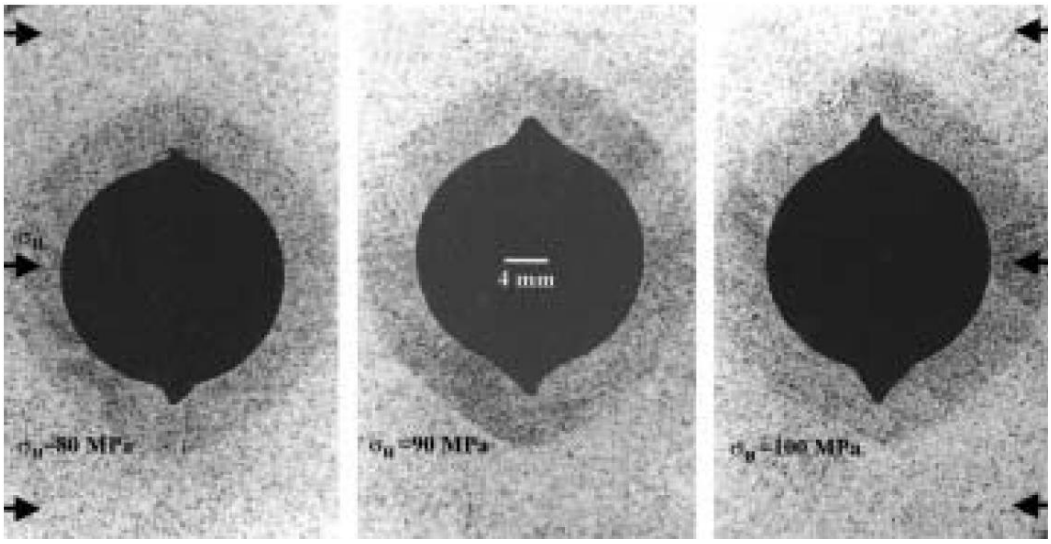

Figure 4.18: Photograph of Berea sand stone under σ_v = 50 MPa, σ_h = 60 MPa, and σ_H varying from 80 to 90 to 100 MPa. (Courtesy of Haimson 2003)

In figure 4.19, a scaled block of sandstone rock type was examined in a lab experiment by Rawling, Barton, Bandis, Addls and Gutlierrez (1993). The block was subjected to three far field loads; vertical stress (σ_v = 1MPa), maximum horizontal stress (σ_H =

0.6MPa) and minimum horizontal stress (σ_h = 0.6MPa).The borehole was created while a small stress was applied to the block sample inside the polyaxial test. The result show a significant reduction in wellbore volume by almost 40% and fracture propagations around the wellbore were observed.

Figure 4.19: photograph of sandstone sample shows the fracture geometry around the drilled borehole (curtesy of Rawling et al, 1993)

Multiple breakouts are shown by an experiment performed in CSIRO labs where intersecting conjugate shear failure planes occurred. As a result, the wellbore enlargement observed (Figure 4.20). A simulation study was carried out to capture the growth and type of fractures pattern observed in lab experiment (Figure 4.20). The model was subjected to far field loading of σ_H = 63MPa and σ_h = 31.5MPa. The failure was dominated by shear

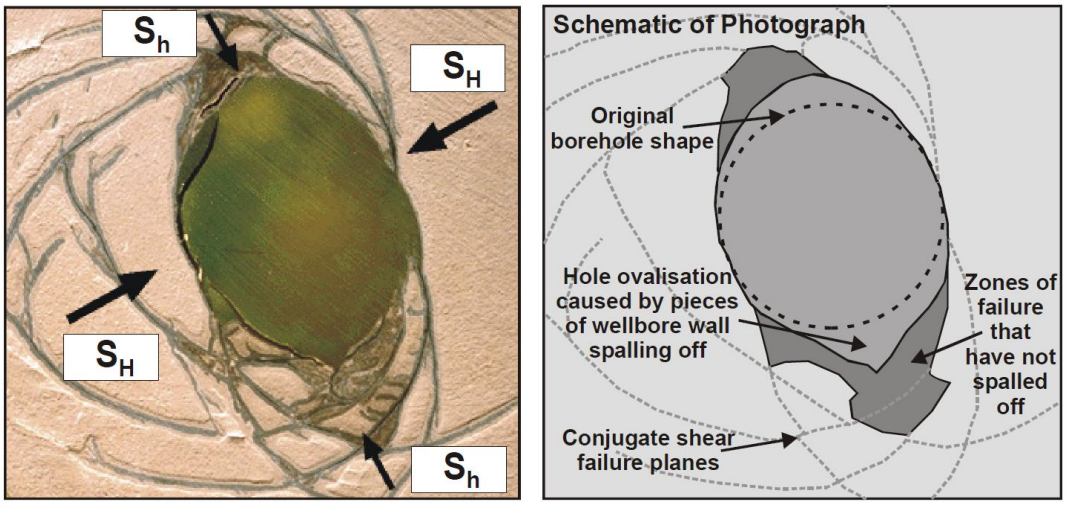

Figure 4.20: Figure shows results of a hollow cylinder lab test simulating borehole breakout (2 unequal horizontal stresses) - CSIRO Division of Geomechanics (J. Reinecker et al., 2003)

4.7 Summary

A series of 2D FEM drilling models of realistic stress states for four sandstone samples are presented. All models were subjected to two different far field loads; a low stress magnitude where σ_H = -20MPa, σ_h = -10MPa and a high stress magnitude where σ_H = -70MPa, σ_h = -30MPa. The combined finite-discrete element method (FDEM code) is utilised to create the results. The tangential, radial and shear stresses are calculated and analysed for each model. The fracture propagation patterns and type of failure are presented for each rock type. After stress state initialization, a progressive reduction of rock stiffness is performed in the region to-be-created hole for each model. The analysis show that the level of stress disturbance in the sandstone Y and Z samples are much larger than in the sandstone X model. The wellbore is significantly less stable when the model is subjected to higher far field stress load. A multiple shear failure occurs around the wellbore in all models except for the sandstone model low far field load. In the claystone model, fractures away from the to-be-created hole are developed prior to drilling. A 2D Berea sandstone drilling model is created and subjected to the same far field loadings used in the previous models. Berea model shows multiple breakouts regions along x-axis. The fractures away from the borehole are also created during drilling. The fractures patterns are somehow similar to the one observed in a laboratory tests performed on sandstone lab samples. Detailed drilling analysis and stimulation responses on Berea sandstone will be presented in the next Chapter.

Chapter 5 – Simulating Hydraulic Fracturing

5.1 Introduction

In Chapter Three, I examined the models which can be selected for use in calculating the post-drilling mechanical state near a wellbore. That analysis reveals that there is a major difference between the methods that calculate stress states in a plate that has a pre-existing hole, and the method that excavates (drills) a hole in a pre-loaded region. I concluded that the excavation, or drilling, approach is likely to be closer to reality, as it captures the physics more realistically. In Chapter Four, I extended the numerical methods still closer to reality by allowing the rock material to fail as a consequence of the drilling process and the resultant perturbed stress state near the wellbore. Those outcomes establish a range of starting points, which exhibit altered stress states and already-failed rocks, for the process of well stimulation that is known as hydraulic fracturing.

In this Chapter, I continue to employ the FDEM simulation tool, and use it to examine how a post-drilling new loading of the wellbore results in the propagation of failures away from the opening into the rock mass. The stimulation-caused failures start at the wellbore wall as shear fractures, with the composite failure zone then extending further away from the wellbore via combinations of shear and opening-mode fracturing.

For the simulations presented in this Chapter, I use the Berea sandstone material that was employed in Chapter Four. I tuned the fracture energy toughness (Mode I and Mode II), which are available parameters in the FDEM model, so that the results are similar to those created using SAVFEM, which does not have a fracture-growth capability. This choice enables me to make a comparison between the FDEM results and those calculated by a continuum method (SAVFEM) which uses a well-calibrated poro-mechanical model of Berea sandstone. The purpose of the comparison of these methods is to give some insight into how well the continuum method might capture the physical processes of the drilling and stimulation, albeit in a framework without induced discontinuities. The comparisons show a similar calculated response, which points towards the use of continuum methods where these are better suited to other aspects of a larger problem.

5.2 Background

Wellbore stimulation engineers are usually presented, by the work of drilling engineers, with a well that is ready for the stimulation job: either as an open-hole completion, or as a cased-hole with liner and cement. Here I consider a case without liner/cement. The state of stress in the reservoir, prior to stimulation, is usually assumed by stimulation engineers to be a version of Kirsch's solution with a pre-existing hole. Then, following the arguments first posed by Hubbert and Willis (1972), it is typically assumed that the imposition of high fluid pressure inside the wellbore causes a breakdown of the wall rock when the bottom-hole pressure reaches or exceeds the least-stress at the wellbore wall. Based on the Kirsch-type analytical expressions, this location is the intersection of the wellbore and the direction of greatest in-plane stress (the y-direction in my work). According to the Kirsch solution, the tangential stress at this point is $= ((\sigma_H + \sigma_h)/2) \times [1+ R^2/r^2] - ((\sigma_H - \sigma_h)/2) \times [1+ R^4/r^4] \times \cos(2\Theta)$. The concept that is typically applied is that the wellbore fluid pressure is able to invade a pre-existing discontinuity in the rock, with the fluid pressure able to "overcome" the least stress and cause the crack to open. That initial opening is argued to cause a local stress concentration at the tip of the crack, which assists in propagating that crack parallel to the maximum in-plane stress (in the y-direction, in the arrangement selected in this thesis). Thus, the breakdown pressure is normally assumed to be equal to the magnitude of the smallest in-plane stress (ignoring cohesion terms).

I showed in Chapter Three that the quantitative difference between the analytical and the FEM pre-hole elastic models, for the low stress loading case, is 10% to 20%, and more for the medium and high stress cases. Although it could be argued that these differences are small enough to be somehow included in the remaining property uncertainty, they could impact the mud weight design, during drilling, or the estimation of the fracturing pressure needed to stimulate a well. A much larger difference was shown for the elastic drilling case, on the order of 50%. Even greater effects were seen in the models described in Chapter Four, where rock failure was enabled. These model results show shear-like deformations at the wellbore wall in the x-direction. These were compared with experimental outcomes that reveal similar patterns of localized deformations propagating away from the borehole wall as it is drilled. Borehole images of wells can show the aftermath of such failures (in cases where they have occurred), which agree with the patterns as calculated by the FDEM simulations. Although borehole images show features that are compatible with the simulations, the images do

not provide evidence of what has happened further away from the wellbore wall, and we have to rely on the simulations to assist in making estimates of those situations.

5.3 Numerical Models

In this model, elements are randomly generated and refined around the wellbore (Figure 5.1). The model consists of 4316 elements and 2199 nodes. It is initialized by boundary tractions of σ_H = -20MPa and σ_h = -10MPa to create an initial stress state. After equilibration from these loads, the model's external boundary is set to a zero velocity (a non-strain boundary condition). The following properties for the numerical model are those for Berea sandstone: E = 20GPa, ν = 0.38, μ = 0.3, ρ = 2650kg/m^3, viscous damping = 1.83E+6kg/(m.s), cohesion = 1.4E+7kg/(m.s^2), tensile strength = 6E+6 kg/(m.s^2), G_I = 750,000N/m, G_{II} = 1,500,000N/m. The model size is 2000mm high by 2000mm wide. The radius, R, of the region which will be drilled out, is 100mm. As before, the drilling is simulated by progressive reduction of the stiffness of the elements that lie within that initial circle, ending with a zero stiffness (so they play no role in the subsequent calculations).

For the finite element method, I use the SAVFEM code (Couples et al., 2007). The model is constructed by 8442 elements and 8555 grid points within the same 2000mm x 2000mm domain. Within the capabilities of the formulation used in SAVFEM, the same loading is used (the difference is how the nodes are treated at the model corners; the results below indicate that this difference is not relevant to the problem investigated here).

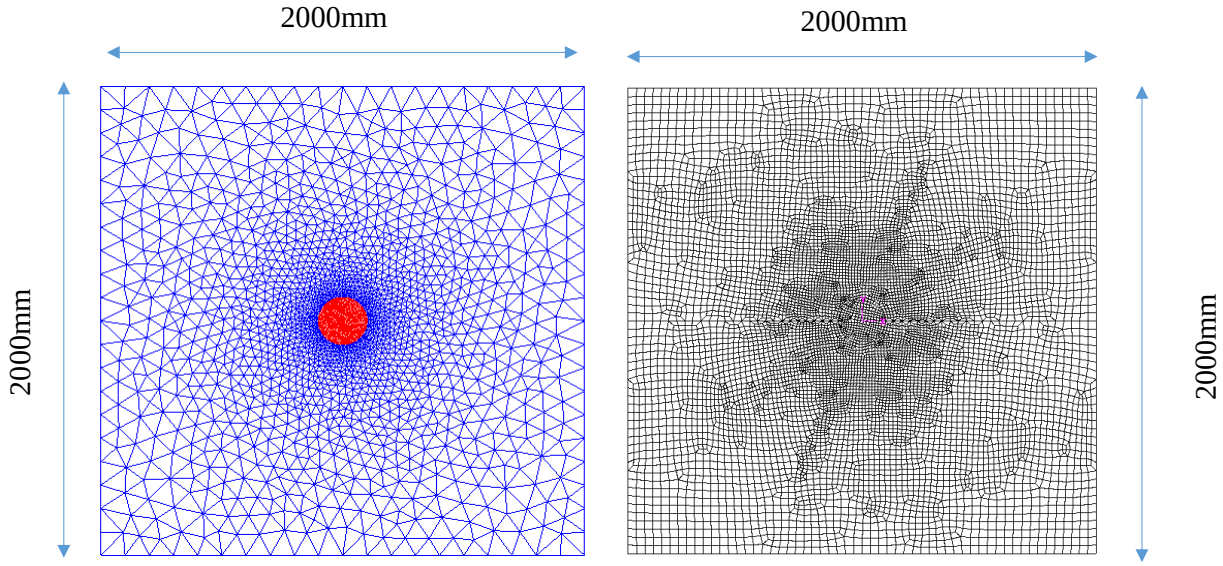

Figure 5.1: FDEM model (left) and SAVFEM model (right)

The overall stress distribution between SAVFEM and FDEM models are in good agreement (Figure 5.2). Due to the difference of the mesh structure between the models, it is not possible to make node-by-node comparisons, but the stress state at critical locations (e.g. along the wellbore wall at the symmetry axes) is almost identical as depicted by the Mohr-circle plots (Figure 5.4 and Figure 5.5). At the wellbore walls along the x-axis, σ_y is a compressional stress with a magnitude of -44.83MPa and -44.62MPa for the SAVFEM model and FDEM model, respectively. Under this loading, for these material properties, the drilling process does not induce any non-elastic response in either simulation.

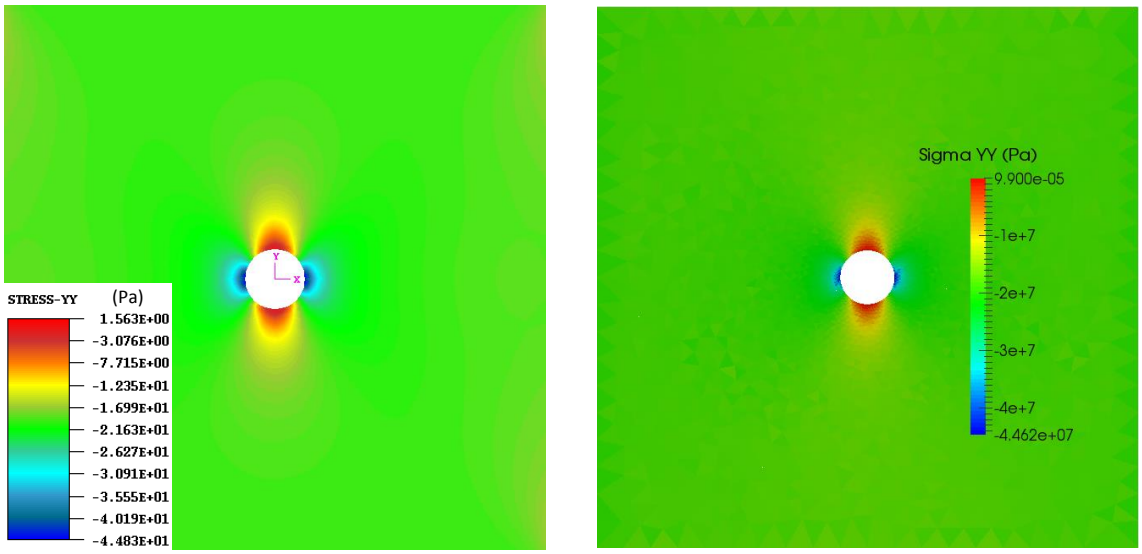

Figure 5.2: Stress plot of σ_{yy} in Pascal for SAVFEM model (left) and FDEM model (right)

After the drilling is completed, the wellbore wall is loaded with a pressure equal to approximately ~55MPa (the breakdown pressure) (Figure 5.4); this is the pressure that occurs when the mass rate is set to 800,000 mass/sec. This pressure replicates the mechanical effect of pumping fluid into the well space without allowing any invasion into the matrix pores. This loading causes fracture-like features to propagate away from the wellbore into the previously-intact rock mass. In the FDEM simulation, the "fluid" pressure (as assigned inside the wellbore) acts also on the open fracture faces after these discontinuities form from the initial continuum configuration.

The nominal configuration resulting from this simulation/loading case is that the deformation arrangement is more-or-less aligned with the direction of the major far-field stress. A closer inspection of the fracture initiation in the FDEM model reveals that the type of failure at the early stage of this propagation is dominated by shear failure near the wellbore. The SAVFEM model, which has a poro-mechanical material law,

shows a sub-planar zone of plastic deformation that forms in the same direction as the failure zone seen in the FDEM model. In the SAVFEM simulation, there is no additional "fluid" loading acting within the plastic strain region, yet there is substantial similarity in response that emerges from the two simulation approaches. This similarity points towards the idea that the induced deformation is a mechanical process and is not related to alterations of effective stress due to fluid invasion into the pore space.

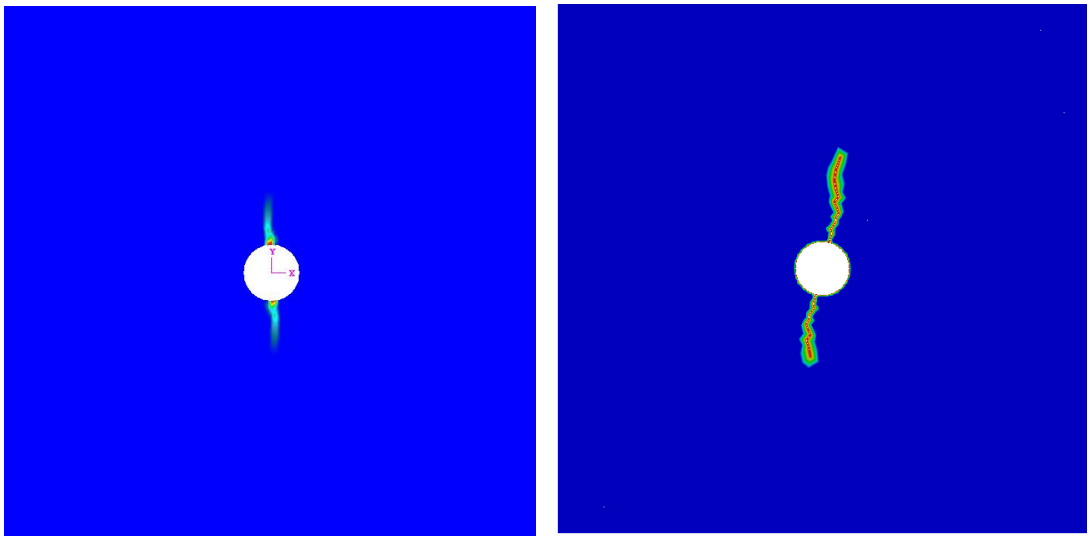

Figure 5.3: hydraulic fracture propagation in SAVFEM model (left) and FEMDEM model (right)

To quantify the comparison between SAVFEM and FDEM models, two points near and away from the wellbore are selected along y and x axes and plotted on Mohr-Coulomb chart (Figure 5.4 and 5.5). The results are in good agreement between the two models. The differences between the two models are in the range of 1% to 3% which is acceptable.

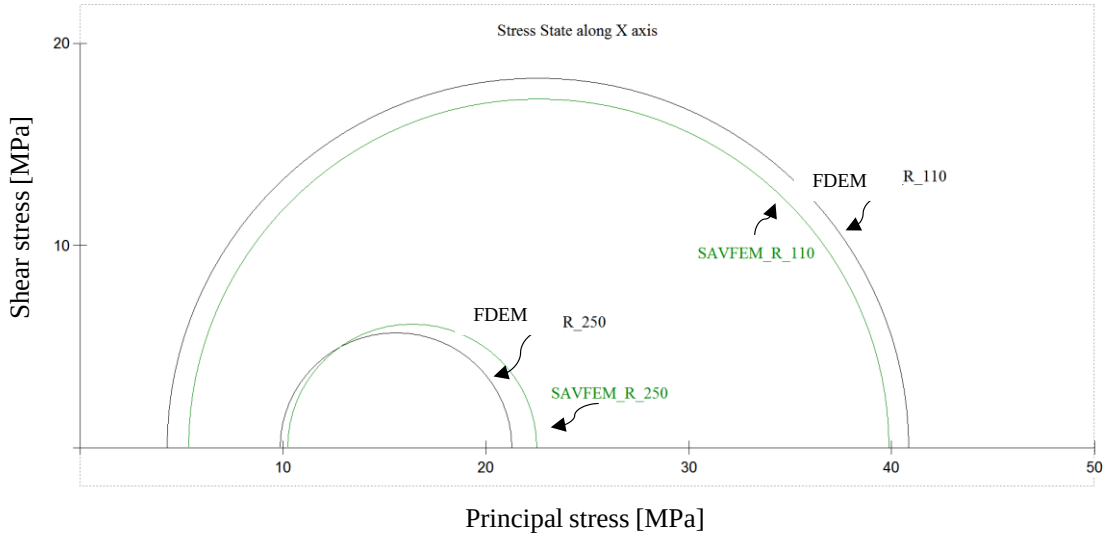

Figure 5.4: stress state plot for FEMDEM and SAVFEM model along x-axis, at r = 110mm and r = 250mm.

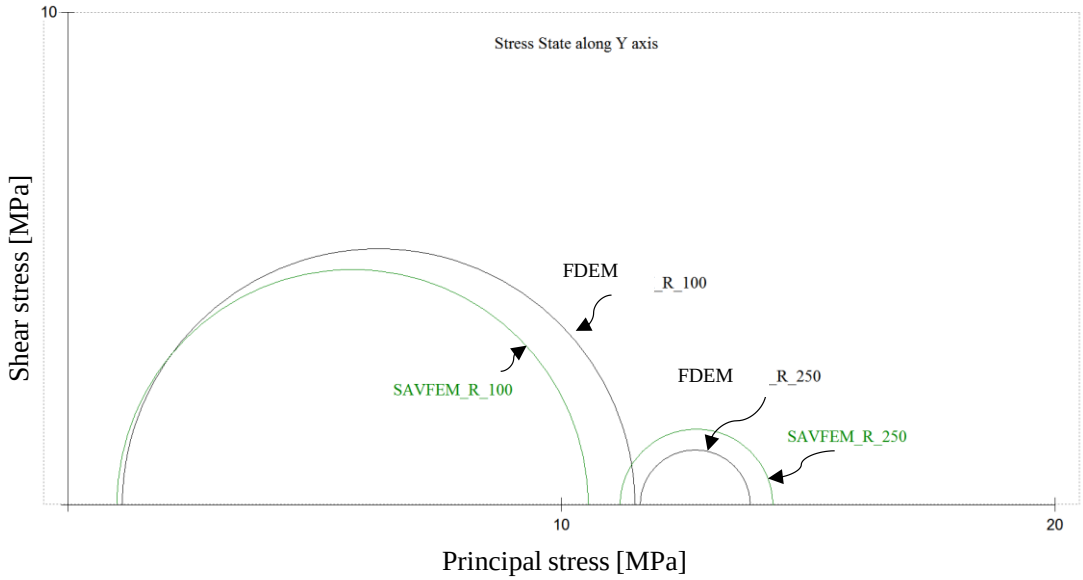

Figure 5.5: stress state plot for FEMDEM and SAVFEM model along x-axis, at r = 110mm and r = 250mm.

In the following section, I will discuss and analyse the FDEM model only under the low stress case and a high stress case.

5.4 Stress State Analysis

Here, I analyse the mechanical state around the wellbore at three different simulation stages (stage one: after drilling (A); stage two: prior to fracture initiation (B) and stage three: at fracture initiation (C)). I will examine the magnitude of displacement of the wellbore wall, the direction and magnitude of the major and minor principal stresses at the region containing the to-be-created fracture, and the mode of failure of the fracture initiation. Later, I will demonstrate and analyse the fracture propagation as a function fluid pressure.

After drilling, the wellbore radius becomes smaller in both x and y directions, as noted in Chapter Three (Figure 5.6 (A)). The maximum displacement in the y and x directions is 0.1715mm and 0.05264mm, respectively. The same wellbore geometry displacement was observed in Chapter Three for the low far field loading case. Prior to the fracture initiation and at the fracture initiation stages, the wellbore diameter has slightly enlarged due to pressure build up inside the borehole (Figure 5.6 (B) (C)). The nodes in the

region of the to-be-created fracture are moving into two directions with varying small angles as a result of the wellbore displacement.

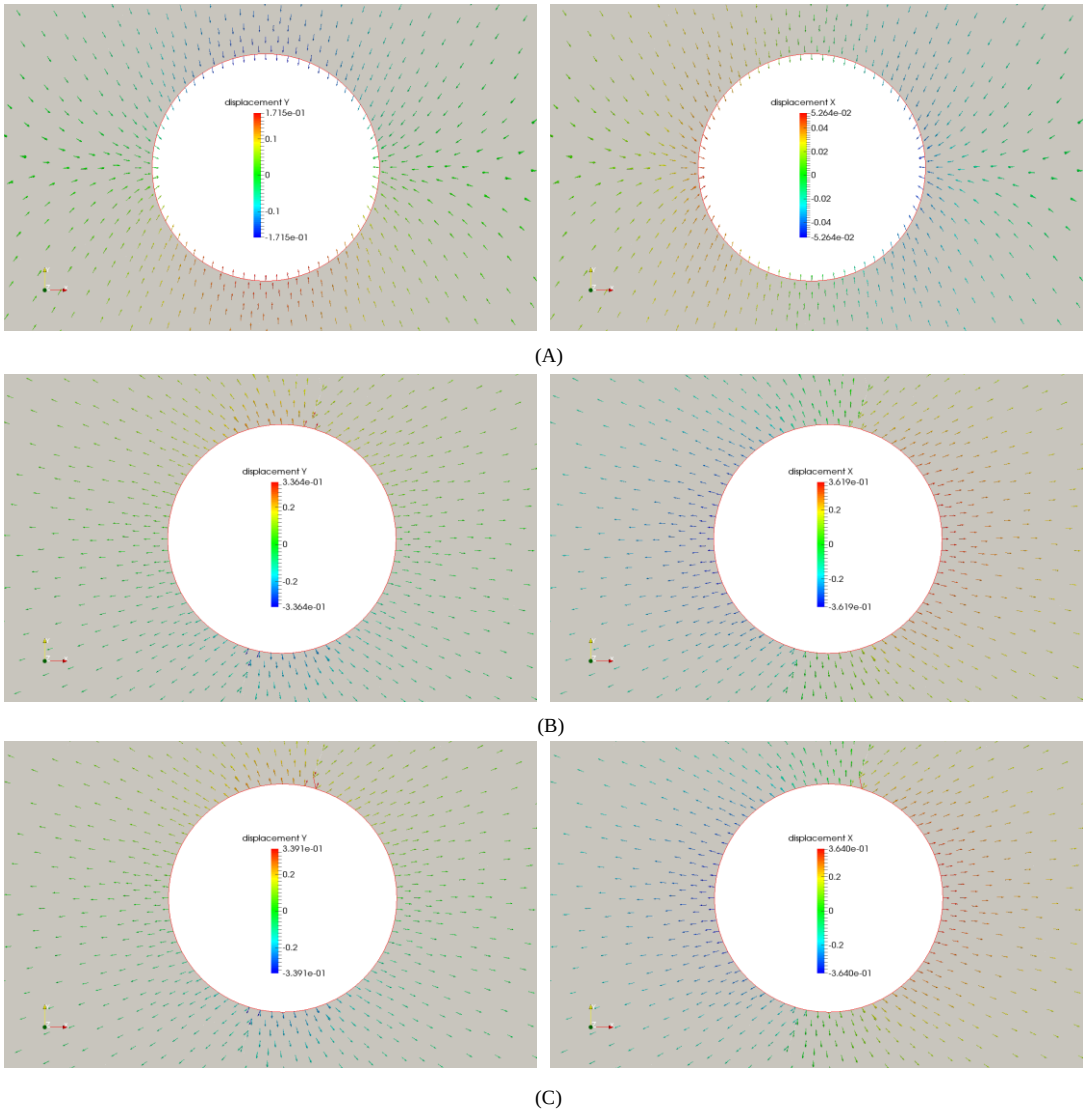

Figure 5.6: wellbore displacements (enlarged view) after drilling (A), prior to fracture initiation (B) and at fracture initiation (C). The arrows show the displacement direction and magnitude of the nodes

By enlarging the picture into the region of the to-be-created fractures (Figure 5.7), it is possible to see that this region has displaced prior to fracture initiation in anti-clockwise rotational way. In other words, the wellbore wall breaks as a result of the displacement acting on the borehole wall. The fluid entered this broken wall to continue propagating the fracture. Later, I will show how the fracture propagates further into the model.

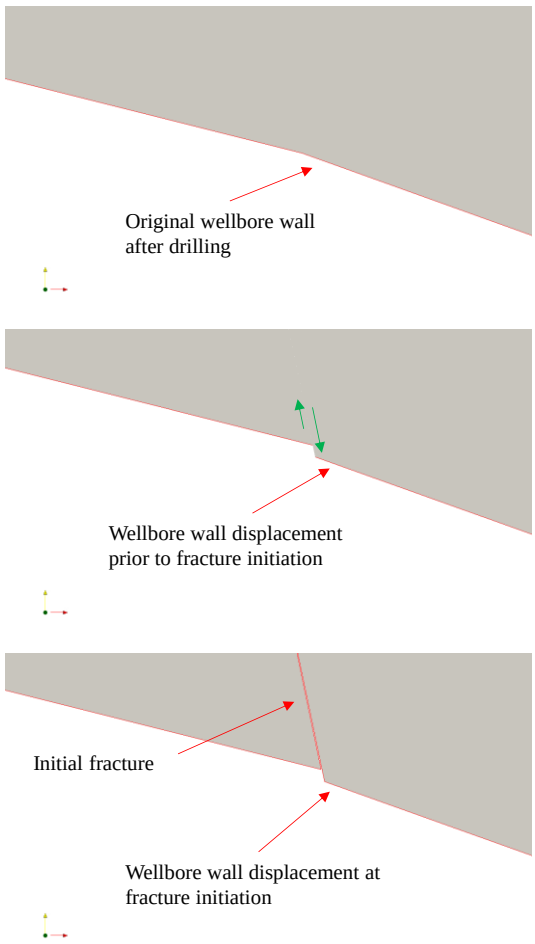

Figure 5.7: wellbore wall displacement at the region to-be-created fracture (this is an enlarged view)

I will focus on the region of the "to-be-created" fracture for the remainder of this analysis. The tangential stress at the fracture initiation region is compressional (Figure 5.8). The compressional state originated due the wellbore wall displacement which creates localised shear planes at this region. The direction and magnitude of the major and minor stresses are shown in Figure 5.9 for the region to-be-created fracture. After drilling (Figure 5.9 (A)), the differences between the major and minor principal stresses are very small, which indicate that the region has not yielded or failed. The principal stresses orientation for stage A are diverging along y axis and converging along x axis. Prior and at the initiation (Figure 5.9 (B) and (C), the differences between the major and minor principal stress become larger which indicates the possibility of yield or failure. The orientation of the major stresses are radially distributed toward the wellbore pressure load while the orientation of the minor stresses are perpendicular to the major stresses (Figure 5.9 (B) and (C)). The increase in radial compressive stress is an indication of the strain caused by the ballooning of the wellbore opening. When the fracture propagates as a function of the fluid pressure, the principal stresses are altered

and show maximum compression in different directions around the fracture "tip", creating high stress regions Figure 5.9 (D)).

To investigate the role of displacement on the stress state at the region to-be-created fracture, Mohr-Coulomb plot is created for the first element that got displaced and eventually broke (Figure 5.10). I calculated Phi, Ɵ, based on the magnitude of principal stresses from the element and used the input parameter of the cohesion to derive the shear slope envelope in the plot. The Mohr-Coulomb circle A and B intersect the envelope which indicate that the element has reached its shear failure. The direction of the stresses are different due to the build-up of pressure and the way that the strains become arranged in locally-variable patterns.

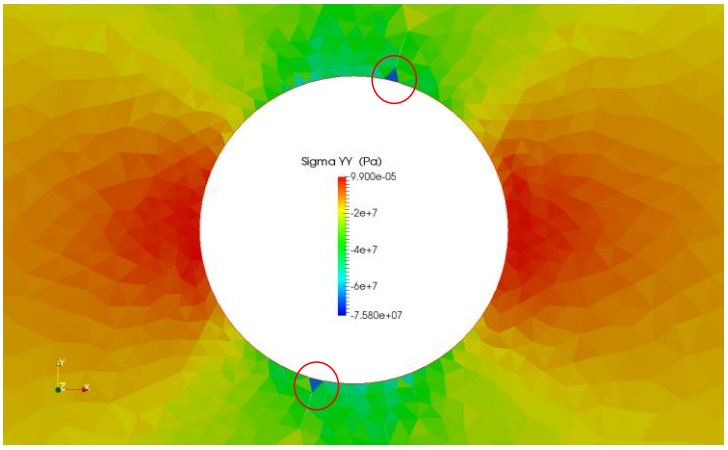

Figure 5.8: enlarged view of wellbore for the tangential stress prior to fracture initiation. The red circle marks the region to-be-created fracture.

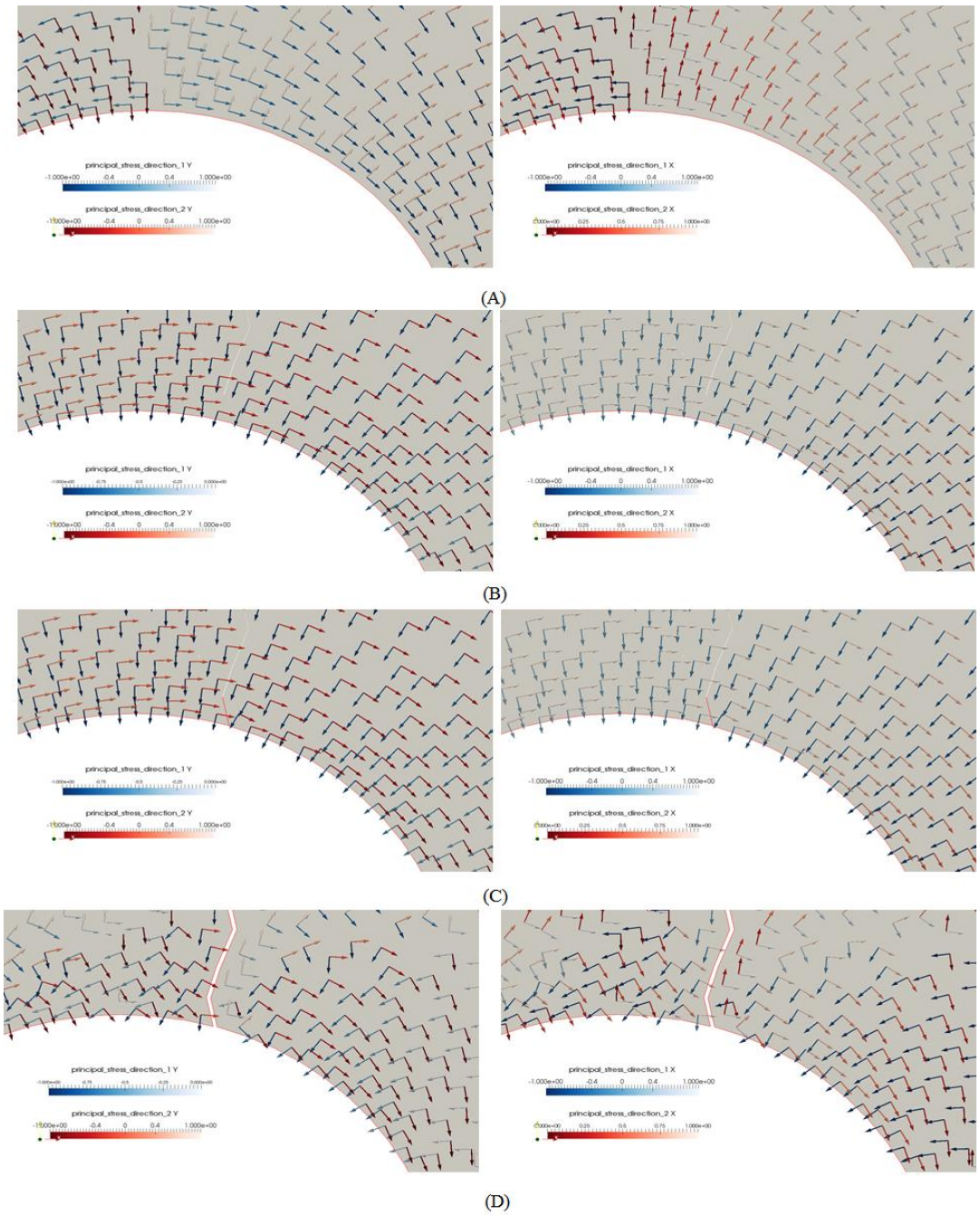

Figure 5.9: Enlarged wellbore images for the major and minor principal stress. (A) stress state after drilling, (B) stress state prior to fracture initiation, (C) stress state at fracture initiation and (D) stress state after fracture propagation

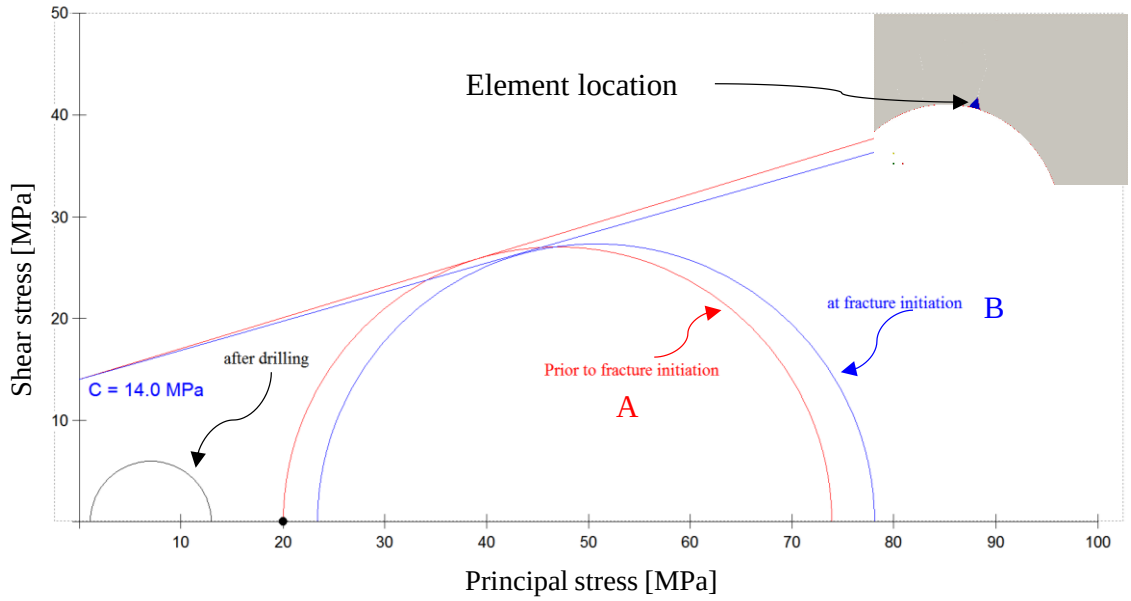

Figure 5.10: stress state al the location to-be-created fracture. (A) stress state prior to fracture initiation and (B) stress state at fracture initiation

The mode of failure is shown in Figure 5.11 for FDEM model. The failure is initiated at the wellbore wall with shear (mode II) type. This behaviour supports the argument by Callanan (1981), Morgenstern (1962), Liunggren, Amadei, Stephansson (1988), Panah, Yanagisawa (1989), Lo, Kaniaru (1990) and Mori, Tamura, Fukui (1990), whom argued that the fracture initiation is the result of shear failure and not a tensile failure.

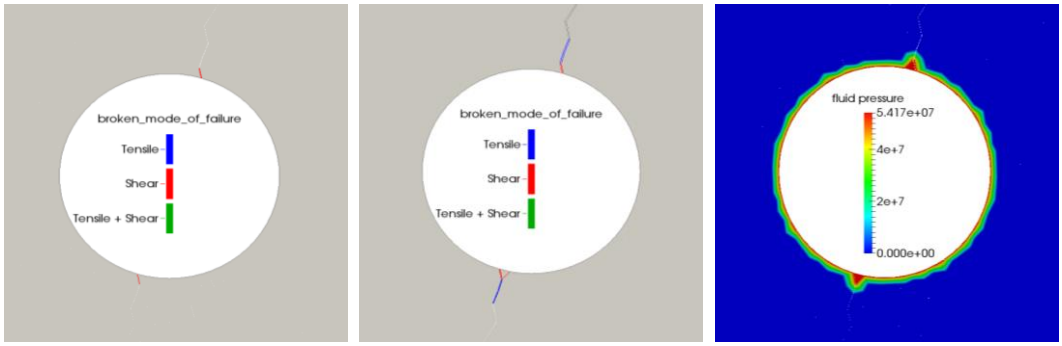

Figure 5.11: initial fracture (left image), fracture propagation in (middle image) and fracture initiation pressure (Pa) in FEMDEM model for ~55 MPa wellbore pressure (right image)

Figure 5.12 shows the hydraulic fracture propagation and related wellbore breakdown pressures. The fracture propagates overall in the direction of the major stress, but not necessarily as a Mode I failure; instead it is a composite zone. The pressure inside the fracture acts as a load on the fracture's wall causing it to create displacements around the propagated fracture. In the following section, I will select few elements ahead of the

fracture and a few elements from one side of the fracture to investigate the possibility of shear/failure in the surrounding elements by created fracture.

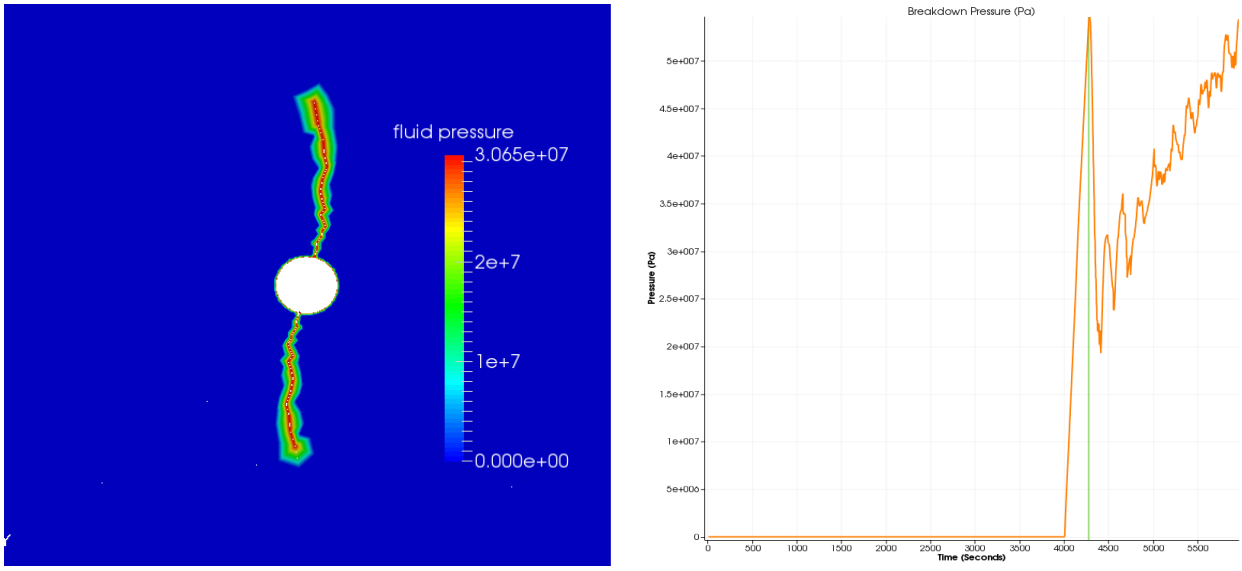

Figure 5.12: hydraulic fracture breakdown and propagation pressure

Figure 5.13 show three elements close to the fracture in Mohr-Coulomb plot. All elements have reached the shear failure criterion as a result of the displacement of the fracture wall. There is no visible fractures on these element due to the size of the mesh. I kept the element size in this region relatively larger to save on the computational time and memory space.

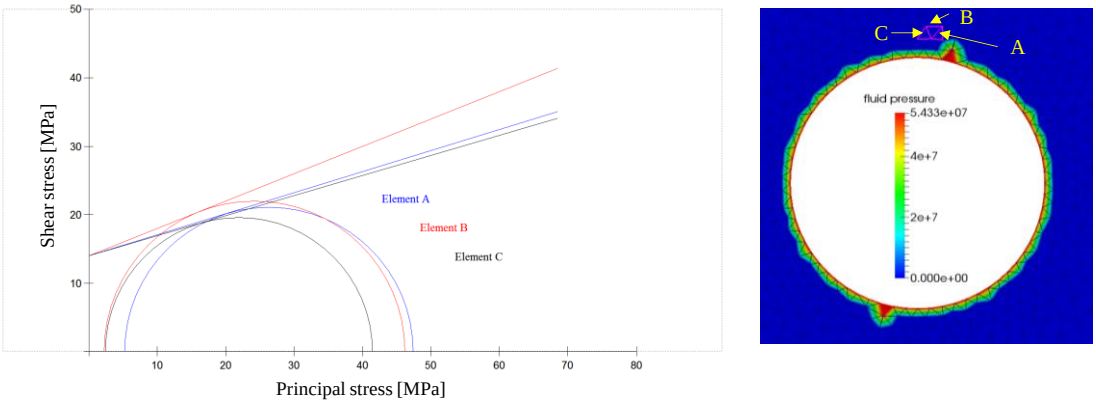

Figure 5.13: stress state and shear envelop of three elements adjacent to the fracture.

Note: the stress state is calculated when the fluid pressure propagates into the fracture.

As the fracture propagates, the displacements become larger. Three elements are selected ahead of the fracture tip to examine the stress state before the fluid comes into the fractured elements (Figure 5.14). The results show that the stress state ahead of the fracture tip is already yielded before entered the broken element and open the fracture in a tensile mode type. The tension is created in a “process zone” ahead of the growing fracture.

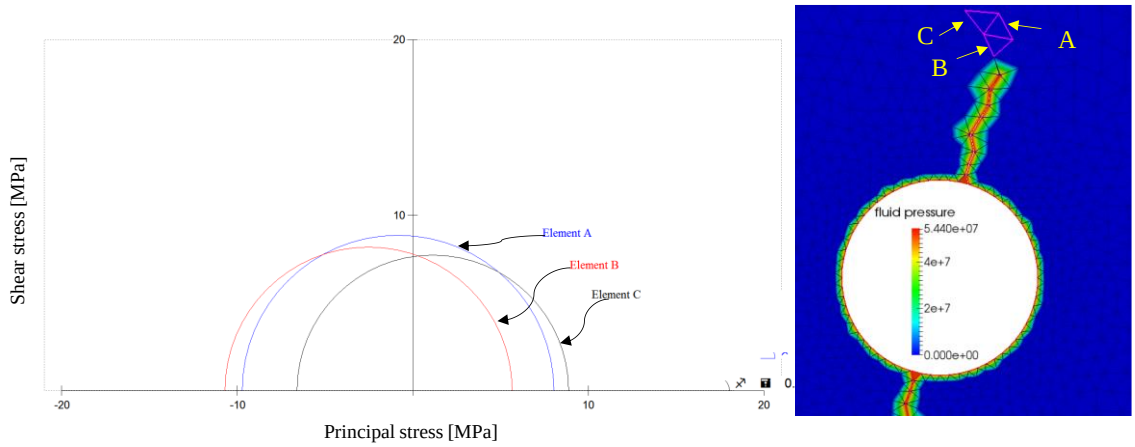

Figure 5.14: stress state of three elements ahead of the fracture tip

The state of stress, prior to stimulation, has a major contribution in predicting the fracture initiation and propagation. Inadequate assumption for predicting that state could leads to major consequences such as high operation cost, low productivity and inaccurate field planning.

The propagation of the fracking fluid is shown in Figure 5.15. As the fluid propagate inside the hydraulic fracture, the fracture exhibit tensile (mode I) stress at the tip of the fracture.

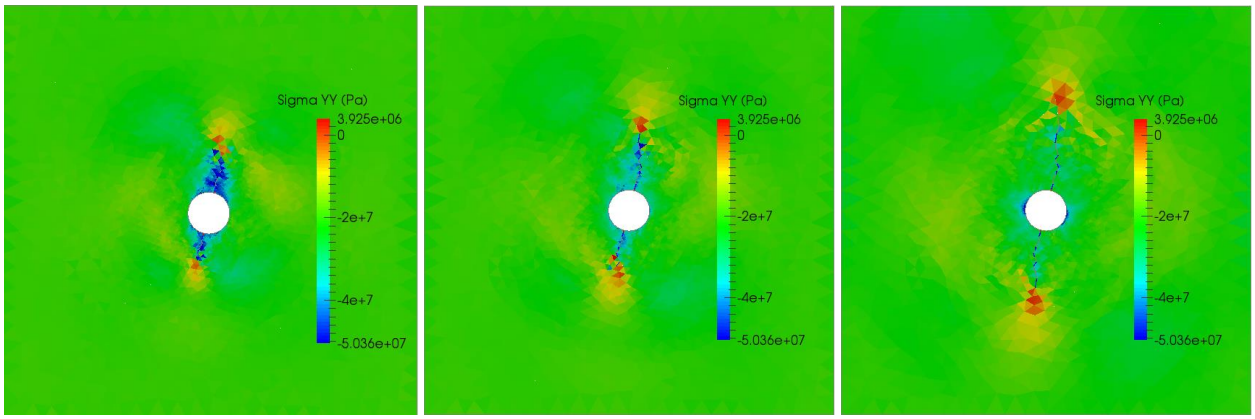

Figure 5.15: plots of σ_{yy} stress with fracture propagation for σ_H = -20MPa, σ_h = -10MPa

5.5 Energy Toughness Sensitivity

In the previous model I tuned the energy toughness (Model I and Mode II) in the FDEM model to derive comparable results with the SAVFEM model. Here, I will vary the energy toughness for testing sensitivity and demonstrate the resulting fracture deformation geometry and type for each model. I used the same Berea sandstone data from the previous analysis, except for the changes in toughness.

Figure 5.16 show the tangential state of stress and mode of failure for Berea sandstone model in high case (A), medium case (B) and low case (C) energy toughness. The low

case exhibits four distinct shear fractures around the wellbore. The high and medium cases show no failure around the wellbore. After drilling, the stress state difference between the medium and low cases is small while the high energy case difference is larger (the high case shows an up to ~25% difference than in the medium and low cases along y-axis and ~6% and 15% difference than in medium and low cases respectively (Figure 3.17)). Note: the percentage difference calculated above is based on the major stress value between all cases.

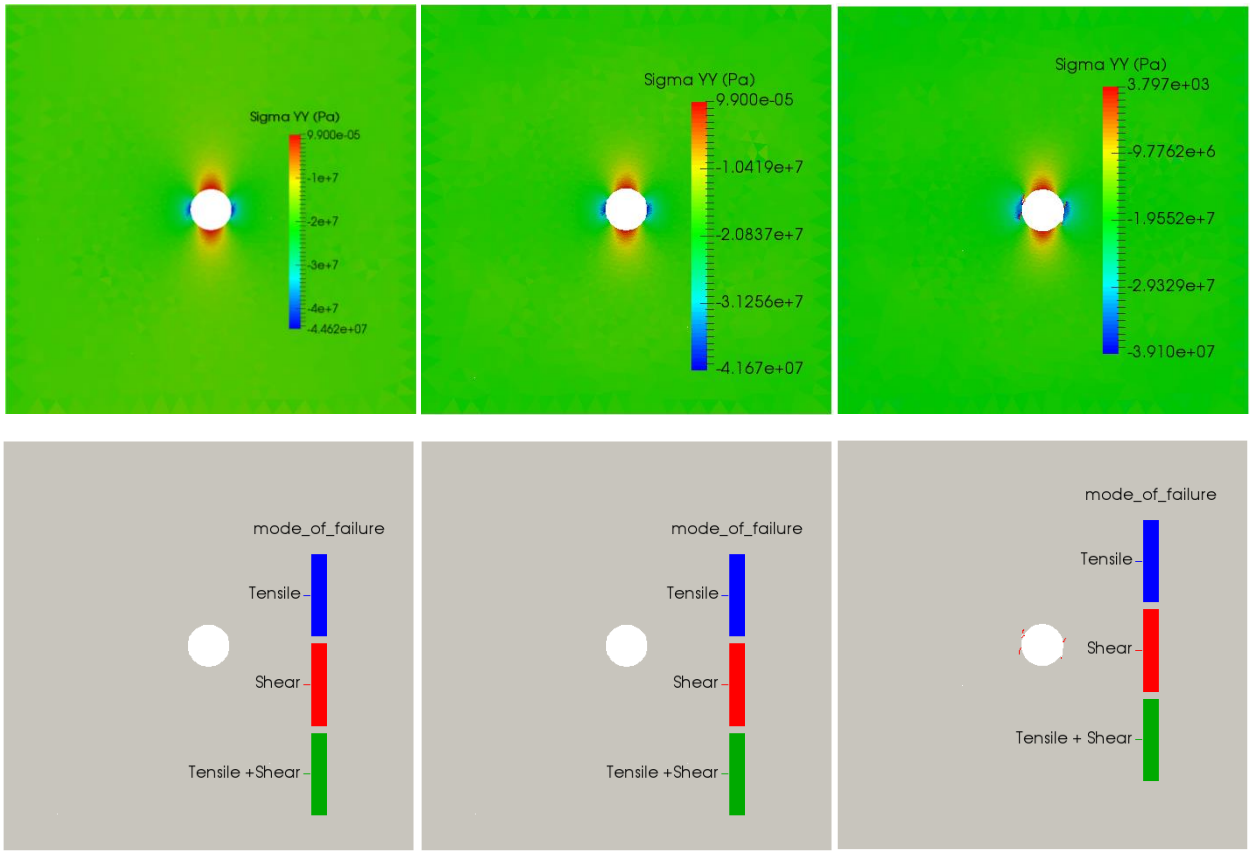

(A)
Mode I = 750,000N/m,
Model II = 1,500,000N/m

(B)
Mode I = 100,000N/m,
Model II = 200,000N/m

(B)
Mode I = 4600N/m,
Model II = 28,000N/m

Figure 5.16: tangential stress and mode of failure for the high (A), medium (B) and low (C) energy toughness cases.

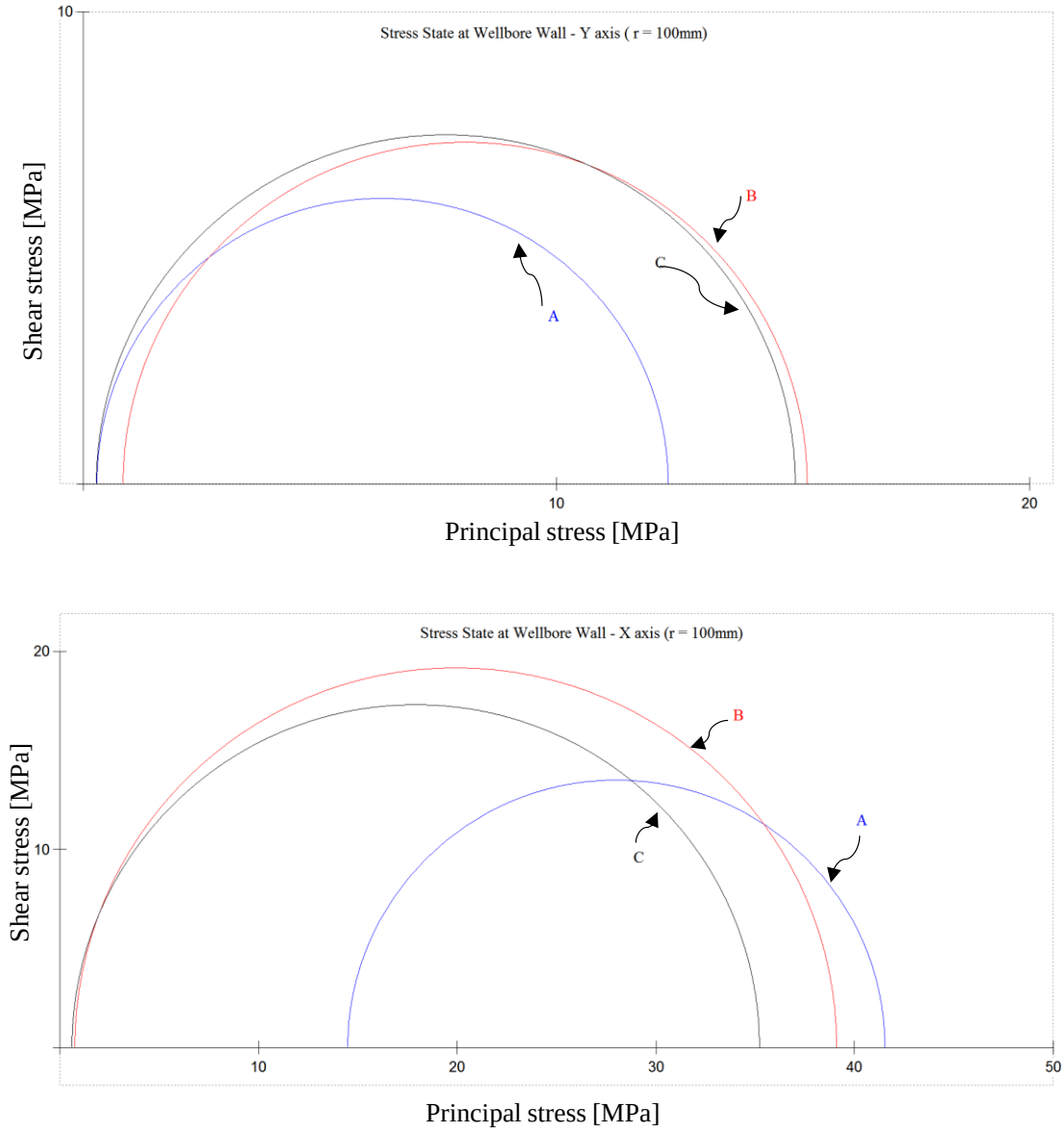

Figure 5.17: stress state at wellbore wall for the high (A), medium (B) and low (C) energy toughness cases

The fluid pressure and mode of failure for Berea sandstone model in the high, medium and low energy toughness cases are shown in Figure 5.18. The high case example was taken from the previous analysis for the sensitivity comparisons. The medium and low energy toughness cases are markedly different than in the high energy toughness case. As the fluid pumping continues, the fracture propagates in four directions for the medium and low cases. The energy toughness can play very important role during drilling and while stimulating the well. The model with lower fracture toughness exhibits more failure than the models with high energy toughness, as would be expected.

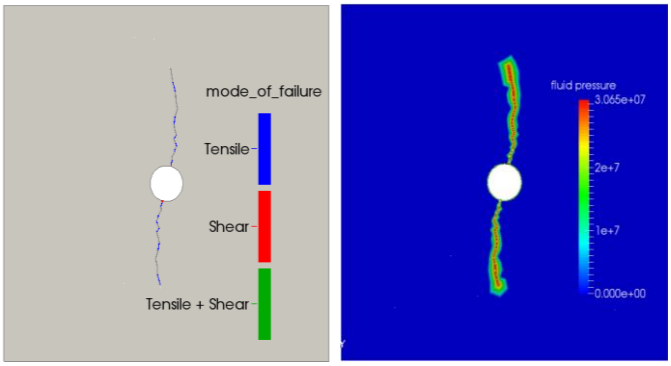

(A) Mode I = 750,000N/m, Model II = 1,500,000N/m

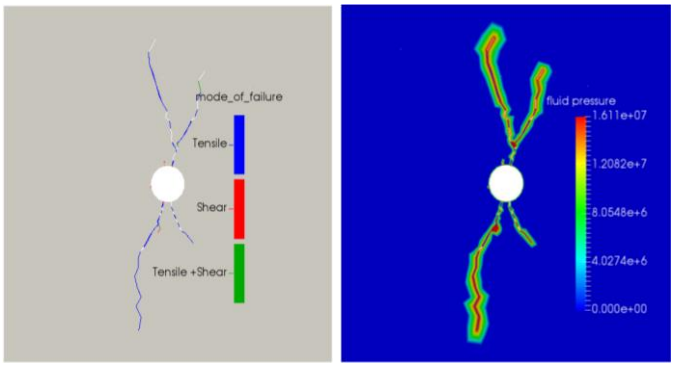

(B) Mode I = 375,000N/m, Model II = 750,000N/m

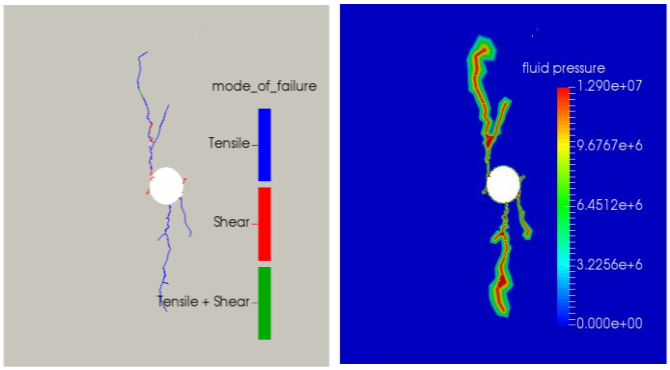

(C) Mode I = 4600N/m, Model II = 28,000N/m

Figure 5.18: mode of failure and fluid pressure images for the high (A), medium (B) and low (C) energy toughness cases. Note: changing the energy toughness influence the failure mode

5.6 Friction Coefficient and Cohesion Sensitivities

Here, I will examine Berea sandstone fracture geometry only by varying the values of the friction coefficient and cohesion. In this sensitivity, all model assigned to the same fracture energy (Mode I = 50,000N/m and Mode II = 100,000N/m). I developed models for the sensitivity scenarios and below is the summary outcomes after stimulation (Figure 5.19). Each model were initialized with far field load similar to the previous models and then drilled.

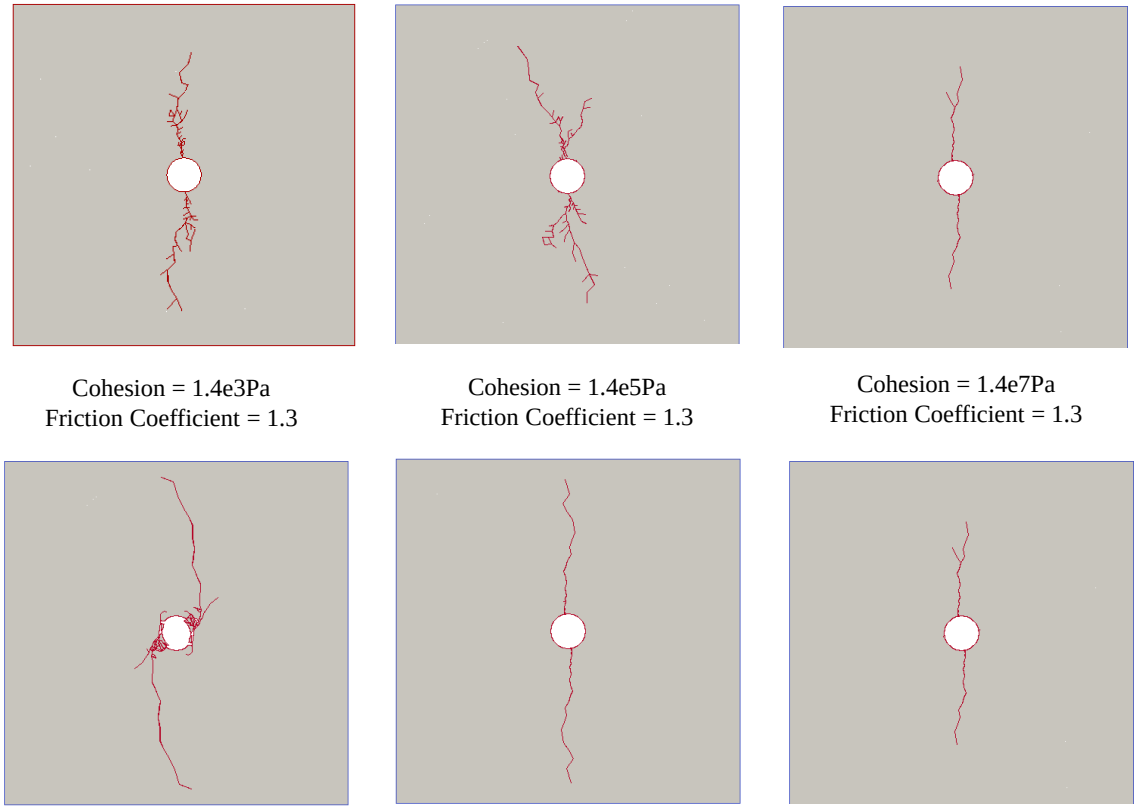

Figure 5.19: FDEM models for friction coefficient and cohesion sensitivities

5.7 Summary

In this chapter, I have investigated and analysed the mechanical state of the hydraulic fracturing treatment in 2D numerical model. I used the SAVFEM and FDEM codes to draw a comparison between the two methods by analysing the drilling and fracturing procedures for Berea sandstone property. SAVFEM code uses the finite element methods formulation while FDEM code uses the explicit numerical formulation of the combined finite-discrete element methods. The fracture energy toughness was tuned to illustrate a comparable results. The compression results between the two models are in good agreement with small differences due to the mesh size and type for each model. FDEM model was investigated and analysed in more details. The analyses were concentrated on the fracture region. The analysis includes wellbore displacement and stress state, displacement of the wellbore wall prior and at fracture initiation and stress state analysis ahead of the fracture tip and on the fracture side. The analysis revealed that the role of displacement has a major impact on rock deformation and the state of stress around the fracture. High shear stress concertation was found on the side of the hydraulic fracture as a result of the fracture's wall displacement. The region ahead of

the fracture tip was dilated before the fluid pressure reached that region. Also, the simulation results agreed with several researchers who argued that the fracture initiation occurred as shear failure. The fracture initiation result type is very dependent on the material properties of the rock (Tatone, 2014).

As mentioned before, the energy toughness was tuned to drive a comparable results with SAVFEM model. So I varied the values of the energy toughness (Mode I and Mode II) in FDEM model. The results demonstrated a significant difference when the energy toughness magnitude is lowered resulting in higher number of fractures after treatment. The stress state at wellbore were analysed and investigated. For low energy toughness case, the wellbore exhibits four distinct fractures before any fluid pumped into the wellbore. For the high and medium energy toughness cases, the two models show no failure around the wellbore wall. Later in this chapter, a friction coefficient and cohesion sensitivities were carried out. The analysis was limited to the investigation of the wellbore deformation after drilling and fracture propagation pattern. The outcomes were different for each model.

Chapter 6 – Discussions

Wellbore stability analysis, and stimulation design, both require a geomechanical analysis of the near-well region, with both seeking to understand the local state of stress and how this may control the next response: such as failure of the wall of the well, or the growth of a fracture away from the well. In many cases, the geomechanical analysis is carried out using simple models that define a simple state of stress. The simplest such model is the one provided by Kirsch (1898), which employs the stress-function approach to derive stress states via analytical expressions. Possibly the next-most-simple model type is the numerical method in which the FEM is used to calculate stresses in an elastic material that contains a pre-existing hole. I showed in Chapter Three that the analytical and pre-hole numerical models are almost the same for the low far-field load, but that the analytical expressions do not equal the solution to any numerical model with any set of elastic material properties. I demonstrated that the analytical expressions cannot be a correct elastic solution for the case of a circular hole in a plate; this analysis raises concerns over the general validity of the stress function approach, although I will not attempt here to examine that possibility further.

I showed that a numerical model, in which the 2D plate is pre-loaded to a given far-field state of stress, and then a circular hole is excavated, leads to markedly different stress states in the near-well region, with perhaps a factor of two difference in stress components at the wellbore wall. I reasoned that these substantial differences, between a pre-hole (or analytical) model, and the one with drilling, are due to the re-arrangement of internal loads (stresses), and hence energy, as the hole is excavated. The stress-state differences, between the pre-hole case and the drilling case, are present to distances of +/-0.5metres away from the wellbore wall. Because the "drilling" model is a better representation of the physical processes that must operate during the creation of a hole, I concluded that the drilling model is a better reference state for use in wellbore stability analysis or for designing or understanding stimulation processes.

I extended my investigations by allowing the rock materials to become non-elastic as a result of the loading (either the pre-drilling state, or the one created by the drilling process). Those simulations showed wellbore breakout patterns that are very like those seen in laboratory experiments, and also as inferred from observations of boreholes and

tunnels. These outcomes reinforce the claim that the drilling method of simulation is a closer representation of physical reality.

I then used the drilling method to establish a post-drilling state which is then used as the basis for simulating hydraulic fracturing. I considered several rock types and far-field stress states to examine how the breakdown occurs as the wellbore pressure is increased. I was able to show that the process is dominantly mechanical, associated with increasing the circumference of the wellbore, and not one where the fluid pressure plays a major role in creating the initial fracturing. Growth of fractures to large distance is likely to be possible only due to the mechanical loading associated with the injected fluid, but the initiation is better explained as a straightforward rock mechanics response.

I have restricted my investigations to mechanics and hydraulics, and have not considered thermal effects or those related to chemical processes. Nor have I investigated the role of effective stress, whether this is caused by fluid invasion or from induced poro-elastic changes of pore-pressure related to the straining of the rocks (or the changes in stress associated with any changes in pore pressure). The reason for the focus on the pure mechanics of the wellbore is because of the likely dominant role for these processes to the wellbore stress state problem. If we physically understand how the wellbore behaves mechanically, the issue of introducing other impacting factors such as thermal and chemical become more realistic to the overall problem. So solving the mechanics first is an essential part to understand how wellbore reacts mechanically.

Most of the wellbore stability approaches use models with a pre-existing hole or derived mathematically based on that assumption. Here I discuss generally the methods used to analyse wellbore stability problem.

A possible reason for the discrepancy that was found, between the analytical solution, and the pre-hole FEM solution, is that the FEM software is faulty. I discount this on the basis of two arguments: the code implementation has been examined by many users, and I have run the code on some simple elastic problems (not with a stress function answer) and its results agree with those cases. Therefore, the discrepancies exist for some other reason.

The FEM method, as we all know, applies loads to a configuration defined by the person creating that model. The loading causes the model domain to deform (elastically, and then possibly in inelastic ways, but I have not allowed that to happen in the examples shown in Chapter three). During this calculated deformation, material points move, which are typically reported as nodal displacements. Such displacements happen with the FEM simulations described here. The square boundaries move, and become non-straight. In the pre-hole model, the nodes that started as being located on a perfect circle move also. They move inwards, but in such a way that they form a slight, approximately-elliptical shape. In the drilling model, the nodes that lie along the to-be-created hole were also located along a perfect circle before loading, and they also move inwards when the far field load is applied, and again as the "hole" material is removed, so they move more than do the same nodes of the mesh of the pre-hole model. The two FEM models represent different physical processes: in the pre-hole model, the concept is loading of a plate with a central hole; in the drilling model, the concept is to create a hole in a plate that previously has a uniform state. The drilling model seems much closer to what we predict and anticipate to occur when we create an opening in the already-loaded subsurface.

In contrast, the analytical model maintains the traction conditions along certain coordinate-defined surfaces (lines) that are fixed in space. Although these lines are often called "boundaries", they do not terminate the solution, which is still defined across the whole of the space (both inside the hole and beyond the model out to infinity). The tensile radial stress that is calculated "inside" the hole – at $r < 100mm$ – is a manifestation of the constraint of $\sigma_{rr} = 0$ applied at $R = 100mm$. In a model that has compressive-stress boundary tractions, the material would move towards the centre, as it does in the FEM solutions. The condition of $\sigma_{rr} = 0$ at $R = 100mm$, can be interpreted as "pulling" the central region outwards into a circular shape, away from the strain configuration it would have with just the far-field loads. Seen from another frame of reference, the condition of $\sigma_{rr} = 0$ occurs at a constant distance $R = 100mm$, and that condition does not change when the material (conceptually) moves across that line. The stress-free circle could be expected to exist only in an unloaded state, and is not compatible with the far-field loads. The analytical solution devised by Kirsch was clever, but not physically sensible. It served a purpose when numerical simulations did not exist, but that is not the current situation.

Similarly, the tractions on the exterior of the analytical model are constant along coordinate lines. This latter point is not the case for Kirsch's original "infinite" model, of course. However, that is not important, as Saleh's solution is almost indistinguishable from the Kirsch solution when the model size exceeds 1500mm, as our example does. The Saleh solution is not strongly influenced by its introduction of a finite "boundary", and this is not the basis for the discrepancies around the central "hole".

I assert here that the FEM pre-hole model is the correct solution (barring numerical round-offs) to the problem of a square region, containing a hole, loaded by far-field tractions. As noted above, the circumference of the hole moves inwards, differentially. The FEM drilling model is asserted to be the correct solution to the problem of a square region, loaded to a given far-field state, with a circular region subsequently excavated in its center. The outline of the to-be-excavated region starts as a circle in the unloaded state, and becomes an ellipse after the far-field load is applied, and then distorts again as the material inside is removed. If we accept these assertions, then we know the displaced coordinates around the initial circle. When we re-calculate the analytical solution with these coordinates, the radial stress component is tensile, while the tangential stress component is slightly altered to a value closer to that of the numerical solution. However, the changes in magnitudes are far smaller than are the discrepancies, so the answer cannot be that we are comparing states from different locations. There is simply a fundamental difference between the analytical solution(s) and those derived from numerical simulation of a mechanical process.

The pre-hole model is slightly dis-similar to the analytical solution, but the drilling model calculates stress states that are very different, in locations close to the wellbore. Choosing one model over the other leads to a significant difference in the state that is calculated – with differences on the order of 2x. Since these calculated post-well states are used as the starting point for other assessments, the choice should be made on the basis of which modelling approach best captures the physics of the real process. The approach that meets this criterion is the FEM drilling model. Plumb and other (2000) presented a geo-mechanical model (the Mechanical Earth Model) to improve wellbore drilling stability control and reduce drilling cost of the exploration wells in the Gulf of Mexico. The stress was initially designed using a classical mechanical model (a pre-hole model). Plumb and other had to reduce the far-field stress 2x smaller to get the prediction to work. The results agree with my approach presented in Chapter three and

that the calculated stress in the FEM drilling model is smaller by a factor of 2 than in the FEM pre-hole model. This reinforce that the classical geo-mechanical model (a model with a pre-existing hole) has issues with predicting a state of stress prior to drilling a well 50% higher than what is anticipated.

Although in Chapter Three we have used the simulation software in such a way as to preclude any non-elastic responses, the code is designed to simulate the creation and operation of discontinuities. Those simulation capabilities have been examined and analysed using the FEM drilling model approach to calculate a mechanical state prior to simulating a well stimulation process, which is calculated after setting the failure criteria to realistic values. An example of the fracture distribution calculated via this workflow is shown in Chapter five. The fracturing is dominated by shear fractures and shear movements, and propagates away from the well. The hydraulic fracture propagate in the same way as in the SAVFEM code, which adopts a poro-mechanical material model. I discounted any discrepancies in the FEMDEM code based on the simulation outcomes from SAVFEM model. SAVFEM results are in good qualitative agreement with FEMDEM results.

The capabilities of the FEMDEM code are substantial. Lisjak and others (2015) have demonstrated the capability of the 3D code in simulating a fluid-pressure-induced fracture nucleation and growth in rock samples. In their study, a three-dimensional (3D) hybrid Finite-Discrete Element Method (FDEM) is used to investigate the complex fracturing behavior around a stimulated wellbore. FDEM (a 3D version of FEMDEM) is an explicit numerical method which combines continuum mechanics principles with discrete element algorithms to simulate multiple interacting deformable fracturable solids. Using FDEM, the stimulation process is modeled in an unconfined 10in x 10in x 10in cube of Indiana limestone with an internal cavity of 1.5in (diameter) x 3in (height), 2in below the cube surface. The pressure pulse is applied on the perimeter of this cavity. The simulation results are verified against laboratory experiments (Al-Nakhli et al, 2014).

The simulation results shed light into the complex fracture growth regime around the cavity. As the pressure pulse is applied, fracturing initiates in Mode I (tensile) on top of the cavity (Figure 7.1). At later stages, Mode II (shear) fractures also develop alongside Mode I fractures and on the periphery of the cavity. This fracturing mechanism continues for as long as the pressure is applied until full rupture of the block. In general,

the simulation results illustrate good agreement with experimental findings including fracture patterns and breakdown pressures. As a result, suitability of 3D FDEM to model the complex rock.

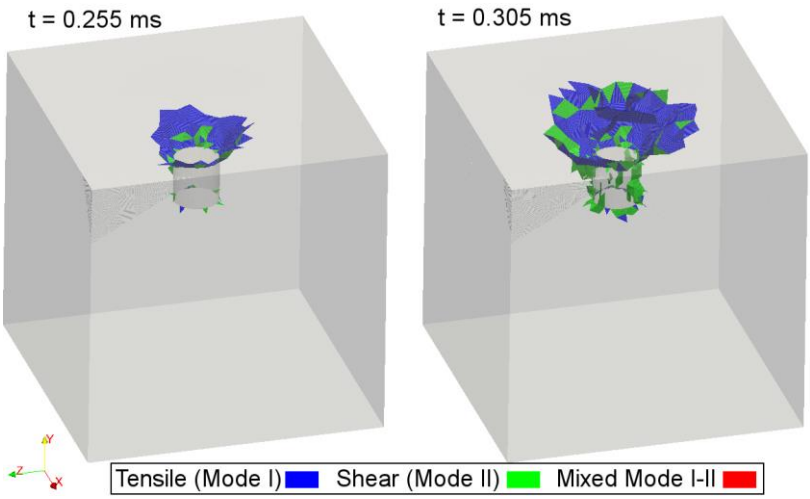

Figure 6.1: mode of fracture after applying pulse pressure (from Lisjak et al., 2015)

On the natural fractures network, the code has showed its vast capability. Grasselli and others (2014) showed the effect of pre-existing discontinuities on the hydraulic fracture initiation. Their model clearly shows that existence of discontinuities results in the initiation of several fractures around the wellbore circumference rather than a bi-wing fractures as generated under the assumption of homogenous conditions (Figure 7.2). The fracture propagate by a pressure-driven load in an anisotropic rock formation with horizontal bedding planes characterised by a horizontal stress of 10 MPa and a vertical stress of 5 MPa. In blue are tensile cracks and in red are shear cracks.

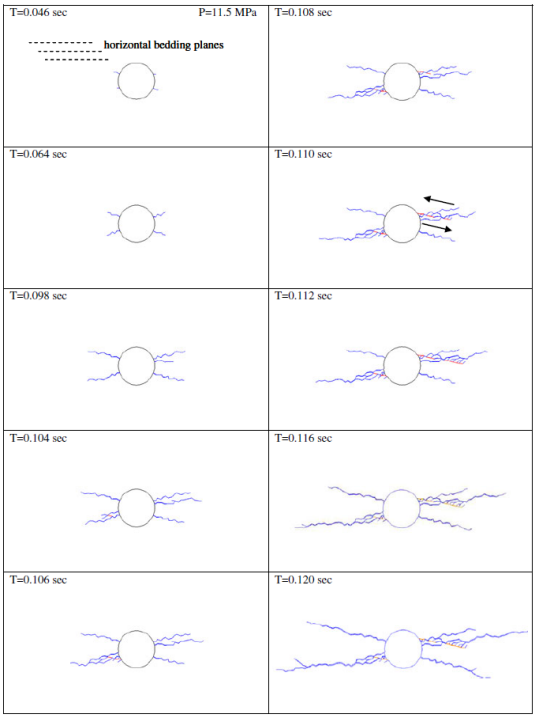

Figure 6.2: fracture propagation in horizontal bedding planes (obtained from Grasselli et. al. 2014)

Several other numerical examples in the mining industry have demonstrated the capability of FEMDEM code in simulating a realistic mechanical deformation of rocks in mines and sea cliffs (Lisjak et al., 2015; Zhao et al., 2015; Grasselli et al 2013)

Chapter 7 – Conclusions

In this chapter, I summarise the key findings and conclusions of this research. Future research work and recommendations are also outlined below.

7.1 Key Findings and Conclusions

- The analytical expressions (here, Saleh's solution) that calculate stresses around an opening are an invalid mechanical solution for the case a circular hole in a plate composed of an elastic solid. The analytical expressions calculate stress component values, at the margin of the hole, and elsewhere in the model domain, that are not like those calculated by the closest-possible model arrangement that uses the FEM simulation method. There are NO combinations of elastic material properties where the analytical and numerical methods agree. Although the differences may only be on the order of 10% or less, there is no consistency in terms of analytical always being larger or smaller, compared to the numerical. The differences, and the analysis they have provoked, reveal a fundamental truth about the analytical solutions: namely, that they are not the solution to an elastic problem, but instead are simply an approximation that was appropriate at a time long ago when proper computation was not routinely feasible.

- In cases with a low far-field load, and while continuing to assume that the material can remain elastic, the stress state calculated by Saleh's solution (a version of Kirsch equation) is only slightly dis-similar to the FEM pre-hole model, but the FEM drilling model calculates stress states that are very different in locations adjacent and near the wellbore. For the medium and high far-field loads, the differences are much larger. Choosing one model over the other leads to a significant difference in the stress state that is calculated – with differences on the order of 2x for the low far-field load, and higher for medium and high far-field loads.

- When the material is allowed to respond in a non-elastic fashion, via either a simple Mohr-Coulomb type of criterion, or via a more-realistic poro-mechanical behavioural model, there is potential for even larger differences between the

states calculated by analytical expression and those resulting from numerical simulation. These differences can extend to larger distances from the nominal wellbore location and result in altered stress states and potentially failed materials across large parts of the model domain. In cases where there is substantial amounts of material failure, the 2m x 2m domain used in this thesis is too small to capture the full process.

- The drilling model is a closer representation of the reality of the physical processes that must operate during the creation of the hole in a pre-stressed region. This statement applies both to cases where only elastic behaviour is admitted, or to those where rocks may fail or yield. Therefore, the "drilling model" approach is a better reference state for use in wellbore stability analysis, or for designing or understanding stimulation processes. The significant stress-state differences, between the FEM pre-hole and the FEM drilling models, are present to distances of +/-0.5metres away from the borehole wall, or further, if the far-field loading is near or at the yield limit of the material.

- The propagation mechanism of fractures, to larger distances, is likely to require the mechanical loading on the fracture faces which is associated with the injected fluid. However, the initiation of deformation at the wellbore wall, and propagation of deformation out to distances on the order of 0.5m, is better explained as a straightforward rock mechanics response to the enlargement of the borehole dimensions. At the borehole wall, the deformation is initiated in a shear (Mode II) type of response that is generally aligned along the far-field maximum loading direction. The fracture "zone" propagates overall in the direction of the major stress, but not as a Mode I failure; instead it is a composite zone that has both shear- and opening-mode responses that can be either tightly localised or somewhat more diffuse.

- In the hydraulic fracture simulations, the stress state ahead of the fracture tip has caused the material to yield before the fluid enters the broken element and hence could be responsible for opening the fracture tip in a tensile mode. The tension that may exist just beyond the crack tip is created in a "process zone" ahead of the growing fracture, associated with dilation of the overall zone, and also local shear strains as one side moves up and the other moves down. The rock walls

along the propagated fracture are likely to possess additional failures that exhibit significant shear (Mode II).

- The magnitude of the fracture toughness can affect the number of zones of fracture propagation. Low toughness leads to a higher number of the propagating fracture zones. Friction coefficient and cohesion parameters also play very important role in the stimulation treatment. Varying these values results in different fracture patterns.

- The hydraulic fracture propagates in the same way in the SAVFEM code, which is based on a poro-mechanical material model. SAVFEM results are in good quantitative agreement with FEMDEM results. Therefore, it is reasonable to discount the idea that the observed outcomes are somehow due solely to some flaw in the FEMDEM code. Instead, the correct conclusion is that the wellbore mechanics and hydraulic stimulation problems need to be evaluated with modern methods of geomechanics, as has been demonstrated herein.

- The outcomes of the drilling models reveal well-organised and repeatable patterns of localized deformations that propagate away from borehole wall as it is drilled. Lab experiments and wellbore images illustrates similar patterns as those observed in the drilling models simulated here. This type of comparison reinforces the claim that the numerical simulation approach, in a drilling mode, is capturing much of the physical reality.

7.2 Future Research Works and Recommendations

Here I list some topics which should be considered for follow-on research, to pursue ideas and issues identified in my thesis work:

1. Adapt the drilling model approach in a larger model domain using the FEMDEM and SAVFEM codes. This will help investigate the stress state around the wellbore at larger scale, and address questions concerning the role of close-by boundary constraints
2. Conduct actual designs for wellbore drilling, calculating a safe mud weight for that drilling, based on material properties and physical states. Selection of cases studies will need to assess quality of the data (material properties and far-field

loading) and the quality of the observed outcomes (stable or failed holes). The literature reports many examples of stability issues, but only some published works may have enough reliable information to enable a robust test of the approach.

3. Advance the fluid flow part of the code formulation, to investigate the role of effective stress, and poro-elastic effects. For models with a pre-existing natural fracture distribution, the fluid flow simulations need to be informed by current best-practice methods used in fractured –reservoir analysis.
4. Integrate other components, such as thermal and chemical effects, to analyse their role in altering the stress state around the wellbore and along the propagating zone of fractures.

REFERENCES

1. Tare, U.A. and Mody, F.K., 2002, April. Managing borehole stability problems: on the learning, unlearning and relearning curve. In *Proceedings of the 2002 AADE Annual Technology Conference, Drilling & Completion Fluids and Waste Management. April* (pp. 2-3).
2. Ewy, R.T., Myer, L.R. and Cook, N.G., 1994. Investigation of stress-induced borehole enlargement mechanisms by a liquid-metal saturation technique. *SPE Drilling & Completion*, *9*(01), pp.65-71.
3. Partin, U.T., Compton, M.T., Nelson, G.R., Livingston, D. and Davis, P., 2010, January. Advanced Modeling Technology: Optimizing Bit-Reamer Interaction Leads to Performance Step Change in Hole Enlargement While Drilling. In *IADC/SPE Drilling Conference and Exhibition*. Society of Petroleum Engineers.
4. Power, D., Ivan, C.D. and Brooks, S.W., 2003, January. The top 10 lost circulation concerns in deepwater drilling. In *SPE Latin American and Caribbean Petroleum Engineering Conference*. Society of Petroleum Engineers.
5. Tare, U.A., Mody, F.K., Mese, A.I., Jiao, D. and Hakimuddin, M., Halliburton Energy Services, Inc., 2003. *Real-time method for maintaining formation stability and monitoring fluid-formation interaction*. U.S. Patent 6,609,067.
6. Ali, A.H.A., Brown, T., Delgado, R., Lee, D., Plumb, D., Smirnov, N., Marsden, R., Prado-Velarde, E., Ramsey, L., Spooner, D. and Stone, T., 2003. Watching rocks change—Mechanical earth modeling. *Oilfield Review*, *15*(1), pp.22-39.
7. Farris, R.F., 1941, January. A practical evaluation of cements for oil wells. In *Drilling and Production Practice*. American Petroleum Institute.
8. Bradley, W.B., 1979. Failure of inclined boreholes. *Journal of Energy Resources Technology*, *101*(4), pp.232-239.
9. Drucker, D.C. and Prager, W., 2013. Soil mechanics and plastic analysis or limit design. *Quarterly of applied mathematics*, *10*.
10. Pariseau, W.G., 1968, January. Plasticity theory for anisotropic rocks and soil. In *The 10th US Symposium on Rock Mechanics (USRMS)*. American Rock Mechanics Association.
11. Hoek, E. and Brown, E.T., 1980. *Underground excavations in rock* (No. Monograph).
12. Paslay, P.R. and Cheatham Jr, J.B., 1963. Rock stresses induced by flow of fluids into boreholes. *Society of Petroleum Engineers Journal*, *3*(01), pp.85-94.

13. Aadnøy, B.S., 1987. *Continuum mechanics analysis of the stability of inclined boreholes in anisotropic rock formations*.
14. Westergaard, H.M., 1940. Plastic state of stress around a deep well.
15. Veeken, C.A.M., Walters, J.V., Kenter, C.J. and Davies, D.R., 1989, January. Use of plasticity models for predicting borehole stability. In *ISRM International Symposium*. International Society for Rock Mechanics.
16. Aadnoy, B.S. and Chenevert, M.E., 1987. Stability of highly inclined boreholes (includes associated papers 18596 and 18736). *SPE Drilling Engineering*, *2*(04), pp.364-374.
17. Cheatham Jr, J.B., 1984. Helical postbuckling configuration of a weightless column under the action of m axial load. *Society of Petroleum Engineers Journal*, *24*(04), pp.467-472.
18. Eaton, B.A., 1969. Fracture gradient prediction and its application in oilfield operations. *Journal of petroleum technology*, *21*(10), pp.1-353.
19. Matthews, W.R. and Kelly, J., 1967. How to predict formation pressure and fracture gradient. *Oil and Gas Journal*, *65*(8), pp.92-106.
20. Wilson, R.C. and Willis, D.N., 1986, January. Successful high angle drilling in the Statfjord field. In *SPE Annual Technical Conference and Exhibition*. Society of Petroleum Engineers.
21. Papanastasiou, P. and Zervos, A., 2004. Wellbore stability analysis: from linear elasticity to postbifurcation modeling. *International Journal of Geomechanics*, *4*(1), pp.2-12.
22. Hubbert, M.K. and Willis, D.G., 1972. Mechanics of hydraulic fracturing.
23. Bredehoeft, J.D., Wolff, R.G., Keys, W.S. and Shuter, E., 1976. Hydraulic fracturing to determine the regional in situ stress field, Piceance Basin, Colorado. *Geological Society of America Bulletin*, *87*(2), pp.250-258.
24. Stock, J.M., Healy, J.H., Hickman, S.H. and Zoback, M.D., 1985. Hydraulic fracturing stress measurements at Yucca Mountain, Nevada, and relationship to the regional stress field. *Journal of Geophysical Research B*, *90*(B10), pp.8691-8706.
25. Haimson, B., 1968. Hydraulic fracturing in porous and nonporous rock and its potential for determining in-situ stresses at great depth.
26. Schmitt, D.R. and Zoback, M.D., 1989, December. Poroelastic effects in the determination of the maximum horizontal principal stress in hydraulic fracturing tests—a proposed breakdown equation employing a modified effective stress

relation for tensile failure. In *International Journal of Rock Mechanics and Mining Sciences & Geomechanics Abstracts* (Vol. 26, No. 6, pp. 499-506). Pergamon.

27. Abou-Sayed, A.S., Brechtel, C.E. and Clifton, R.J., 1978. In situ stress determination by hydrofracturing: a fracture mechanics approach. *Journal of Geophysical Research: Solid Earth*, *83*(B6), pp.2851-2862.
28. Rummel, F., 1987. FRACTURE NMECHANICS APPROACH TO HYDRAUL| C FRACTURING STRESS NMEASURENMENTS. *Fracture mechanics of rock*, p.217.
29. Xie, L.M., Min, K.B. and Shen, B., 2014, August. Displacement discontinuity method modelling of hydraulic fracturing with pre-existing fractures. In *48th US Rock Mechanics/Geomechanics Symposium*. American Rock Mechanics Association.
30. Serati, M. and Williams, D.J., 2015. THE RING TEST UNDER GENERAL INTERIOR AND EXTERIOR LOADING. In *The 13th International Congress of Rock Mechanics-ISRM CONGRESS 2015*.
31. Mitchell, T.M. and Faulkner, D.R., 2006, December. On the Origin and Distribution of Fracture Damage Surrounding Strike-Slip Fault Zones. In *AGU Fall Meeting Abstracts* (Vol. 1, p. 07).
32. Zhou, Z., Mu, L., Li, X., Wang, W., Zhao, W., Wang, X., Bu, X. and Pang, P., 2012, January. Hybrid Fracturing Treatments Unleash Tight Oil Reservoirs Consisting of Sand/Shale Sequences in the Changqing Oilfield. In *IADC/SPE Asia Pacific Drilling Technology Conference and Exhibition*. Society of Petroleum Engineers.
33. Liu, X., Chang, Y., Lu, H., Chen, B., Li, J., Qi, Y. and Wang, C., 2012, January. Optimizing fracture stimulation in low-permeability oil reservoirs in the Ordos Basin. In *SPE Asia Pacific Oil and Gas Conference and Exhibition*. Society of Petroleum Engineers.
34. McLean, M.R. and Addis, M.A., 1990, January. Wellbore stability analysis: a review of current methods of analysis and their field application. In *SPE/IADC Drilling Conference*. Society of Petroleum Engineers.
35. Ito, T. and Hayashi, K., 1991, July. Physical background to the breakdown pressure in hydraulic fracturing tectonic stress measurements. In *International journal of rock mechanics and mining sciences & geomechanics abstracts* (Vol. 28, No. 4, pp. 285-293). Pergamon.

36. Clark, J.B., 1949. A hydraulic process for increasing the productivity of wells. *Journal of Petroleum Technology*, *1*(01), pp.1-8.
37. Perkins, T.K. and Kern, L.R., 1961. Widths of hydraulic fractures. *Journal of Petroleum Technology*, *13*(09), pp.937-949.
38. Nordgren, R.P., 1972. Propagation of a vertical hydraulic fracture. *Society of Petroleum Engineers Journal*, *12*(04), pp.306-314.
39. Khristianovic, S. and Zheltov, Y., 1955, June. Formation of vertical fractures by means of highly viscous fluids. In *Proc. 4th world petroleum congress, Rome* (Vol. 2, pp. 579-586).
40. Geertsma, J. and De Klerk, F., 1969. A rapid method of predicting width and extent of hydraulically induced fractures. *Journal of Petroleum Technology*, *21*(12), pp.1-571.
41. Green, A.E. and Sneddon, I.N., 1950. The distribution of stress in the neighbourhood of a flat elliptical crack in an elastic solid. In *Mathematical Proceedings of the Cambridge Philosophical Society* (Vol. 46, No. 01, pp. 159-163). Cambridge University Press.
42. Guo, H., Tang, X., Yang, S. and Shen, Z., 2008. Effect of indigenous bacteria on geochemical behavior of arsenic in aquifer sediments from the Hetao Basin, Inner Mongolia: Evidence from sediment incubations. *Applied Geochemistry*, *23*(12), pp.3267-3277.
43. Zhang, J., Standifird, W.B., Roegiers, J.C. and Zhang, Y., 2007. Stress-dependent fluid flow and permeability in fractured media: from lab experiments to engineering applications. *Rock Mechanics and Rock Engineering*, *40*(1), pp.3-21.
44. Taleghani, A.D. and Olson, J.E., 2009, January. Analysis of multistranded hydraulic fracture Propagation: an improved model for the interaction between induced and natural fractures. In *SPE Annual Technical Conference and Exhibition*. Society of Petroleum Engineers.
45. Settari, A. and Cleary, M.P., 1986. Development and testing of a pseudo-three-dimensional model of hydraulic fracture geometry. *SPE Production Engineering*, *1*(06), pp.449-466.
46. Morales, R.H. and Abou-Sayed, A.S., 1989. Microcomputer analysis of hydraulic fracture behavior with a pseudo-three-dimensional simulator. *SPE production engineering*, *4*(01), pp.69-74.

47. Green, C.A., Barree, R.D. and Miskimins, J.L., 2007, January. Hydraulic Fracture Model Sensitivity Analyses of a Massively Stacked, Lenticular, Tight Gas Reservoir. In *Production and Operations Symposium*. Society of Petroleum Engineers.
48. Kresse, O., Weng, X., Gu, H. and Wu, R., 2013. Numerical modeling of hydraulic fractures interaction in complex naturally fractured formations. *Rock mechanics and rock engineering*, *46*(3), pp.555-568.
49. Hossain, M.M., 2001. *Reservoir stimulation by hydraulic fracturing: Complexities and remedies with reference to initiation and propagation of induced and natural fractures*. University of New South Wales.
50. Economides, M.J. and Hill, A.D., 1994. Ehlig-Economides C. *Petroleum Production Systems*, pp.402-405.
51. Dershowitz, W.S., Cottrell, M.G., Lim, D.H. and Doe, T.W., 2010, January. A discrete fracture network approach for evaluation of hydraulic fracture stimulation of naturally fractured reservoirs. In *44th US Rock Mechanics Symposium and 5th US-Canada Rock Mechanics Symposium*. American Rock Mechanics Association.
52. Rogers, S., Elmo, D., Dunphy, R. and Bearinger, D., 2010, January. Understanding hydraulic fracture geometry and interactions in the Horn River Basin through DFN and numerical modeling. In *Canadian Unconventional Resources and International Petroleum Conference*. Society of Petroleum Engineers.
53. Last, N.C. and Harper, T.R., 1990. Response of fractured rock subject to fluid injection part I. Development of a numerical model. *Tectonophysics*, *172*(1), pp.1-31.
54. McLennan, J.D., Tran, D.T., Zhao, N., Thakur, S.V., Deo, M.D., Gil, I.R. and Damjanac, B., 2010, January. Modeling fluid invasion and hydraulic fracture propagation in naturally fractured formations: a three-dimensional approach. In *SPE International Symposium and Exhibiton on Formation Damage Control*. Society of Petroleum Engineers.
55. Ben, Y., Xue, J., Miao, Q., Wang, Y. and Shi, G.H., 2012, January. Simulating hydraulic fracturing with discontinuous deformation analysis. In *46th US Rock Mechanics/Geomechanics Symposium*. American Rock Mechanics Association.

56. Fu, P., Johnson, S.M., Hao, Y. and Carrigan, C.R., 2011, January. Fully coupled geomechanics and discrete flow network modeling of hydraulic fracturing for geothermal applications. In *The 36th Stanford Geothermal Workshop*.
57. Ong, S.H. and Roegiers, J.C., 1995, January. Fracture initiation from inclined wellbores in anisotropic formations. In *International Meeting on Petroleum Engineering*. Society of Petroleum Engineers.
58. Daneshy, A.A., 1974, January. Hydraulic fracture propagation in the presence of planes of weakness. In *SPE European Spring Meeting*. Society of Petroleum Engineers.
59. Wang, S.Y., Sun, L., Au, A.S.K., Yang, T.H. and Tang, C.A., 2009. 2D-numerical analysis of hydraulic fracturing in heterogeneous geo-materials. *Construction and Building Materials*, *23*(6), pp.2196-2206.
60. Hecker, M.T. and Downie, R.C., 1996, January. Process changes improve fracture treatment designs in the Hugoton Gas Field. In *SPE Mid-Continent Gas Symposium*. Society of Petroleum Engineers.
61. Love, A.E.H., 1927. *The mathematical theory of elasticity*.
62. Muskhelishvili, N. I. (1953). *Singular Integral Equations: Boundary Problems of Functions Theory and Their Application to Mathematical Physics*. J. R. M. Radok (Ed.). P. Noordhoff.
63. Savin, G.N., 1961. *Stress concentration around holes* (Vol. 1). Pergamon Press.
64. Whittaker, B.N., 1988. Analytical and computational methods in engineering rock mechanics, edited by By ET Brown Allen and Unwin, London, 1987, No. of pages: 259. Price:£ 30.
65. Lisjak, A., Mahabadi, O.K., Tatone, B.S.A., Alruwaili, K., Couples, G.D., Ma J, J. and Al-Nakhli, A., 2015, November. 3D simulation of fluid-pressure-induced fracture nucleation and growth in rock samples. In *49th US Rock Mechanics/Geomechanics Symposium*. American Rock Mechanics Association.
66. Kirsch, G., 1898. *Die theorie der elastizität und die bedürfnisse der festigkeitslehre*. Springer.
67. Saleh, K., 1985. *Détermination de l'état de contrainte et des propriétés élastiques d'un massif rocheux par inversion des données récoltées lors d'un essai de fracturation pressiométrique* (Doctoral dissertation, Châtenay-Malabry, École centrale Paris).
68. Love, A.E.H., 1927. *The mathematical theory of elasticity*.

69. Timoshenko, S., Timoshenko, S. and Goodier, J.N., 1951. *Theory of Elasticity, by S. Timoshenko and JN Goodier,...* McGraw-Hill book Company.
70. Poulos, H.G. and Davis, E.H., 1974. *Elastic solutions for soil and rock mechanics*. John Wiley.
71. Jaeger, J.C. and Cook, N.G., W. 1979. Fundamentals of Rock Mechanics. *Chapman and Hall, London*, p.593.
72. Hoek, E. and Bray, J.W., 1977. Rock Slope Engineering, 2nd. *Edn., The Institute of Mining and Metallurgy, London*, *527*.
73. Zienkiewicz, O.C., 1971. The finite element in engineering science. *McGrau Hill, London*.
74. Munjiza, A. (1992) RG combined finite discrete element code - C++, 1990-1992.
75. Mahabadi, O.K., Lisjak, A., Munjiza, A. and Grasselli, G., 2012. Y-Geo: new combined finite-discrete element numerical code for geomechanical applications. *International Journal of Geomechanics*, *12*(6), pp.676-688.
76. Hudson, J.A. and Harrison, J.P., 2000. *Engineering rock mechanics-an introduction to the principles*. Elsevier.
77. Sanford, A.R., 1959. Analytical and experimental study of simple geologic structures. *Geological Society of America Bulletin*, *70*(1), pp.19-52.
78. Bell, J.S. and Gough, D.I., 1979. Northeast-southwest compressive stress in Alberta evidence from oil wells. *Earth and Planetary Science Letters*, *45*(2), pp.475-482.
79. Shamir, G. and Zoback, M.D., 1992. Stress orientation profile to 3.5 km depth near the San Andreas fault at Cajon Pass, California. *Journal of Geophysical Research: Solid Earth*, *97*(B4), pp.5059-5080.
80. Haimson, H.C. and Herrick, C.G., 1986, August. Borehole breakouts-a new tool for estimating in situ stress?. In *ISRM International Symposium*. International Society for Rock Mechanics.
81. Lee, M. and Haimson, B., 1993, December. Laboratory study of borehole breakouts in Lac du Bonnet granite: a case of extensile failure mechanism. In *International journal of rock mechanics and mining sciences & geomechanics abstracts* (Vol. 30, No. 7, pp. 1039-1045). Pergamon.
82. Dyskin, A.V., Germanovich, L.N. and Ustinov, K.B., 2000. Asymptotic analysis of crack interaction with free boundary. *International journal of solids and structures*, *37*(6), pp.857-886.

83. Germanovich, L.N. and Dyskin, A.V., 2000. Fracture mechanisms and instability of openings in compression. *International Journal of Rock Mechanics and Mining Sciences*, *37*(1), pp.263-284.
84. Jizba, D.L., 1991. *Mechanical and acoustical properties of sandstones and shales*. Stanford University, Department of Geophysics, School of Earth Sciences.
85. Zoback, M.D., Moos, D., Mastin, L. and Anderson, R.N., 1985. Well bore breakouts and in situ stress. *Journal of Geophysical Research: Solid Earth*, *90*(B7), pp.5523-5530.
86. Bell, J.S., 1990. Investigating stress regimes in sedimentary basins using information from oil industry wireline logs and drilling records. *Geological Society, London, Special Publications*, *48*(1), pp.305-325.
87. Hubbert, M.K. and Willis, D.G., 1972. Mechanics of hydraulic fracturing.
88. Haimson, B.C., 2003. Borehole breakouts in Berea sandstone reveal a new fracture mechanism. In *Thermo-Hydro-Mechanical Coupling in Fractured Rock* (pp. 813-831). Birkhäuser Basel.
89. Rawlings, C.G., Barton, N.R., Bandis, S.C., Addis, M.A. and Gutierrez, M.S., 1993. Laboratory and numerical discontinuum modeling of wellbore stability. *Journal of Petroleum Technology*, *45*(11), pp.1-086.
90. Zipf, K., 2006, January. Numerical modeling procedures for practical coal mine design. In *Golden Rocks 2006, The 41st US Symposium on Rock Mechanics (USRMS)*. American Rock Mechanics Association.
91. Callanan, M.J., 1981. Hydraulic fracture initiation by shear failure in formations at great depths. In *Proc. Workshop on hydraulic fracturing stress measurements, Monterey, CA, 181M189*.
92. Morgenstern, N., 1962. A relation between hydraulic fracture pressures and tectonic stresses. *Geofisica pura e applicata*, *52*(1), pp.104-114.
93. Ljunggren, C., Amadei, B. and Stephansson, O., 1988. Use of the Hoek and Brown failure criterion to determine in situ stresses from hydraulic fracturing measurements. *Proc. Care*, *88*, pp.133-142.
94. Panah A. K., and Yanagisawa, E., 1989. Laboratory studies on hydraulic fracturing criteria in soil. *Soil foundat*, *29*(4), pp.14-22.
95. Lo, K.Y. and Kaniaru, K., 1990. Hydraulic fracture in earth and rock-fill dams. *Canadian Geotechnical Journal*, *27*(4), pp.496-506.

96. Mori A., Tamura M. and Fukui Y., 1990. Fracturing pressure of soil ground by viscous materials. *Soil foundat*, *30*(3), pp.129-136.
97. Couples, G., Ma, J., Lewis, H., Olden, P., Quijano, J., Fasae, T. and Maguire, R., 2007. Geomechanics of faults: impacts on seismic imaging. *first break*, *25*(10).
98. Al-Nakhli, A.R., H. Abass, M. Khan, V. Hilab, and A. Rizq. 2014. Chemically-induced pressure pulse to increase stimulated reservoir volume in unconventional reservoirs. In *Proceedings of the Unconventional Resources Technology Conference*. Society of Petroleum Engineers.
99. Grasselli, G., Lisjak, A., Mahabadi, O.K. and Tatone, B.S., 2015. Influence of pre-existing discontinuities and bedding planes on hydraulic fracturing initiation. *European Journal of Environmental and Civil Engineering*, *19*(5), pp.580-597.
100. Lisjak, A., Garitte, B., Grasselli, G., Müller, H.R. and Vietor, T., 2015. The excavation of a circular tunnel in a bedded argillaceous rock (Opalinus Clay): short-term rock mass response and FDEM numerical analysis. *Tunnelling and Underground Space Technology*, *45*, pp.227-248.
101. Zhao, Q., Lisjak, A., Mahabadi, O.K. and Grasselli, G., 2015. Numerical investigation of the influences of rock fabrics on hydraulic fracturing operations.
102. Grasselli, G., Lisjak, A. and Vietor, T., 2013. BRINGING FDEM TO PRACTICE-STUDY OF FAILURE MECHANISMS THAT CONTRIBUTE TO THE DEVELOPMENT OF THE DAMAGED AREA AROUND EXCAVATIONS IN LAYERED ROCK FORMATIONS.
103. Tatone BSA, 2014. "Investigating the evolution of rock discontinuity asperity degradation and void space morphology under direct shear.". Ph.D. Thesis, University of Toronto. Toronto, Canada.

```
/*General_Description:
*/
/YD/YDC/MCSTEP 10000
/YD/YDC/DCSTEC 1e-5
/YD/YDC/ICOUTF 500
/YD/YDC/DCGRAY 0
/YD/YDC/DCSIZC 100
/YD/YDC/DCSIZF 1e7
/YD/YDC/DCSIZV 100
/YD/YDC/DCSIZS 1e6
/YD/YDC/ICOUTI 0
/YD/YDC/ICOUTP 4
 /YD/YDC/ICRESF
/YD/YDC/DCTIME 0
/YD/YDC/NCSTEP 0

/*              ELEMENTS          */
/YD/YDE/MELEM 43160
/YD/YDE/NELEM 4316
/YD/YDE/MELST   2  /YD/YDE/NELST 2
/YD/YDE/MELNO   4  /YD/YDE/NELNO 3
/YD/YDE/D2ELST 21 2 0


/*              INTERACTION              */
/YD/YDI/MICOUP 300000
/YD/YDI/DIEZON 0.025
/YD/YDI/NICOUP 0
/YD/YDI/IIECFF -2
/YD/YDI/DIEDI 200
/YD/YDI/D1IESL 0
/YD/YDI/I1IECT 0
/YD/YDI/I1IECN 0
```

```
/YD/YDI/MISTATE 6

/*              HYDRO-FRACTURING      */
/YD/YDHF/IUSEHF 1
/YD/YDHF/IHFTYP 1
/YD/YDHF/DHFFLP 0
/YD/YDHF/DHFFLQ 800000
/YD/YDHF/HFAROW 4
/YD/YDHF/D2HFAF 21 2 4
0       0
1       0
1.00005         1
10      1
/YD/YDHF/FLUPRES 101.325
/YD/YDHF/FLUPRES0 101.325
/YD/YDHF/FLURHO0 1000
/YD/YDHF/FLUBULK 2.2e9
/YD/YDHF/FRADIM 2
/YD/YDHF/GRAVACC 9.81
/YD/YDHF/D2WTLEV 21 2 2
0       0
0       0

/*              IN SITU STRESSES  */
/YD/YDIS/IUSEIS 0
/YD/YDIS/DCSTXX -10e6
/YD/YDIS/DCSTXY 0
/YD/YDIS/DCSTYY -20e6
/YD/YDIS/DCSYXX 0
/YD/YDIS/DCSYXY 0
/YD/YDIS/DCSYYY 0
/YD/YDIS/DCSRFY 0

/*              PROPERTY - ELEMENTS           */
/YD/YDPE/MPROP 2
```

```
/YD/YDPE/NPROP 2

/YD/YDPE/D1PEEM 2
2E+10 2e10
/YD/YDPE/D1PENU 2
0.38     0.38
/YD/YDPE/D1PELA 2
2.29469E+10  2.29469E+10
/YD/YDPE/D1PEMU 2
7.24638E+09  7.24638E+09
/YD/YDPE/D1PERO 2
2650    2650
/YD/YDPE/D1PEKS 2
1.82003E+06  1.82003E+06
/YD/YDPE/I1PTYP 2
5         5
/* Transversely isotropic elastic constants */
/YD/YDPE/I1USAN 2
0         0
/YD/YDPE/D1PEEX 2
2E+10 2e10
/YD/YDPE/D1PEEY 2
2E+10 2e10
/YD/YDPE/D1PEMX 2
0.38     0.38
/YD/YDPE/D1PEMY 2
0.38     0.38
/YD/YDPE/D1PEG 2
7.24638E+09  7.24638E+09
/* Excavation flag */
/YD/YDPE/I1PEXC 2
0         0

/YD/YDPE/MPEROW 3
/YD/YDPE/D2PEINT 21 5 3
```

```
0       0       1.3     2E+11 2E+10
0       1       1.3     2E+11 2E+10
1       1       1.3     2E+11 2E+10

/YD/YDPE/I1PEFR 2
0       0
/YD/YDPE/D1PSEM 2
0       0
/YD/YDPE/I1PEMB 2
0       0
/YD/YDPE/I1PSDE 2
0       0
/*              PROPERTY - COHESIVE CRACKS              */
/YD/YDPJ/MPJSET 1
/YD/YDPJ/NPJSET 1

/YD/YDPJ/D1PJFR 1
1.3
/YD/YDPJ/D1PJCO 1
1.4e7
/YD/YDPJ/D1PJFS 1
0
/YD/YDPJ/D1PJFT 1
6E+06
/YD/YDPJ/D1PJGF 1
750000
/YD/YDPJ/D1PJGS 1
1500000
/YD/YDPJ/D1PJPE 1
1E+11
/YD/YDPJ/I1PTYP 1
3
/YD/YDPJ/I1PSDE 1
0
/* Anisotropic joint fracture model */
```

```
/YD/YDPJ/D1USAF 1
0
/YD/YDPJ/D1PJAL 1
0
/YD/YDPJ/D1PJFD 1
1.3
/YD/YDPJ/D1PJCR 1
1.4e7
/YD/YDPJ/D1PJTR 1
6E+06
/YD/YDPJ/D1PJGR 1
750000
/YD/YDPJ/D1PJSR 1
1500000
/*              PROPERTY - MESHING              */
/YD/YDPM/MPMCOM 1
/YD/YDPM/MPMCOL 4
/YD/YDPM/I2PMSET 21 4 1
2       3       0       1

/YD/YDPM/MPMROW 3
/YD/YDPM/I2PMIJ 21 3 3
0       0       0
0       1       0
1       1       0

/*              BOUNDARY CONDITIONS             */
/YD/YDPN/MPNSET 3
/YD/YDPN/NPNSET 3

/YD/YDPN/D1PNAX 3
0       0       0
/YD/YDPN/D1PNAY 3
0       0       0
/YD/YDPN/D1PNAP 3
```

```
0       0       0
/YD/YDPN/D1PNAT 3
0       0       0
/YD/YDPN/I1PNFX 3
1       3       1
/YD/YDPN/I1PNFY 3
1       3       1
/YD/YDPN/D1PNXX 3
1       1       1
/YD/YDPN/D1PNXY 3
0       0       0
/YD/YDPN/D1PNYX 3
0       0       0
/YD/YDPN/D1PNYY 3
1       1       1

/* First modulus reduction inside borehole */
$YDOIT
/YD/YDC/MCSTEP 20000
/YD/YDPE/D1PEEM 2
2E+10 2E+9

/* Second modulus reduction inside borehole */
$YDOIT
/YD/YDC/MCSTEP 30000
/YD/YDPE/D1PEEM 2
2E+10 2E+8

/* Excavate borehole completely */
$YDOIT
/YD/YDC/MCSTEP 2000000
/* Excavation flag */
/YD/YDPE/I1PEXC 2
0       1
```

/* Start pumping water inside borehole */

$YDOIT

/YD/YDC/MCSTEP 3000000

/YD/YDHF/IHFTYP 2

$YDOIT

$YSTOP